Inaugural–Dissertation
zur
Erlangung der Doktorwürde
der
Naturwissenschaftlich–Mathematischen Gesamtfakultät
der
Ruprecht–Karls–Universität Heidelberg

vorgelegt von
Johannes L. Herold
aus Bayreuth

Tag der mündlichen Prüfung:

.....

Mathematical modeling, simulation, and optimization of loading schemes for isometric resistance training

Advisors:
Prof. Dr. Dr. h.c. mult. Hans Georg Bock
Prof. Dr. Christian Kirches

Further referees:
Prof. Dr. Dr. h.c. mult. Willi Jäger

Abstract

In this thesis, we present a novel mathematical model-based approach to optimize loading schemes of isometric resistance training (RT) sessions for different training goals. To this end, we develop a nonlinear ordinary differential equation model of the time course of maximum voluntary isometric (MVIC) force under external isometric loading. To validate the model, we set up multi-experiment parameter estimation problems using a comprehensive dataset from the literature. We solve these problems numerically via direct multiple shooting and the generalized Gauss-Newton method. Moreover, we use the proposed model to examine hypotheses about fatigue and recovery of MVIC force. Then, we mathematically formulate key performance indicators and optimality criteria for loading schemes of isometric RT sessions identified in sports science and incorporate these into multi-stage optimal control problems. We solve these problems numerically via direct multiple shooting and structure-exploiting sequential quadratic programming. We discuss the results from a numerical and sports scientific point of view. Based on the proposed model, we additionally formulate the estimation of critical torque as a nonlinear program. This allows us to reduce the experimental effort compared to conventional testing when estimating these quantities. Furthermore, we formulate multi-stage optimum experimental design problems to reduce the statistical uncertainty of the parameter estimates when calibrating the model. We solve these problems numerically via direct single shooting and sequential quadratic programming. We discuss the solutions from a numerical and physiological point of view. For our approach, a small amount of data obtained in a single testing session is sufficient. Our approach can be extended to more elaborate physiological models and other forms of resistance training once suitable models become available.

Zusammenfassung

In dieser Arbeit stellen wir einen neuen mathematischen modellbasierten Ansatz zur Optimierung von Belastungsschemata isometrischer Krafttrainingseinheiten für verschiedene Trainingsziele vor. Dafür entwickeln wir ein nichtlineares gewöhnliches Differentialgleichungsmodell des Zeitverlaufs der maximalen willentlichen isometrischen Kraft unter externer isometrischer Belastung. Um das Modell zu validieren, stellen wir Mehrfachexperiment-Parameterschätzprobleme auf und verwenden einen umfassenden Datensatz aus der Literatur. Wir lösen diese Probleme numerisch mit der Mehrzielmethode und dem verallgemeinerten Gauß-Newton-Verfahren. Weiterhin verwenden wir das entwickelte Modell um Hypothesen bezüglich Ermüdung und Erholung der maximalen willentlichen isometrischen Kraft zu untersuchen. Danach formulieren wir Leistungskennzahlen und Optimalitätskriterien für Belastungsschemata isometrischer Krafttrainingseinheiten mathematisch, die in den Sportwissenschaften identifiziert wurden, und binden diese in mehrphasige Optimalsteuerungsprobleme ein. Wir lösen diese Probleme numerisch mit der Mehrzielmethode und sequentieller quadratischer Programmierung. Wir diskutieren die Resultate aus numerischer und sportwissenschaftlicher Sicht. Basierend auf dem entwickelten Modell, formulieren wir zusätzlich die Schätzung von „Critical Torque“ als nichtlineares Programm. Dies erlaubt es uns den experimentellen Aufwand gegenüber einer konventionellen Schätzung zu reduzieren. Weiterhin formulieren wir mehrphasige Versuchsplanungsprobleme, um die statistische Unsicherheit der Modellparameter beim Kalibrieren des Modells zu reduzieren. Wir lösen diese Probleme numerisch mit dem Einfachschießverfahren und sequentieller quadratischer Programmierung. Wir diskutieren die Resultate aus numerischer und physiologischer Sicht. Mit unserem Ansatz ist eine geringe Menge an Daten, die in einer einzigen Testeinheit erhoben werden kann, ausreichend. Unser Ansatz kann auf umfangreichere physiologische Modelle und andere Formen des Krafttrainings erweitert werden sobald geeignete Modelle zur Verfügung stehen.

Table of contents

Titlepage **3**

Abstract **5**

Table of contents **9**

List of acronyms and abbreviations **13**

List of selected symbols **15**

Introduction **17**
Motivation 17
Contributions 17
Publications 21
Computing environment 22
Thesis overview 22

I Optimization of dynamic processes **23**

1 Dynamic processes **25**
1.1 Ordinary differential equation models 25
1.2 Handling explicit switches 25

2 Optimal control **27**
2.1 Multi-stage optimal control problems 27
2.2 Numerical solution via direct multiple shooting 28
2.3 Sequential quadratic programming 30
2.4 Generating derivatives 33

3 Parameter estimation **35**
3.1 Multi-experiment parameter estimation problems 35
3.2 Numerical solution via direct multiple shooting 36
3.3 Generalized Gauss-Newton method 36
3.4 Sensitivity analysis of the solution 37

4 Optimum experimental design **41**
4.1 Multi-stage optimum experimental design problems 41
4.2 Numerical solution via direct single shooting 42

II Resistance training **45**

5 Basic concepts of resistance training **47**
5.1 Definition of resistance training 47
5.2 Goals and types of resistance training 47
5.3 Describing a resistance training program 48
5.4 Principles of specificity, progression, and periodization 49

6 Key performance indicators for loading schemes of isometric resistance training sessions **51**
6.1 Increasing maximum strength 51
6.2 Increasing muscle mass 52
6.3 Increasing muscle endurance 52
6.4 Increasing power 53

III Results **55**

7 General outline of the approach **57**
7.1 Prerequisites for a suitable model 57
7.2 Literature overview 58
7.3 Working with small amounts of data 59

8 Developing a mathematical model of the time course of maximum voluntary isometric contraction force **61**
8.1 Quantifying muscle fatigue 61
8.2 Prerequisites for a real-life use of a model 62
8.3 Literature overview 63
8.4 Suitable models from the literature 65
8.5 Proposed nonlinear ordinary differential equation model 66
8.6 Formulating a multi-stage variant of the model 67
8.7 Available data 68
8.8 Multi-experiment parameter estimation problems 70
8.9 Numerical solution via direct multiple shooting 70
8.10 Numerical results 71
8.11 Discussion 84
8.12 Limitations and future work 86
8.13 Conclusion 87

9 Analyzing the time course of maximum voluntary isometric contraction force **89**
9.1 Simulated scenarios 89
9.2 Numerical results 90
9.3 Discussion 90
9.4 Conclusion 92

10 Optimizing loading schemes for different training goals **93**
10.1 Multi-stage optimal control problems 93
10.2 Numerical solution via direct multiple shooting 94
10.3 Optimized scenarios 96
10.4 Numerical results 100
10.5 Discussion 110
10.6 Limitations and future work 113
10.7 Conclusion 114

11 Mathematical model-based estimation of critical torques **117**
11.1 Critical power and critical torque 117
11.2 A nonlinear program formulation of critical torque 118
11.3 Numerical results 120
11.4 Discussion 124
11.5 Limitations and future work 125
11.6 Conclusion 126

12 Optimizing testing sessions for model calibration **127**
12.1 Experimental setting 127
12.2 Multi-stage optimum experimental design problems 128
12.3 Numerical solution via direct single shooting 130
12.4 Optimized scenarios 131
12.5 Numerical results 132
12.6 Discussion 138
12.7 Conclusion 138

Conclusion and outlook **139**

Danksagung **141**

Bibliography **143**

List of figures **165**

List of tables **171**

List of acronyms and abbreviations

AD	automatic differentiation
AIC	Akaike information criterion
BFGS	Broyden-Fletcher-Goldfarb-Shanno
GGN	generalized Gauss-Newton
IND	internal numerical differentiation
KKT	Karush-Kuhn-Tucker
KPI	key performance indicator
MAE	mean absolute error
MSO	modeling, simulation, and optimization
NLP	nonlinear program
NLS	nonlinear least-squares
OC	optimal control
ODE	ordinary differential equation
OED	optimum experimental design
PE	parameter estimation
QP	quadratic program
SD	standard deviation
SQP	sequential quadratic programming
WRSS	weighted residual sum of squares

1RM	one repetition maximum
DCER	dynamic constant external resistance
FTI	force-time integral
MVIC	maximum voluntary isometric contraction
RFD	rate of force development
RT	resistance training
SAID	specific adaptation to imposed demands
TUT	time-under-tension

List of selected symbols

c	path constraints
C	variance-covariance matrix
f	right-hand side
G_v	sensitivities of the states w.r.t variable v
h	observable
J	Jacobian
n_c	number of path constraints
n_{con}	number of control intervals
n_e	number of experiments
n_m	number of measurements
n_{ms}	number of shooting intervals
n_p	number of parameters
n_q	number of control quantities
n_s	number of model stages
n_u	number of control functions
n_x	number of differential states
p	parameters
q	control quantities
s	shooting variables
t	time
T	stage duration
u	control functions
x	differential states
ϵ	measurement error
η	measurements
σ	standard deviation of the measurement error
τ^{con}	control grid
τ^{ms}	shooting grid
Φ	objective functional

Introduction

Motivation

Resistance training (RT) is a popular choice among athletes, rehabilitation patients, and the general public to improve physical performance. Benefits of RT include increased muscular strength and endurance, improved body composition, or enhanced functional capacity and quality of life [Williams et al., 2007]. To optimize results, individualized RT is necessary [Fleck and Kraemer, 2014]. Therefore, training variables such as exercise selection, frequency, volume, or intensity need to be adjusted to the trainee and the training goals. These adjustments are commonly performed by the trainee or a coach via trial-and-error [Clarke and Skiba, 2013].

To complement such a manual decision-making, many research areas like chemical or mechanical engineering have adopted methods from scientific computing, e.g., modeling, simulation, and optimization (MSO). For this reason, scientific computing is often considered to be the third pillar of methodology in science next to theory and experiment [Oberkampf and Roy, 2010]. Nevertheless, sports science and exercise physiology are only slowly realizing the potential of model-based approaches [Arandjelović, 2017]. In particular, reports of applications covering loading schemes for resistance training are very limited.

A model-based optimization of loading schemes for RT could provide valuable impulses for practitioners and complement the predominantly manual program design. By calibrating the model to the trainee, personalized parameters are obtained. Then, optimized RT programs could be computed specifically for this trainee, exercise, and training goal based on a key performance indicator (KPI) included in the model. Furthermore, a comparison of effective loading schemes in practice and algorithmically optimized loading schemes could help to identify the driving stimuli for adaptations, e.g., the contributions of mechanical loading, metabolic stress, and muscle damage to hypertrophic adaptations [Schoenfeld, 2010], or the effect of different mechanical stimuli on strength and power adaptations [Crewther et al., 2005]. Moreover, RT programs could be designed to induce the same level of metabolic disturbances. This would allow to increase the comparability between training approaches, e.g., between blood flow restriction training and conventional training.

Contributions

In this thesis, we present a novel mathematical model-based approach to optimize loading schemes of RT sessions for different training goals. The main contributions in the fields of mathematics, applied physiology, and sports science are as follows.

Proposal of a novel mathematical model-based approach to optimize loading schemes of RT sessions for different training goals

To complement the manual decision-making of trainees and coaches in RT planning, an algorithmic optimization of loading schemes appears promising. However, two fundamental challenges arise. First, mathematical or computational modeling is not well-established in the RT literature and therefore only few phenomenological models are available [Arandjelović, 2017] of which – to the best of our knowledge – none are suitable for our purpose (see Chapter 7). Thus, a new model is necessary. Second, the physiological processes taking place in the human body during and after RT are not fully understood by researchers and data for these phenomena is only sparsely available – especially for long-term adaptation processes. Hence, a first principles modeling approach directly connecting the loading schemes to RT outcomes seems to be practically infeasible. Thus, we propose a novel approach. First, we model the varying force capacities of a trainee during a training session depending on the loading scheme. Then, we mathematically formulate key performance indicators and optimality criteria for isometric RT sessions identified in sports science and incorporate these into multi-stage optimal control problems. Based on these problem formulations, we can then optimize the loading schemes. For our approach, a small amount of data obtained in a single testing session is sufficient. This renders an optimization of RT sessions feasible. Details on this approach are given in Chapter 7.

Development of a nonlinear ordinary differential equation model of the time course of maximum voluntary isometric contraction force

To algorithmically optimize the loading schemes of RT sessions, a model-based prediction of the time-dependent force capacities of the trainee is necessary. Such a dynamic model should satisfy several prerequisites (see Chapter 8). However, to the best of our knowledge, a suitable model is not available. Therefore, we develop a nonlinear ordinary differential equation (ODE) model of the time course of maximum voluntary isometric contraction (MVIC) force of a muscle group. As input, the model takes the absolute external isometric load over time and gives the resulting MVIC force capacities of the muscle group as output. The states of the model separate the fast and the slow processes of muscle fatigue and recovery [Carroll et al., 2017]. Their dynamics are based on physiological principles and phenomenological observations. The intrinsic parameters of the model describe the fatigue and recovery properties of the muscle group under consideration and can be identified solely through force measurements. The model is based on previous work by Freund and Takala [2001] and Fayazi et al. [2013]. Due to the chosen structure, it is suitable for our purpose. A parametrization of the input function furthermore allows to use the trainee's effort as input, which enables a simulation of maximum efforts. This results in an additional coupling of the states. Details on the proposed model are given in Chapter 8.

Numerical validation of the proposed model in a multi-experiment parameter estimation setting based on a comprehensive real-life data set

To ensure a practical benefit of the proposed model for sports scientists and exercise physiologists, a validation of its descriptive and predictive abilities is necessary. We use published data of the time course of MVIC force of the elbow flexors under different loading schemes. To the best of our knowledge, we compile the most comprehensive dataset in the literature for this purpose. As data of the available single experiments is not sufficient for a reliable model calibration, we formulate a multi-experiment parameter estimation problem using a subset of the available experiments. The resulting weighted least-squares problem constrained by an ODE system is transcribed to finite-dimensional form via the direct multiple shooting method [Bock, 1987] and solved with the reduced generalized Gauss-Newton method [Bock, 1987; Schlöder, 1988]. We quantify the uncertainty of the parameter estimates and use the calibrated model to predict the remaining experiments. This approach guarantees reliable parameter estimates and an efficient estimation procedure, which is necessary when scaling our approach to multiple muscle groups and individuals. We cross-validate our results by interchanging experiments in the calibration and prediction sets. The model is able to describe and predict the data with a mean absolute error of 0.02 to 0.04 %. Details on the validation process are given in Chapters 3 and 8.

Physiological analysis of the time course of MVIC force via numerical simulations

To examine or validate hypotheses about the time course of MVIC force under different loading schemes, extensive experimental effort is necessary (see, e.g., the works of Rozand et al. [2015] or Rashedi and Nussbaum [2017]). We demonstrate how numerical simulations of the calibrated model can be used to reduce the experimental effort. Namely, we examine the history-dependence of force recovery [Rashedi and Nussbaum, 2017] and the influence of the force-time integral on fatigue [Rozand et al., 2015]. Such simulations complement the experimental work of practitioners and contribute to the understanding of fatigue and recovery of MVIC force. Details on these numerical simulations are given in Chapter 9.

Mathematical formulation of KPIs and optimality criteria for different training goals of isometric RT sessions as multi-stage optimal control problems

The sports science literature identifies four so-called "trainable characteristics" for RT – muscle strength, muscle mass, muscle endurance, and muscle power [American College of Sports Medicine, 2009]. However, due to the obstacles mentioned above, the proposed model does not link the training input directly to these training goals. Therefore, we mathematically formulate multi-stage optimal control (OC) problems to model KPIs and optimality criteria identified in the sports

science and exercise physiology literature for the loading schemes. We choose multi-stage OC problems as these reflect the RT reality of grouping a session into sets and repetitions. Furthermore, this multi-stage setting allows a straightforward extension to other contraction modes once suitable data becomes available. The KPIs we identify from the literature and which can be used in the model are intensity, volume, time-under-tension, and fatigue. Using these different KPIs and variants thereof, enables us to analyze how sensitive the optimized loading schemes are to changing the training goals. Details on the mathematical setup of the OC problems are given in Chapters 2 and 10.

Numerical solution of the proposed OC problems with subsequent sports scientific analysis of the optimized isometric RT sessions

To solve the multi-stage optimal control problems, we employ a first-discretize-then-optimize strategy. We transcribe them to a finite-dimensional form via the direct multiple shooting method and solve the resulting nonlinear program with a structure-exploiting sequential quadratic programming method [Bock and Plitt, 1984; Leineweber et al., 2003a,b]. We choose this approach as we need an efficient and flexible framework to solve many of these OC problems for different individuals and different training goals. Furthermore, the control discretization of the direct approach reflects common practice in RT, where external loading is constant during a set. This allows a direct interpretation of the computed solutions by trainees and coaches. Moreover, we analyze these solutions and compare their structure to prevailing RT practice. Details on the numerical solution process of the OC problems are given in Chapters 2 and 10.

Formulation of critical torque estimation as nonlinear program to reduce the experimental effort compared to conventional methods

Critical torque is an important fatigue threshold in exercise physiology and can be used to analyze, predict, or optimize performance [Craig et al., 2019]. However, its practical estimation is rather costly and several testing sessions on separate days are necessary. We formulate the estimation of critical torque as a nonlinear program (NLP). This enables us to determine these quantities with substantially less experimental effort compared to conventional approaches. Details on the model-based estimation of critical torques are given in Chapter 11.

Mathematical formulation of optimum testing sessions as multi-stage optimum experimental design problems to reduce the experimental effort for model calibration

Before an individualized algorithmic optimization of loading schemes is possible, the model needs to be calibrated to the subject's muscle group. To reduce the experimental effort when calibrating the model, we set up multi-stage optimum experimental design (OED) problems. These non-standard optimal control prob-

lems operate on the variance-covariance matrix of the underlying parameter estimation problem and thus allow us to minimize the uncertainty of the resulting parameter estimates [Körkel, 2002]. We choose to minimize their average variance and ensure that the practical realization of an experiment is correctly represented by the mathematical formulation. Details on the mathematical formulation of the multi-stage OED problems are given in Chapters 4 and 12.

Numerical solution of the proposed OED problems with subsequent physiological and numerical analysis of the optimized testing sessions

Due to their non-standard structure, the multi-stage optimum experimental design problems with continuous measurements are challenging to solve [Bock et al., 2013]. Furthermore, we need to ensure a possible transfer of the numerical solution into practice. We choose to transcribe the OED problems to finite-dimensional form via the direct single shooting method and solve the resulting NLP with a sequential quadratic programming method [Körkel, 2002]. We choose this approach as we need an efficient and flexible framework to solve many of these OED problems for different individuals. Moreover, the control discretization of the direct approach reflects common practice in RT, where external loading is constant during a set. This allows a direct interpretation of the computed solutions by trainees and coaches. We analyze these solutions and compare their structure to prevailing testing practice. Our approach allows to calibrate the model in a single testing session. Furthermore, we demonstrate how the parameter uncertainties propagate through the model and influence other quantities of interest, e.g., critical torque. Details on the numerical solution of the multi-stage OED problems are given in Chapters 4 and 12.

Publications

Results of this thesis have been peer-reviewed and published in:

- Herold et al. [2018]: J. L. Herold, C. Kirches, and J. P. Schlöder. A phenomenological model of the time course of maximal voluntary isometric contraction force for optimization of complex loading schemes. *European Journal of Applied Physiology*, 118(12):2587–2605, 2018. doi: 10.1007/s00421-018-3983-z. URL `https://doi.org/10.1007/s00421-018-3983-z`.

- Herold and Sommer [2020a]: J. L. Herold and A. Sommer. A model-based estimation of critical torques reduces the experimental effort compared to conventional testing. *European Journal of Applied Physiology*, 2020. doi: 10.1007/s00421-020-04358-w. URL `https://doi.org/10.1007/s00421-020-04358-w`.

- Herold and Sommer [2020b]: J. L. Herold and A. Sommer. A mathematical model-based approach to optimize loading schemes of isometric resistance

training sessions. *Sports Engineering*, 2020. doi: 10.1007/s12283-020-00337-8 URL https://doi.org/10.1007/s12283-020-00337-8.

Computing environment

All results of this thesis were obtained on a machine with a quad-core Intel Core i7-6700K CPU @ 4.00 GHz and 32 GB memory running Ubuntu 18.04 LTS. The maximum number of available threads was 8.

Thesis overview

This thesis is structured into three main parts. Following this introduction, in the first part, we derive the mathematical problem formulations chosen for our approach and present the numerical solution methods chosen. This includes notes on optimal control, multi-experiment parameter estimation, and optimum experimental design for multi-stage ODE models. In the second part, we introduce basic concepts of RT and present possible KPIs for isometric RT sessions. In the third part, we present the results obtained in this thesis in the order listed above. We end this thesis with a conclusion and an outlook on possible further research directions.

Part I

Optimization of dynamic processes

Chapter 1

Dynamic processes

In this chapter, we introduce dynamic processes modeled by ordinary differential equations (ODEs). In the first section, we present the general notation for the ODE models used in this thesis. In the second section, we discuss how we handle possibly occurring explicit switches.

Here and in the following chapters, we expect the reader to be familiar with the basics of nonlinear optimization and the numerical solution of ODEs – in particular with backward differentiation formulas and Runge-Kutta-Fehlberg methods. We refer to the books of Nocedal and Wright [2006], Hairer et al. [1993], and Hairer and Wanner [1996] for a comprehensive introduction to these topics.

1.1 Ordinary differential equation models

Many dynamic processes in nature can be modeled by autonomous systems of ODEs given in the form

$$\frac{\mathrm{d}}{\mathrm{d}t}x(t) = f(x(t), u(t), q, p). \tag{1.1}$$

Here, $\frac{\mathrm{d}}{\mathrm{d}t}$ denotes the total derivative w.r.t. variable t. The differential states $x : [0,T] \to \mathbb{R}^{n_x}$ describe the evolution of the system on the time horizon $t \in [0,T] \subset \mathbb{R}$ and the laws of the system are modeled by the right-hand side $f : \mathbb{R}^{n_x} \times \mathbb{R}^{n_u} \times \mathbb{R}^{n_q} \times \mathbb{R}^{n_p} \to \mathbb{R}^{n_x}$, representing, e.g., lactate kinetics during exercise. Furthermore, the model contains parameters $p \in \mathbb{R}^{n_p}$, which describe internal properties of the system, e.g., buffering capacity of the trainee's muscle group. These parameters can usually not be measured directly and therefore have to be estimated from measurement data. We refer to Chapter 3 for an introduction to parameter estimation.

Additionally, the system can be controlled externally. In this work, we use piecewise constant control functions $u \in PC^0$ on a chosen grid $\{\tau_i^{\mathrm{con}}\}_{0 \le i \le n_{\mathrm{con}}}$ with $u(t) = w_i \in \mathbb{R}^{n_u}$ for $t \in [\tau_i^{\mathrm{con}}, \tau_{i+1}^{\mathrm{con}}] \subseteq [0,T]$ and constant control quantities $q \in \mathbb{R}^{n_q}$ describing, e.g., the force generated by the muscle group or joint angles which are constant during the exercise. Chapter 2 gives an introduction to optimal control.

1.2 Handling explicit switches

ODE models can contain so-called switches, which induce a discontinuous jump in the differential states or a change of the right-hand side and therefore of the

model dynamics. We distinguish between explicit and implicit switches.

Explicit switches (also called externally forced switches or time events) occur at a priori known time instances during the process, e.g., when the trainee changes the contraction mode from concentric to eccentric. Explicit switches can be handled by stopping and restarting the integration at those time points. If necessary, sensitivity updates need to be provided.

In contrast, implicit switches (also called internally forced switches or state events) occur at a priori unknown time instances when certain conditions on the states are satisfied, e.g., when muscle glycogen is depleted. Implicit switches are more challenging to handle and several approaches have been proposed, e.g., by Bock [1987], Mombaur [2001], Kirches [2006], Albersmeyer [2010], or [Meyer, 2020]. Again, sensitivity updates need to be provided need if necessary.

In this thesis, we use a multi-stage approach [Leineweber et al., 2003a] for the optimization of such systems, which is suitable when the sequence of model changes is known a priori. In the next chapter, we introduce the concept of multi-stage optimal control problems tailored to our needs.

Chapter 2

Optimal control

In this chapter, we introduce the specific formulation of multi-stage optimal control (OC) problems used in this thesis and the numerical methods used to solve these problems.

In the first section, we formulate the multi-stage OC problems. In the second section, we introduce the direct multiple shooting approach to reduce the optimization problems to finite-dimensional form. In the third section, we give an overview on sequential quadratic programming (SQP) used to solve the resulting nonlinear programs (NLPs). In the last section, we discuss how to efficiently generate derivatives necessary for these algorithms.

For an overview on the topic, we refer to the work of Leineweber et al. [2003a,b], which is based on the work of Bock and Plitt [1984], and the references therein.

2.1 Multi-stage optimal control problems

Often, it is desirable to steer the system (1.1) in such a way that a certain objective functional $\Phi(x) \in \mathbb{R}$ is min- or maximized, e.g., min- or maximizing the accumulation of metabolites during a training session. To this end, the control functions u and the control quantities q are used. During the process, certain constraints have to be satisfied by the system, e.g., a certain heart rate may not be exceeded. We model this by the inclusion of path constraints

$$0 \leq c(t, x(t), u(t), q, p) \in \mathbb{R}^{n_c}. \tag{2.1}$$

Initial conditions are given by

$$x(0) = x_0(q, p) \in \mathbb{R}^{n_x}. \tag{2.2}$$

To deal with possible changes in the right-hand side, we divide the time interval into n_s subintervals called stages. The corresponding model components on stage $i \in \{1, \ldots, n_s\}$ are denoted by a superscript. The stages are defined on time intervals $[0, T^i]$. Continuous transitions between model stages are modeled by

$$x^{i+1}(0) = x^i(T^i). \tag{2.3}$$

Possible dimensional changes or discontinuous state jumps could be incorporated by special transition function and stages [Leineweber et al., 2003a].

The multi-stage optimal control problems in this thesis can be formulated as

$$\min_{x^i(\cdot), u^i(\cdot), q^i} \quad \Phi(x^{n_s}(T^{n_s})) \tag{2.4a}$$

$$\text{s.t.} \quad x^1(0) = x_0(q^1, p) \tag{2.4b}$$

$$\sum_{i=1}^{n_s} T^i \leq C_T \tag{2.4c}$$

$$\text{and for} \quad i \in \{1, \ldots, n_s - 1\} :$$

$$x^{i+1}(0) = x^i(T^i) \tag{2.4d}$$

$$\text{and for} \quad i \in \{1, \ldots, n_s\} \text{ and } t \in [0, T^i] :$$

$$\frac{\mathrm{d}}{\mathrm{d}t} x^i(t) = f^i(x^i(t), u^i(t), q^i, p) \tag{2.4e}$$

$$0 \leq c^i(t, x^i(t), u^i(t), q^i, p). \tag{2.4f}$$

The stage durations T^i are either part of the control quantities q^i or fixed, in which case the constraint (2.4c) and the upper bound $C_T \in \mathbb{R}$ can be neglected. The performance index Φ is of Mayer type and is only evaluated at the end of the last stage. Performance indices of Bolza or Lagrange type are reformulated as Mayer type in this thesis.

2.2 Numerical solution via direct multiple shooting

Several approaches exist to solve the OC problems formulated above. In this work, we choose a direct multiple shooting approach introduced by Bock and Plitt [1984], which transcribes the problems to finite-dimensional form. The resulting nonlinear programs are then solved with structure-exploiting methods, which we discuss in the next section. In the following, we give a short overview of the basic ideas. We use a single-stage problem for illustration.

2.2.1 Discretization of the control functions

First, the time horizon $[0, T]$ is divided into n_{con} control intervals

$$0 = \tau_0^{\mathrm{con}} < \tau_1^{\mathrm{con}} < \cdots < \tau_{n_{\mathrm{con}}-1}^{\mathrm{con}} < \tau_{n_{\mathrm{con}}}^{\mathrm{con}} = T \tag{2.5}$$

on a chosen control grid $\{\tau_i^{\mathrm{con}}\}_{0 \leq i \leq n_{\mathrm{con}}}$. Usually, a suitable discretization of the control functions is then chosen on these intervals. However, as we use piecewise constant control functions, this is not necessary in this work. For the remainder of this chapter, we append the values $w_i \in \mathbb{R}^{n_u}$ of the piecewise constant control functions in front of the control quantities, which then yields a vector $q \in \mathbb{R}^{n_{\mathrm{con}} n_u + n_q}$.

2.2.2 Parametrization of the states

Furthermore, we introduce a shooting grid $\{\tau_i^{\mathrm{ms}}\}_{0 \leq i \leq n_{\mathrm{ms}}}$ and shooting variables $s_i \in \mathbb{R}^{n_x}$ with $0 \leq i \leq n_{\mathrm{ms}}$. These shooting variables serve as initial values for a decoupled solution of the ordinary differential equation (ODE) system on these intervals. We denote the solution of the ODE on the i-th shooting interval by

$x(t; s_i, q, p)$ with $0 \leq i \leq n_{ms} - 1$ and $t \in [\tau_i^{\text{ms}}, \tau_{i+1}^{\text{ms}}]$. Adding so-called matching conditions

$$x(\tau_{i+1}^{\text{ms}}; s_i, q, p) - s_{i+1} = 0 \quad \text{for} \quad 0 \leq i \leq n_{\text{ms}} - 1 \tag{2.6}$$

to the problem then again ensures the continuity of the state trajectories in the solution. Thus, simulation and optimization of the system are performed simultaneously.

Single shooting can be seen as a special case of multiple shooting with $n_{\text{ms}} = 1$. Here, only the control variables q are subject to optimization and the states are treated as dependent variables. Thus, simulation and optimization are performed as separate tasks.

2.2.3 Discretization of the constraints and objective

Next, the constraints

$$0 \leq c(t, x(t), q, p) \in \mathbb{R}^{n_c}. \tag{2.7}$$

are discretized to hold pointwise on a grid. Here, we choose this grid to be identical with the shooting grid:

$$0 \leq c(\tau_i^{\text{ms}}, s_i, q, p) \in \mathbb{R}^{n_c} \quad \text{for} \quad 0 \leq i \leq n_{\text{ms}}. \tag{2.8}$$

In general, this does not need to be the case.

Last, evaluating the Mayer-type objective $\Phi(x(T))$ then corresponds to evaluating $\Phi(s_{n_{\text{ms}}})$ at the last shooting node.

2.2.4 Resulting nonlinear program

Taken together, the resulting NLP reads as

$$\begin{aligned}
\min_{s,q} \quad & \Phi(s_{n_{\text{ms}}}) && \text{(2.9a)}\\
\text{s.t.} \quad & c(\tau_i^{\text{ms}}, s_i, q, p) \geq 0 \quad \text{for} \quad 0 \leq i \leq n_{\text{ms}}, && \text{(2.9b)}\\
& x(\tau_{i+1}^{\text{ms}}; s_i, q, p) - s_{i+1} = 0 \quad \text{for} \quad 0 \leq i \leq n_{\text{ms}} - 1, && \text{(2.9c)}\\
& s_0 = x_0(p, q). && \text{(2.9d)}
\end{aligned}$$

The structure of this NLP can be exploited efficiently. We refer to Section 2.3.1 for some short remarks.

2.2.5 Advantages over other approaches

The direct multiple shooting approach offers several advantages over other approaches, which is why we choose it here. Direct methods circumvent the problem of formulating necessary optimality conditions in function space or finding suitable initial guesses for states and co-states when using indirect methods. Moreover, dividing the time interval into smaller intervals allows to reduce the nonlinearity of

the problem and reduce the error propagation on longer time intervals. This lifting allows for a more stable behavior compared to other direct methods, e.g., direct single shooting. Furthermore, due to the decoupling on the shooting intervals, the integration of the ODE can be parallelized in a straightforward manner.

2.3 Sequential quadratic programming

To solve the NLPs obtained by transcribing the OC problems to finite-dimensional form, we employ structure-exploiting sequential quadratic programming. For a thorough introduction to SQP methods, we refer to the book of Nocedal and Wright [2006] and the references therein.

The resulting NLPs are of the general form

$$\min_{v} \quad f(v) \tag{2.10a}$$

$$\text{s.t.} \quad g(v) = 0, \tag{2.10b}$$

$$h(v) \geq 0, \tag{2.10c}$$

with $v \in \mathbb{R}^{n_v}$, $f : \mathbb{R}^{n_v} \to \mathbb{R}$, $g : \mathbb{R}^{n_v} \to \mathbb{R}^{n_g}$, and $h : \mathbb{R}^{n_v} \to \mathbb{R}^{n_h}$. For the algorithm to work reliably, we require f, g, and $h \in \mathcal{C}^2$. The Lagrangian of this problem is defined as

$$\mathcal{L}(v, \lambda, \mu) = f(v) - \lambda^\top g(v) - \mu^\top h(v) \tag{2.11}$$

with Lagrange multipliers $\lambda \in \mathbb{R}^{n_g}$ and $\mu \in \mathbb{R}^{n_h}$.

Algorithm 1 illustrates a basic line search SQP method to solve these problems. Here, we solve a linearly constrained quadratic problem (QP) at the current iterate to obtain a search direction. Using a suitable globalization strategy, we determine a new iterate along this direction and repeat this step until a previously determined convergence criterion is satisfied.

Algorithm 2 illustrates a basic trust region SQP method to solve these problems. Here, we solve a linearly constrained quadratic problem at the current iterate until we obtain a sufficiently better iterate by adjusting the trust region radius. Again, we repeat this step until a previously determined convergence criterion is satisfied.

Several aspects have to be worked out in detail before Algorithms 1 and 2 can be used in practice. Some important aspects are:

- The linearly constrained quadratic program can be solved by a variety of methods, e.g., active set or interior point methods. Active set methods exhibit favorable warm start properties, when similar QPs are solved sequentially. In this thesis, we use the active set methods QPOPT [Gill et al., 1995] and SQOPT [Gill et al., 2005].

- The globalization strategy has to be specified. We use a line search method on augmented Lagrangian merit functions [Gill et al., 2005] and a boxstep trust region approach [Leineweber, 1999].

Algorithm 1 Line search sequential quadratic programming

1: **Require** an initial guess (v_0, λ_0, μ_0) and a convergence criterion.
2: Set $k = 0$.
3: **while** the convergence criterion is not satisfied **do**
4: Compute $f(v_k)$, $g(v_k)$, and $h(v_k)$ as well as the Jacobians $F = \nabla_v f(v_k)$, $G = \nabla_v g(v_k)$, and $H = \nabla_v h(v_k)$ evaluated at the current iterate and an approximation L of the Hessian of the Lagrangian $\nabla^2_{vv}\mathcal{L}(v_k, \lambda_k, \mu_k)$.
5: Solve the linearly constrained quadratic program

$$\min_{\Delta v} \quad \frac{1}{2}\Delta v^\top L \Delta v + F\Delta v \tag{2.12a}$$
$$\text{s.t.} \quad G\Delta v + g(v_k) = 0, \tag{2.12b}$$
$$H\Delta v + h(v_k) \geq 0, \tag{2.12c}$$

to obtain Δv and the Lagrange multipliers λ^{QP} and μ^{QP}.
6: Determine a step size $\alpha \in (0, 1]$ by a suitable globalization strategy.
7: Set

$$v_{k+1} = v_k + \alpha \Delta v, \tag{2.13a}$$
$$\lambda_{k+1} = \lambda_k + \alpha(\lambda^{\mathrm{QP}} - \lambda_k), \tag{2.13b}$$
$$\mu_{k+1} = \mu_k + \alpha(\mu^{\mathrm{QP}} - \mu_k). \tag{2.13c}$$

8: Set $k = k + 1$.
9: **end while**
10: **Return** the solution $(\hat{v}, \hat{\lambda}, \hat{\mu}) = (v_k, \lambda_k, \mu_k)$.

Algorithm 2 Trust region sequential quadratic programming

Require an initial guess (v_0, λ_0, μ_0), an initial trust region radius $\delta > 0$, and a convergence criterion.
Set $k = 0$.
while the convergence criterion is not satisfied **do**
  Compute $f(v_k)$, $g(v_k)$, and $h(v_k)$ as well as the Jacobians $F = \nabla_v f(v_k)$, $G = \nabla_v g(v_k)$, and $H = \nabla_v h(v_k)$ evaluated at the current iterate and an approximation L of the Hessian of the Lagrangian $\nabla^2_{vv}\mathcal{L}(v_k, \lambda_k, \mu_k)$.
  while $v_k + \Delta v$ is not sufficiently better than v_k **do**
    Solve the linearly constrained quadratic program

$$\begin{aligned} \min_{\Delta v} \quad & \frac{1}{2}\Delta v^\top L \Delta v + F\Delta v && \text{(2.14a)} \\ \text{s.t.} \quad & G\Delta v + g(v_k) = 0, && \text{(2.14b)} \\ & H\Delta v + h(v_k) \geq 0, && \text{(2.14c)} \\ & \|\Delta v\| \leq \delta, && \text{(2.14d)} \end{aligned}$$

    to obtain Δv and the Lagrange multipliers λ^{QP} and μ^{QP}.
    if $v_k + \Delta v$ is sufficiently better than v_k **then**
      Choose a trust region radius $\delta' \geq \delta$.
    else
      Decrease the trust region radius $\delta' < \delta$.
    end if
    Set $\delta = \delta'$.
  end while
  Set $v_{k+1} = v_k + \Delta v$ and the multipliers λ_{k+1} and μ_{k+1} depending on whether the trust region constraint is active.
  Set $k = k + 1$.
end while
Return the solution $(\hat{v}, \hat{\lambda}, \hat{\mu}) = (v_k, \lambda_k, \mu_k)$.

- A convergence criterion needs to be defined. We use the so-called Karush-Kuhn-Tucker (KKT) tolerance [Hoffmann et al., 2014] and the maximum complementarity gap [Gill et al., 2005].
- The approximation of the Hessian has to be chosen. This is usually realized by update formulas, which reduce the computational effort compared to computing the exact Hessian or ensure positive definiteness. We choose limited memory Broyden-Fletcher-Goldfarb-Shanno (BFGS) updates – either block-wise [Leineweber, 1999] or full [Gill et al., 2005].

2.3.1 Structure exploitation for multiple shooting

Due to the artificially introduced shooting variables, the dimensions of the resulting NLP increase. However, the structure of the NLP can be exploited. To this end, a condensing algorithm [Bock and Plitt, 1984] is used before solving the QP, which eliminates the shooting variables and the matching conditions. This reduces the computational effort for solving the QP and renders it similar to an effort necessary for single shooting. The shooting variables and the multipliers for the matching conditions can then be computed recursively. For certain problem types, other variants of condensing can be more efficient. Kirches et al. [2012], e.g., proposed a complementary condensing approach for OC problems with many controls, e.g., arising from convexifying mixed-integer OC problems.

Furthermore, tailored block updates are employed to preserve the diagonal block structure of the Hessian [Bock and Plitt, 1984; Leineweber, 1999].

2.4 Generating derivatives

To use the derivative-based SQP method – and the generalized Gauss-Newton method introduced in the following chapter, we need to provide the derivatives of the model functions as well as the sensitivities of the states.

2.4.1 Derivatives of the model functions

We apply two different methods for generating derivatives of the model functions – automatic differentiation (AD) and finite difference approximations. Other methods for generating derivatives of the model functions include, e.g., analytic differentiation by hand, symbolic differentiation via computer algebra systems, or complex step differentiation.

For AD, the function under consideration is represented as a composition of elementary operations, for which the derivatives are provided analytically. Repeatedly applying the chain rule then allows to compute the derivative of the composite function. Not considering potential rounding errors, the thus determined derivatives are exact. Depending on the desired type of derivatives, one evaluates the computational graph of the function either in forward or backward direction. A further variant of AD is the propagation of Taylor polynomials. For a

comprehensive introduction to the topic of AD, we refer to the book of Griewank and Walther [2008].

Furthermore, one-sided

$$\frac{\partial f}{\partial x}(x) = \frac{f(x+h) - f(x)}{h} + \mathcal{O}(h) \tag{2.15}$$

or central finite difference approximations

$$\frac{\partial f}{\partial x}(x) = \frac{f(x+h) - f(x-h)}{2h} + \mathcal{O}(h^2) \tag{2.16}$$

are obtained to approximate the derivatives of a model function.

Second-order derivatives are obtained by applying these methods to the first-order derivatives.

2.4.2 Sensitivities of the states

Apart from derivatives of the model functions, we need to provide the sensitivities $G_v(t) = \frac{\mathrm{d}x}{\mathrm{d}v}(t)$, with $v = (s, q, p)$ representing the shooting variables, the discretized control functions and control quantities, and the parameters. Furthermore, the sensitivities G_p are explicitly part of the optimum experimental design (OED) problems introduced in Chapter 4.

One approach to obtain those sensitivities is to set up the variational differential equations and solve the system

$$\frac{\mathrm{d}}{\mathrm{d}t}x(t) = f(x(t), v) \tag{2.17a}$$

$$\frac{\mathrm{d}}{\mathrm{d}t}G_v(t) = \frac{\partial}{\partial x}f(x(t), v)G_v(t) + \frac{\partial}{\partial v}f(x(t), v) \tag{2.17b}$$

$$x(0) = x_0(v) \tag{2.17c}$$

$$G_v(0) = \frac{\mathrm{d}}{\mathrm{d}v}x_0(v) \tag{2.17d}$$

simultaneously. This is equivalent to using internal numerical differentiation (IND) [Bock, 1981] to generate the sensitivities. The main idea of IND is to fix the adaptive components of the integrator and to differentiate the discretization scheme. This yields the exact derivatives of the approximate solution of the nominal ODE.

For higher order sensitivities

$$G_{vw}(t) = \frac{\mathrm{d}G_v}{\mathrm{d}w}(t) = \frac{\mathrm{d}^2 G}{\mathrm{d}v\mathrm{d}w}(t), \tag{2.18}$$

with $w = (s, q, p)$, we can use the same approach. This is, e.g., necessary when computing G_{pq} for solving the OED problems of Chapter 4.

Another approach is to use external numerical differentiation – a finite difference approximation obtained by integrating the nominal trajectory with perturbed values. This is straightforward to implement but suffers serious drawbacks concerning numerical precision.

Chapter 3

Parameter estimation

In this chapter, we introduce the specific formulation of multi-experiment parameter estimation (PE) problems and the numerical methods used to solve these problems.

In the first section, we formulate the multi-experiment PE problems. In the second section, we present the constrained nonlinear least-squares (NLS) problem resulting from the multiple shooting discretization. In the third section, we introduce the generalized Gauss-Newton (GGN) method used to solve these problems. In the last section, we present an approach to examine the statistical quality of the parameter estimates.

For an overview on the topic, we refer to the book of Bard [1974] and the papers of Bock et al. [2007, 2013] – which are based on the dissertation of Bock [1987] – and the references therein.

3.1 Multi-experiment parameter estimation problems

For the ordinary differential equation (ODE) model (1.1) to be able to accurately describe real-world processes, we need to calibrate the model and provide estimates of the parameters $p \in \mathbb{R}^{n_p}$. As these usually can not be measured directly, one conducts experiments and fits the model to measurement data $\eta \in \mathbb{R}^{n_m}$.

We assume the model to be correct and the measurement errors ϵ_j to be additive, independent, and normally distributed with expected value $\mu_j = 0$ and standard deviation $\sigma_j > 0$. Consequently, the n_m measurements η_j can be modeled as

$$\eta_j = h_j(t_j, x^*(t_j), q, p^*) + \epsilon_j, \qquad j = 1, \dots, n_m, \tag{3.1}$$

where $h_j : [0,T] \times \mathbb{R}^{n_x} \times \mathbb{R}^{n_q} \times \mathbb{R}^{n_p} \to \mathbb{R}$ denotes the measurement function, t_j the time of the measurement, p^* the 'true' but unknown parameter values, and x^* the corresponding states. Note that different measurements could be conducted at the same point in time. Following these assumptions, the maximum likelihood estimator of p^* can be obtained [Bard, 1974] by solving the weighted NLS problem

$$\min_{p, x^{k,i}(\cdot)} \quad \frac{1}{2} \sum_{k=1}^{n_e} \sum_{i=1}^{n_s^k} \sum_{j=1}^{n_m^{k,i}} \left(\frac{h_j^{k,i}(t_j^{k,i}, x^{k,i}(t_j^{k,i}), q^{k,i}, p) - \eta_j^{k,i}}{\sigma_j^{k,i}} \right)^2 \tag{3.2a}$$

$$\text{s.t. for} \quad k \in \{1, \dots, n_e\} :$$

$$x^{k,1}(0) = x_0^{k,1}(q^{k,1}, p) \tag{3.2b}$$

$$\text{and for} \quad k \in \{1, \dots, n_e\} \text{ and } i \in \{1, \dots, n_s^k - 1\}:$$
$$x^{k,i+1}(0) = x^{k,i}(T^{k,i}) \tag{3.2c}$$
$$\text{and for} \quad k \in \{1, \dots, n_e\},\ i \in \{1, \dots, n_s^k\},\ \text{and } t \in [0, T^{k,i}]:$$
$$\frac{\mathrm{d}}{\mathrm{d}t} x^{k,i}(t) = f^{k,i}(x^{k,i}(t), u^{k,i}(t), q^{k,i}, p). \tag{3.2d}$$

Here, the superscript k denotes the experiment under consideration and the superscript i denotes the model stage. Since the experiments are already conducted, the control functions $u^{k,i}$ and quantities $q^{k,i}$ are known during the parameter estimation. The same holds true for the stage durations $T^{k,i}$.

3.2 Numerical solution via direct multiple shooting

We use a single-experiment single-stage problem for illustration of the numerical solution. The transcription of the infinite-dimensional PE problem is done as described in Section 2.2 for the optimal control problem. Here, the resulting constrained NLS problem takes the form

$$\min_{s,p} \quad \frac{1}{2} \sum_{j=1}^{n_m} \left(\frac{h_j(t_j, x(t_j; s_{k(j)}, q, p), q, p) - \eta_j}{\sigma_j} \right)^2 \tag{3.3a}$$
$$\text{s.t.} \quad x(\tau_{i+1}^{\mathrm{ms}}; s_i, q, p) - s_{i+1} = 0 \quad \text{for} \quad 0 \le i \le n_{\mathrm{ms}} - 1, \tag{3.3b}$$
$$s_0 = x_0(p, q), \tag{3.3c}$$

with $0 \le k(j) \le n_{\mathrm{ms}}$ chosen such that t_j lies in the shooting interval $[\tau_k^{\mathrm{ms}}, \tau_{k+1}^{\mathrm{ms}}]$.

Depending on the chosen shooting grid and type of measurements, we can additionally initialize parts of the shooting variables with measurement data. This allows for a better convergence behavior compared to other direct methods, e.g., direct single shooting.

3.3 Generalized Gauss-Newton method

To solve the constrained NLS problems obtained by transcribing the PE problems, we employ the generalized Gauss-Newton method [Bock, 1987; Schlöder, 1988]. The NLS problems can be written in the general form

$$\min_{v} \quad \frac{1}{2} \left\| F_1(v) \right\|_2^2 \tag{3.4a}$$
$$\text{s.t.} \quad F_2(v) = 0, \tag{3.4b}$$

with $v \in \mathbb{R}^{n_v}$, $F_1 : \mathbb{R}^{n_v} \to \mathbb{R}^{n_1}$ and $F_2 : \mathbb{R}^{n_v} \to \mathbb{R}^{n_2}$. Again, we require F_1 and $F_2 \in \mathcal{C}^2$ for a reliable performance of the algorithm.

Algorithm 3 illustrates the basic idea of the GGN. Therefore, we solve a linearized constrained least-squares problem at the current iterate to obtain a search

Algorithm 3 Generalized Gauss-Newton method

1: **Require** an initial guess v_0 and a convergence criterion.
2: Set $k = 0$.
3: **while** the convergence criterion is not satisfied **do**
4: Compute $F_1(v_k)$ and $F_2(v_k)$ and the Jacobians $J_1 = \nabla_v F_1(v_k)$ and $J_2 = \nabla_v F_2(v_k)$ evaluated at the current iterate.
5: Solve the linearized constrained least-squares problem

$$\min_{\Delta v} \frac{1}{2} \|F_1(v_k) + J_1 \Delta v\|_2^2 \tag{3.5a}$$

$$\text{s.t. } F_2(v_k) + J_2 \Delta v = 0. \tag{3.5b}$$

for the increment Δv.
6: Determine a step size $\alpha \in (0, 1]$ by a suitable globalization strategy.
7: Set $v_{k+1} = v_k + \alpha \Delta v$.
8: Set $k = k + 1$.
9: **end while**
10: **Return** the solution $\hat{v} = v_k$.

direction. Using a suitable globalization strategy, we determine a new iterate and repeat this step until a previously determined convergence criterion is satisfied.

The linearized constrained least-squares problem (3.5) can be solved analytically using only first-order derivative information [Bock, 1987]. This avoids the computationally expensive calculation of the Hessian necessary for other methods. As globalization strategy, we choose the restricted monotonicity test [Bock et al., 2000], which has shown favorable results in practice. Other approaches are possible as well, e.g., line search approaches on suitable merit functions [Nocedal and Wright, 2006].

The constrained NLS problem could also be solved by other methods, e.g., sequential quadratic programming or the Levenberg-Marquardt method. However, the GGN possesses some beneficial statistical properties which guarantee reliable parameter estimates, i.e., it is typically not attracted by statistically unstable local minima [Bock, 1987]. The latter property is necessary to ensure the predictive capability of the calibrated model and can therefore be seen as an advantage over other solution methods for least-squares problems, although this might not be apparent at first.

3.4 Sensitivity analysis of the solution

Since the measurement data η is subject to random measurement errors, the solution $\hat{v}$ of problem (3.4a) is a random variable [Bock, 1987]. Assuming

$$\text{rank } J_2 = n_2, \qquad \text{(constraint qualification)} \tag{3.6a}$$

$$\text{rank } J = n_v, \qquad \text{(positive definiteness)} \tag{3.6b}$$

with

$$J = \begin{pmatrix} J_1 \\ J_2 \end{pmatrix}, \tag{3.6c}$$

one can approximate [Bock, 1987; Janka, 2015] its variance-covariance matrix by

$$C = \begin{pmatrix} \mathrm{I} & 0 \end{pmatrix} \begin{pmatrix} J_1^\top J_1 & J_2^\top \\ J_2 & 0 \end{pmatrix}^{-1} \begin{pmatrix} \mathrm{I} \\ 0 \end{pmatrix} \in \mathbb{R}^{n_v \times n_v}. \tag{3.6d}$$

It can be shown that the variance-covariance matrix of the constrained problem projected on the upper left $(n_v - n_2) \times (n_v - n_2)$ part equals the variance-covariance matrix $C = J_1^\top J_1$ of the unconstrained problem [Janka, 2015]. This is a desired property, as the multiple shooting discretization which induces the equality constraints in our case, is chosen arbitrarily. Thus, the variance-covariance matrix of PE problem (3.2) can be approximated by

$$C = (J^\top J)^{-1} \in \mathbb{R}^{n_p \times n_p}. \tag{3.7a}$$

with

$$J = \begin{pmatrix} J_1^{1,1} \\ J_2^{1,1} \\ \dots \\ J_1^{1,2} \\ J_2^{1,2} \\ \dots \\ J_1^{2,1} \\ J_2^{2,1} \\ \dots \end{pmatrix} \in \mathbb{R}^{n_m \times n_p}, \tag{3.7b}$$

the rows given as

$$J_j^{k,i} = \frac{1}{\sigma_j^{k,i}} \left(\frac{\partial h_j^{k,i}}{\partial x^{k,i}} G_p^{k,i}(t_j^{k,i}) + \frac{\partial h_j^{k,i}}{\partial p}(t_j^{k,i}) \right) \Bigg|_{p=\hat{p}} \in \mathbb{R}^{n_p}, \tag{3.7c}$$

and $n_m = \sum_{k=1}^{n_e} \sum_{i=1}^{n_s^k} n_m^{k,i}$ being the total number of measurements. Here, the sensitivities of the model states w.r.t. the parameters are denoted by $G_p(t) = \frac{\mathrm{d}x}{\mathrm{d}p}(t)$. To increase readability, we partially omitted function arguments.

The approximation C describes a confidence ellipsoid around the estimates $\hat{p}$. Different criteria $\Phi(C)$ can then be used to measure the statistical quality of the estimates [Pukelsheim, 1993]. Often used criteria are, e.g.,

- the A-criterion: $\Phi_A(C) = \frac{1}{n_p} \mathrm{tr}(C)$,
- the D-criterion: $\Phi_D(C) = \det(C)^{\frac{1}{n_p}}$,
- the E-criterion: $\Phi_E(C) = \max\{\lambda_i \mid \lambda_i \text{ eigenvalue of } C\}$,

- and the M-criterion: $\Phi_M(C) = \max\{C_{\mathrm{ii}} \mid i \in \{1, \ldots, n_p\}\}$.

These criteria can be interpreted geometrically with regard to the confidence ellipsoid. The A-criterion is proportional to the mean half-axis, the D-criterion to the volume of an enclosing box, the E-criterion to the largest principal half-axis, and the M-criterion to the longest edge of an enclosing box.

Chapter 4

Optimum experimental design

In this chapter, we introduce the specific formulation of multi-stage optimum experimental design (OED) problems and the numerical methods used to solve these problems.

In the first section, we formulate the multi-stage OED problems. In the second section, we present the nonlinear program (NLP) resulting from the single shooting discretization of these problems.

For an overview on the topic, we again refer to the papers of Bock et al. [2007] and Bock et al. [2013] and the references therein. For a more detailed introduction, we refer to the dissertations of Körkel [2002] and Janka [2015].

4.1 Multi-stage optimum experimental design problems

As shown in the previous chapter, the variance-covariance matrix $C = C(u, q, p)$ (3.7) resulting from the underlying parameter estimation problem (3.2) depends on the control functions u, on the control quantities q, and on the current guess $\hat{p}$. However, it does not depend on the measurement data η. This enables us to design experiments which reduce the statistical uncertainty of the estimates. This idea is illustrated in Figure 4.1.

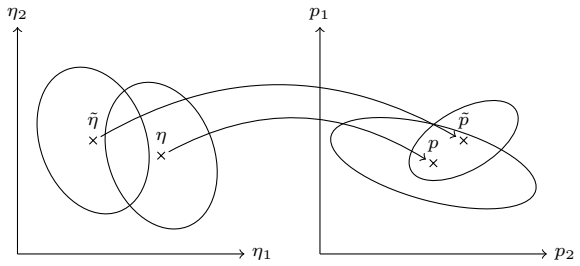

Figure 4.1: Different experimental conditions result in different parameter estimates and confidence regions thereof. The measurement data obtained by two different experiments are denoted by η and $\tilde{\eta}$. The corresponding parameter estimates are denoted by p and $\tilde{p}$. Confidence regions are illustrated by ellipses. Smaller confidence regions increase the probability of the estimates being close to the 'true' but unknown value. Redrawn in modified form from Walter [2012].

The single-experiment multi-stage optimum experimental design problems in this thesis take the following form:

$$\min_{x^i(\cdot),G_p^i(\cdot),u^i(\cdot),q^i} \quad \Phi(C) \tag{4.1a}$$

$$\text{s.t.} \quad x^0(0) = x_0(q^1, p) \tag{4.1b}$$

$$G_p^0(0) = \frac{\mathrm{d}}{\mathrm{d}p} x_0(q^1, p) \tag{4.1c}$$

$$\sum_{i=1}^{n_s} T^i \leq C_T \tag{4.1d}$$

$$\text{and for} \quad i \in \{1, \ldots, n_s - 1\} :$$

$$x^{i+1}(0) = x^i(T^i) \tag{4.1e}$$

$$G_p^{i+1}(0) = G_p^i(T^i) \tag{4.1f}$$

$$\text{and for} \quad i \in \{1, \ldots, n_s\} \text{ and } t \in [0, T^i] :$$

$$\frac{\mathrm{d}}{\mathrm{d}t} x^i(t) = f^i(x^i(t), u^i(t), q^i, p)) \tag{4.1g}$$

$$\frac{\mathrm{d}}{\mathrm{d}t} G_p^i(t) = \frac{\partial f^i}{\partial x^i} G_p^i(t) + \frac{\partial f^i}{\partial p} \tag{4.1h}$$

$$0 \leq c^i(t, x^i(t), u^i(t), q^i, p). \tag{4.1i}$$

The stage durations T^i are either part of the control quantities q^i or fixed, in which case the constraint (4.1d) and the upper bound $C_T \in \mathbb{R}$ can be neglected. As outlined in Section 3.4, several choices for the objective functional Φ are possible. In this thesis, we choose the A-criterion, which can be also be interpreted as the mean variance of the parameters. If desired, a weighting of the parameters can be achieved by an internal scaling of the parameters.

4.2 Numerical solution via direct single shooting

We use a single-stage OED problem for illustration of the numerical solution via single shooting. The transcription of the infinite-dimensional OED problem is done as described in Section 2.2 for the optimal control problem. Here, the resulting NLP takes the form

$$\min_{s,q} \quad \Phi(C) \tag{4.2a}$$

$$\text{s.t.} \quad c(\tau_i^{\mathrm{ms}}, s_i, q, p) \geq 0 \quad \text{for} \quad 0 \leq i \leq n_{\mathrm{ms}}, \tag{4.2b}$$

$$s_0 = x_0(p, q). \tag{4.2c}$$

For the single shooting approach, a reformulation of the nonstandard objective functional, which is nonlinearly coupled in time, is not necessary compared to a direct multiple shooting approach [Janka, 2015]. A sequential quadratic

programming (SQP) method with limited memory Broyden-Fletcher-Goldfarb-Shanno (BFGS) updates is chosen to solve the resulting NLP as it does not require the computation of second order derivatives. Due to the objective functional operating on the variance-covariance matrix – and thus the sensitivities – of the underlying parameter estimation problem, already the first order derivatives are challenging to compute. SQP methods usually need less function and derivative evaluations compared to interior point methods and perform favorably when only first order derivatives are available [Gill et al., 2015], which is a further reason for our choice.

Part II

Resistance training

Chapter 5

Basic concepts of resistance training

In this chapter, we present the basic concepts of resistance training (RT). In the first section, we give a definition of RT. In the second section, we summarize the possible goals and different types of RT. In the third section, we explain how to describe an RT program. In the fourth section, we present the principles of specificity, progression, and periodization.

For a comprehensive introduction to the multifaceted topic of RT, we refer to the book of Fleck and Kraemer [2014]. If not mentioned otherwise, we follow their work in this chapter.

5.1 Definition of resistance training

The American College of Sports Medicine [2013] defines RT as "a form of physical activity that is designed to improve muscular fitness by exercising a muscle or a muscle group against external resistance."

5.2 Goals and types of resistance training

According to the American College of Sports Medicine [2009], trainable characteristics include

- muscle strength – the maximum force or torque that a muscle can produce,
- muscle mass / hypertrophy – the amount of muscle tissue,
- muscle power – the amount of work that a muscle can perform in a certain time interval,
- and muscle endurance – the ability of the muscle to withstand prolonged loading.

Apart from these primary characteristics, RT offers a variety of health benefits, e.g., increased functional capacity and quality of life, or improved body composition [Williams et al., 2007]. Furthermore, improvements in RT can also transfer to sports-specific skills [American College of Sports Medicine, 2009]. In practice however, RT programs are commonly designed to increase (or maintain) a subset of the trainable characteristics.

RT is characterized by exercising muscles. The different contraction modes are

- isometric – where no movement of the joint occurs,

- concentric – where a shortening of the active muscle occurs
- and eccentric – where a lengthening of the active muscle occurs.

Isometric contractions are also called static contractions. Concentric and eccentric contractions are summarized as dynamic contractions.

Based on the exercises performed, RT can be categorized into the non-mutually exclusive types [Fleck and Kraemer, 2014]

- dynamic constant external resistance (DCER) training – also called isoinertial or isoload training, where force is produced against a constant external resistance during a dynamic movement, e.g., when lifting a dumbbell,
- variable resistance training – where force is produced against a varying external resistance during a dynamic movement, e.g., when using resistance bands or certain RT machines,
- isokinetic training – where the joint angular velocity is constant during a movement,
- isotonic training – where the force exerted by the muscle (group) is constant during a movement, often used as a misnomer for DCER training,
- and isometric training – where only isometric contractions are performed.

5.3 Describing a resistance training program

Classically, six variables are used to describe RT programs of a single exercise [Toigo and Boutellier, 2006]:

- intensity – defined by absolute load, repetition maxima, velocity, rating of perceived exertion, or similar,
- number of repetitions – a repetition is defined as one complete motion of the exercise,
- number of sets – a set is defined as a group of repetitions,
- inter-set rest – the duration of rests between two adjacent sets,
- training frequency – the number of training sessions,
- and duration of the training program.

Additionally, the ambiguous terms volume, defined as the sum of repetitions over all sets, or volume load, defined as the sum of load times repetitions over all sets, are often used as variables of RT programs.

However, as Toigo and Boutellier [2006] showed, the classical variables are not sufficient to allow for a unique description. Therefore, further variables are proposed:

- cadence – the temporal distribution of isometric, concentric, and eccentric parts of the motion,
- inter-repetition rest – the duration of rests between repetitions in a set,
- time-under-tension (TUT) – the accumulated contraction time, which can also be calculated from the number of repetitions and cadence,
- muscular failure – whether or not muscular failure was reached during the training session,
- range of motion – usually described by lower and upper bounds on the joint angles,
- inter-session rest – the duration of rests between training sessions,
- and execution of the exercise – the anatomical definition of the exercise.

Not all of these variables are relevant for or applicable to all types of RT. For an isometric RT exercise, for example, only the joint angle (given by the execution of the exercise) and not the range of motion needs to be specified.

Commonly, a variety of exercises is performed by the trainee. Then, possible interactions between the exercises (e.g., working the same muscle group) have to be considered. A combination of their descriptions then yields the full RT program.

5.4 Principles of specificity, progression, and periodization

Three principles are commonly followed when designing RT plans [Fleck and Kraemer, 2014].

First, for RT, the principle of a "specific adaptation to imposed demands (SAID)" applies, which states that results are specific to the RT program employed. Thus, RT has to be individualized to optimize the desired results.

Second, to elicit further adaptations, a continuous increase of stress placed on the body is necessary. This principle is termed progression and can be achieved by various means, e.g., increasing intensity, increasing volume, or decreasing rest.

Third, periodization denotes a planned variation of training variables – most commonly training intensity and volume – with various goals in mind, e.g., to manage fatigue or to avoid overtraining and injury. Periodization can take several forms, e.g., linear with monotonous changes to the training variables for several weeks or nonlinear (also called undulating) with more frequent non-monotonous changes possibly on a daily basis. However, although commonly used in practice, it is still much debated whether or not there are any advantages of non-periodized compared to periodized approaches or in-between the various forms of periodization [Harries et al., 2015; Williams et al., 2017, 2018; Nunes et al., 2018; Grgic et al., 2017, 2018a; Evans, 2019].

Chapter 6

Key performance indicators for loading schemes of isometric resistance training sessions

In this work, we examine loading schemes for isometric resistance training (RT) sessions of a single exercise. Therefore, this chapter provides an overview of key performance indicators (KPIs) for isometric RT sessions based on recommended loading schemes to increase the four trainable characteristics muscle strength, mass, power, and endurance. We follow the recent reviews of Oranchuk et al. [2019] and Lum and Barbosa [2019] if not mentioned otherwise. We assume the exercise and the joint angle to be previously determined.

In our setting, a loading scheme compromises the RT variables intensity, number of repetitions, number of sets, inter-set rest, inter-repetition rest, and duration of the contractions. From these variables, we can furthermore calculate time-under-tension (TUT) and the force-time integral (FTI) defined as the integral of load over time. The FTI is often used as an analogue for physical work during isometric contractions, where no actual work is performed [Rozand et al., 2015]. TUT corresponds to volume in dynamic constant external resistance (DCER) training. FTI corresponds to volume load in DCER training.

The literature on isometric RT is not as comprehensive as on the more commonly used DCER training. Thus, to fill potential gaps and enable comparisons, we also report results for DCER training in the following. For this, we follow the position stand of the American College of Sports Medicine [2009] if not mentioned otherwise.

6.1 Increasing maximum strength

Maximum strength can be defined in various ways. For isometric RT, maximum voluntary isometric contraction (MVIC) force and MVIC torque are commonly used. The equivalent for DCER training used in practice is the one repetition maximum (1RM) – the maximum load which can be lifted for one repetition.

To increase maximum strength, the American College of Sports Medicine [2009] recommends high loads for DCER training, i.e., 60 – 70 % of the 1RM for 8 – 12 repetitions for novice to intermediate trainees and 80 – 100 % of the 1RM for advanced trainees. This advantage of high loads has been confirmed by other authors, e.g., in the meta-analysis of Schoenfeld et al. [2017]. For isometric RT however, Oranchuk et al. [2019] found no benefit of higher contraction intensities in their systematic review. In contrast, Lum and Barbosa [2019] concluded in their narrative review that isometric RT should be performed at 80 – 100 % of

MVIC force with sustained contractions of 1 – 5 s and a total contraction time of 30 – 90 s per sessions to increase maximum strength.

Apart from intensity, RT volume (or volume load) seems to drive strength gains [Grgic et al., 2018b] for DCER training. Similarly, for isometric RT, Lum and Barbosa [2019] postulate that the magnitude of strength gains could be determined by total TUT per training session. TUT can be manipulated by the number of sets, the number of repetitions, and the contraction durations. FTI, the equivalent of volume load, furthermore depends on contraction intensity.

Schott et al. [1995] demonstrated that longer sustained contractions resulted in greater increases of isometric strength. For DCER training, Grgic et al. [2018c] note in their review that rest intervals longer than 2 min might be required to optimize strength development for advanced trainees. Both observations might be based on a higher possible training volume or intensity when using longer rests.

6.2 Increasing muscle mass

Changes in muscle mass can be detected by various methods, e.g., circumference, magnetic resonance imaging, computerized tomography, ultrasound, biopsy, dual energy X-ray absorptiometry, or densitometry [Schoenfeld et al., 2016].

Oranchuk et al. [2019] note in their review that higher training volumes seem to be better for inducing muscle hypertrophy. A similar dose-response relationship has been advocated for DCER by Krieger [2010].

Training intensity does not seem to influence the hypertrophic adaptations for DCER if all sets are performed to momentary muscle failure [Schoenfeld et al., 2017]. Oranchuk et al. [2019] noted similar results for isometric RT if volume is equated. However, Lum and Barbosa [2019] recommend contractions at 70 – 75 % of MVIC force sustained for 3 – 30 s and a total TUT of 80 – 150 s per session.

6.3 Increasing muscle endurance

For DCER training, muscle endurance can be measured by repetitions to failure at a prescribed intensity [Campos et al., 2002]. For isometric RT, endurance times at submaximal intensities are commonly used [Vøllestad, 1997].

To increase muscle endurance in DCER training, the American College of Sports Medicine [2009] recommends light to moderate loads (40 – 60 % of 1RM) for a high number of repetitions (more than 15) and short rests (shorter than 90 s). For advanced trainees, the American College of Sports Medicine [2009] furthermore recommends multiple sets to achieve a higher training volume. For isometric RT, Lum and Barbosa [2019] find that prolonged contractions might be beneficial to increase muscle endurance. Here, submaximal intensities allow a greater TUT.

6.4 Increasing power

In RT, power is commonly measured as the product of force and velocity. Mean and peak power are both of interest for practitioners. According to the American College of Sports Medicine [2009], the neuromuscular contributions to maximum muscle power are the maximum rate of force development (RFD), force production at slow and fast contraction velocities, stretch-shortening cycle performance, and coordination of movement pattern and skill. Assuming a transfer from isometric to dynamic muscle performance, isometric RT can then influence power by increasing maximum force and the maximum RFD. However, such a transfer seems to be limited [Wilson and Murphy, 1996; Oranchuk et al., 2019].

To increase power by DCER training, the American College of Sports Medicine [2009] recommends maximizing strength and light loads (0 – 60 % of 1RM) moved at fast contraction velocities with 3 – 5 min inter-set rest and 3 – 5 sets per exercise. To improve isometric RFD, Oranchuk et al. [2019] find that ballistic or explosive contractions are more beneficial than gradually increasing contraction intensities.

Part III

Results

Chapter 7

General outline of the approach

In this chapter, we present the general outline of our approach and explain the reasons for our choices. In the first section, we discuss necessary prerequisites for a model to be used for an algorithmic optimization of loading schemes. In the second section, we provide an overview of model-based approaches used to simulate or optimize an individual's response to single resistance training (RT) sessions or to long-term RT plans in terms of strength, power, muscle mass, or local muscular endurance by varying the loading scheme. In the third section, we explain how our novel approach allows to work with small amounts of data.

Remark. We emphasize that substantial parts of Herold and Sommer [2020b] have been incorporated into this chapter either with only slight changes or without any changes.

7.1 Prerequisites for a suitable model

To enable a real-life application for practitioners, the model used should fulfill several criteria. First, the inputs and outputs of the model, which correspond to the training plan and training responses of the trainee, have to be interpretable for practitioners. As such, using quantities that reduce the dimensionality of the training input [Toigo and Boutellier, 2006] is not desirable. For example, using only volume load (defined as weight $\times$ number of repetitions $\times$ number of sets) [Bird et al., 2005] to describe the loading scheme of an RT session provides no information about the intensity distribution and is therefore unsuitable. Second, the parameters of the model should be identifiable through commonly available data, e.g., from force measurements, to avoid an overly laborious model calibration. Third, due to the high number of possible training inputs, the model should be suitable for high-dimensional optimization, i.e., for derivative-based optimization (see Part I). Fourth, the model should allow to incorporate real-life constraints into the optimization problem, e.g., days or weeks off [Schaefer et al., 2015]. Last, the model should be assessed for its predictive capability. We classify a model as predictive if it has been fit to a subset of the available data and the resulting parameter estimates can be used to predict the remaining data. We emphasize this, as the terminology is sometimes used differently and models are already classified as predictive if they fit the whole dataset, a property we call descriptive. However, overparameterization or other model deficiencies might diminish the model's capability to predict unknown datasets. Benzekry et al. [2014], for

example, demonstrated this issue illustratively for tumor growth modeling. Furthermore, fit and prediction should be evaluated by suitable measures [Spiess and Neumeyer, 2010] and should not be judged based on the plots alone, as those are heavily depending on the chosen visualization.

7.2 Literature overview

Banister et al. [1975] introduced a model based on the assumption that each training load induces a negative effect (fatigue) and a positive effect (fitness) on performance. As the original paper can not be found easily, we refer to Calvert et al. [1976] for a description of the model. The ordinary differential equation (ODE) model has been adopted for various settings and several modifications have been proposed. The model is commonly known as Banister model or Fitness-Fatigue model and predominantly given in a time-discrete formulation. Busso et al. [1990, 1992] fitted variants of the Banister model to data from Olympic weightlifters. The authors used weighted weekly training volume as input and clean and jerk performance as output and tried to derive correlations between model components and various hormones. However, the predictive capability of the model was not tested, i.e., the whole dataset was used for fitting the model. Model variants were furthermore used by Philippe et al. [2015] to describe the response of rats to resistance training. In a subsequent work, the authors used exponential growth functions for this purpose [Philippe et al., 2019]. In both works, model prediction was not tested.

Mader [1988, 1990] developed an ODE model of the active adaptation and regulation of protein synthesis on a cellular level. The model uses intensity of the functional activity as input and gives protein mass as an indicator of functional capacity as the most important output. The model is able to describe supercompensation as well as overtraining, which is demonstrated by simulating different scenarios. An extended version of the model has been proposed by Ullmer and Mader [1992]. None of the variants were experimentally validated.

Gatti et al. [2008] computed training plans for shoulder rehabilitation by determining the optimal number of sets per exercise for increasing maximum isometric strength given a time constraint. Two different objective functions were examined and compared to current practice. No statements about training intensity were made.

Gacesa et al. [2010] used a nonlinear dynamic system to separately fit fatigue data and muscular growth data of the triceps brachii. The predictive capability of the model was not tested.

Arandjelović [2010] introduced a model of neuromuscular adaption to resistance training. In this model, the so-called capability profile of an athlete is modified depending on the execution of an exercise. The author subsequently used simulations to examine the influence of using fixed loads or accommodating loads on the training stimulus. Furthermore, the author proposed a framework to calibrate the model from video data [Arandjelović, 2013a, 2017]. The model was found

to successfully predict performance in the bench press and the squat. Resistance training can then be adjusted via trial-and-error by inspecting the simulated adaptations. Additionally, Arandjelović used the model to examine training strategies to overcome the sticking point of an arm curl [Arandjelović, 2011], to examine the influence of externally supplied momentum on the hypertrophy stimulus of a shoulder lateral raise [Arandjelović, 2013b], and to examine different loading mechanisms of a Smith machine [Arandjelović, 2012]. Although these three studies are mainly of biomechanical nature, we mention them here, as they specifically aim at increasing force or muscle mass by a model-based examination of possible adaptations.

Wisdom et al. [2015] proposed ODE models of muscle adaptation to chronic overstretch, overload, understretch, and underload and compared those models to experimental data. The predictive capability of the models was not tested. Zhou et al. [2018] used similar dynamics to describe hypertrophy and atrophy of a muscle fiber given as cross-sectional area with muscle activation level as input. After fitting their model to experimental data, the authors simulated muscle atrophy during a spaceflight and how different exercises could serve as countermeasures.

Torres et al. [2017] extended an energy balance model to account for the hypertrophic effects of resistance training and used the model for simulation studies. Moreover, the model was fit to data from elderly subjects following a resistance training routine. Resistance training input is described via a single scaling variable and has no direct interpretation in terms of volume, intensity, or frequency.

Remark. Here, we do not include work that is restricted to the biomechanical analysis of RT exercises, the description of muscular fatigue during RT, or general models of the training-performance relationship without a specific application to RT, as a thorough literature overview including these fields of research is far beyond the scope of this work. However, we would like to mention that substantial work has been done in these fields – either close or synergetic to ours. For example, model-based approaches are stronger established in endurance sports to analyze optimum pacing strategies [Atkinson et al., 2007; Zignoli and Biral, 2020], training strategies [Eriksson et al., 2016], or long-term adaptations [Wood et al., 2005]. Furthermore, as soon as a suitable extension of the model to dynamic movements is available, possible synergies could arise from existing works which analyze and compute optimum movements [Eriksson and Nordmark, 2011; Hatz, 2014]. For the interested reader, we refer to these exemplary works and the references therein.

7.3 Working with small amounts of data

The works presented above do not fulfill all criteria necessary for an algorithmic optimization of loading schemes to be used in practice. In most cases a thorough validation of the model is lacking. Two issues provide the main reasons for this. First, adaptation processes to RT are not fully understood by researchers (see, e.g., the review by Wackerhage et al. [2019] on stimuli and sensors of hypertrophy or

the review of Crewther et al. [2005] on stimuli for strength and power adaptation). Second, data on adaptation processes is only sparsely available, as most studies are based on small sample sizes (see, e.g., the review by Schoenfeld et al. [2016]) and cover only a few weeks of training [Jones et al., 1989]. Additionally, a continuous monitoring of adaptations is often too laborious [Brown et al., 2017] or taxing on the trainees [Zourdos et al., 2016].

Thus, we propose a novel approach. First, we model the varying force capacities of a trainee during a training session depending on the loading scheme. Then, we mathematically formulate key performance indicators and optimality criteria for isometric RT sessions identified in sports science and incorporate these into multi-stage optimal control problems. Based on these problem formulations, we can then optimize the loading schemes.

Chapter 8

Developing a mathematical model of the time course of maximum voluntary isometric contraction force

In this chapter, we describe and validate the proposed ordinary differential equation (ODE) model. In the first section, we discuss our choice of maximum voluntary isometric contraction (MVIC) force as indicator of muscle fatigue. In the second section, we give necessary prerequisites for a model to be used in our approach. In the third section, we provide a literature overview of mathematical and computational models to predict the time course of MVIC force during voluntary isometric contractions. In the fourth section, we demonstrate that a new model is necessary, as existing models suitable for our intentions do not perform satisfactorily. In the fifth section, we present the proposed model. In the sixth section, we validate our model with a comprehensive set of published data. In the seventh section, we discuss our results. In the eighth section, we mentions limitations and future directions for research. In the ninth section, we draw conclusions for this chapter.

Remark. We emphasize that substantial parts of Herold et al. [2018] have been incorporated into this chapter either with only slight changes or without any changes.

8.1 Quantifying muscle fatigue

Muscle fatigue is defined as an exercise-induced reduction in the ability to generate force or power [Gandevia, 2001] and multiple task-specific mechanisms contribute to this complex phenomenon [Enoka and Duchateau, 2008]. These mechanisms are categorized as peripheral (arising distal from the neuromuscular junction) or central (originating at spinal or supraspinal level). For a comprehensive overview of the physiological mechanisms, we refer to the works of Allen et al. [2008] and Gandevia [2001].

Due to this complex nature, several criteria can be used to measure muscle fatigue, e.g. the MVIC force. MVIC force is defined as the force that can be measured during an MVIC effort. To distinguish between peripheral and central contributions, one can furthermore superimpose external stimuli during MVIC efforts either electrically to the nerve trunk or to the muscle belly [Shield and Zhou, 2004], or magnetically to the motor cortex [Todd et al., 2003]. The result-

ing force increment then provides information about the origin of fatigue. Other measurement possibilities are, for example, the maximum voluntary power, the rate of force development, the one-repetition-maximum, or the repetition strength [Brown and Weir, 2001; Vøllestad, 1997; Rodríguez-Rosell et al., 2017].

In this work, we examine muscle fatigue by assessing MVIC force. This is motivated by several reasons. First, MVIC force is considered one of the gold standards for determining muscle fatigue [Vøllestad, 1997], as its measurements are easy to standardize and to conduct. It is therefore used extensively by physiologists and sports scientists. Second, although most everyday movements are of a dynamic nature, isometric contractions contribute to stabilization during those movements [American College of Sports Medicine, 2009]. For this reason, isometric strength capacities and especially their connection to possible injuries are of high interest, e.g. in ergonomics [Keyserling et al., 1980; Granata and Gottipati, 2008] or sports [Leetun et al., 2004]. Third, isometric strength is an important physical characteristic for a variety of athletes, e.g. wrestlers, gymnasts [Tan, 1999], or climbers [Fleck and Kraemer, 2014]. Due to the specificity of adaptations, instead of dynamic exercises, isometric training is favorable for these athletes. Finally, isometric resistance training can be used as part of a rehabilitation program, e.g. when joint movements are restricted or not advisable [Kisner et al., 2017].

To be able to describe MVIC force at any point in time, one modifies its definition to be the force that could theoretically be measured if an MVIC effort were to be conducted. This allows us to discuss the time courses of MVIC force even when there are no actual measurements, i.e. during submaximal contractions and at rest. For a review of these time courses, we refer to the work of Carroll et al. [2017].

Remark. During isometric contractions, force and torque normalized to baseline are equivalent. Thus, we do not differentiate between the two terms in the following.

8.2 Prerequisites for a real-life use of a model

Several mathematical and computational models have been proposed to predict the time course of MVIC force during voluntary isometric contractions (see next section) or the behavior of maximal evocable isometric force under external stimulation. As fatigue is highly task-dependent and substantial differences exist between evoked and voluntary contractions [Maffiuletti, 2010], we do not consider models created for external stimulation for our approach. Furthermore, we assume that all models can be applied at joint level and account for peripheral and central factors contributing to MVIC force generation.

Mathematical optimization problems dealing with the optimal use of MVIC force capacities are inherently high-dimensional, owing to the large number of possible combinations of contraction intensities and durations. Thus, derivative-based methods have to be employed for an efficient solution, which imposes several

mathematical requirements on model candidates.

As a consequence, we put a special focus on the following criteria necessary for our intentions:

1. Can the model predict fatigue of MVIC force at joint level under complex patterns of voluntary isometric contractions, i.e. maximal, submaximal, sustained, and intermittent contractions of varying intensity?

2. Does the model include recovery of MVIC force?

3. Is the model suitable for real-life applications, i.e. is the number of parameters low and are all parameters identifiable through MVIC force measurements?

4. Is the model suitable for high-dimensional optimization, i.e. is the model suitable for derivative-based solution methods?

Many physiology-based models implement a feedback loop with some kind of proportional-integral-derivative controller to imitate force adjustments by the nervous system and match simulated to target force (see Section 8.3). Unfortunately, these closed-loop controllers violate the last criterion as they are usually not suitable for derivative-based optimization methods without considerable effort spent on reformulations. From a mathematical point of view, this is the main obstacle for the use of most existing models. In addition, those models that fulfill the mathematical criteria do not describe the physiological observations satisfactorily (see Section 8.11).

8.3 Literature overview

First attempts to quantify the development of muscle fatigue were made around 1960 by Monod and Scherrer [1957, 1965] and Rohmert [1960], who mathematically described the nonlinear relationship between contraction intensity and endurance time with algebraic equations. Subsequently, several authors proposed similar equations or developed joint-specific versions [El ahrache et al., 2006; Frey-Law and Avin, 2010]. However, these models neither allow to evaluate the time course of MVIC force for more complex contraction scenarios nor do they include recovery.

Fuglevand et al. [1993] constructed a model of recruitment and rate coding of a pool of motor units. As the model does not include fatigue effects, it was later on extended by Dideriksen et al. [2010]. The fatigue-induced changes of the model require a controller to maintain target force. Potvin and Fuglevand [2017] proposed another modification to the original model [Fuglevand et al., 1993], which has yet to be extended to be able to describe force recovery.

Hawkins and Hull [1993] incorporated fatigue effects into a previously developed fiber based model [Hawkins, 1990]. The model does not describe recovery after work and employs an if-else structure to account for the recruitment order of different fiber types.

Based on the work of Rich [1960] and Deeb et al. [1992], Wood et al. [1997] proposed a model and subsequently used it to minimize fatigue during work schedules consisting of intermittent contractions with constant intensities and duty cycles. The least fatiguing setting was found by an exhaustive search through the parameter space. Although their approach pursued a similar goal as this work, the fixed duty cycles impose an undesired limitation on the loading schemes. Similarly, Marina et al. [2014] developed an algebraic equation to describe the force decay during an intermittent handgrip protocol. As the equation needs to be tailored to a specific protocol, it is unsuitable for our purpose as well.

Freund and Takala [2001] constructed a biomechanical model of the forearm and introduced a simple ODE to account for effects of fatigue and recovery. Ma et al. [2009, 2010, 2015] utilized similar dynamics but separated fatigue and recovery, which resulted in a branchwise definition of the ODE's right-hand-side. Riener et al. [1996] modeled the effects of fatigue and recovery for externally stimulated contractions. Although they chose muscle activation as model input, the proposed dynamics are closely related to the ones of Freund and Takala [2001] and Ma et al. [2010], which is why we include it here. Fayazi et al. [2013] based their model on that of Ma et al. [2010], but modeled fatigue and recovery to occur simultaneously as originally proposed by Freund and Takala [2001] for voluntary contractions and by Riener et al. [1996] for stimulated contractions. Fayazi et al. [2013] used their model subsequently to calculate optimal pacing strategies for a cyclist.

Liu et al. [2002] introduced a three-compartment model distinguishing between active, fatigued, and resting motor-units. Fatigue and recovery effects are represented by flows between the compartments and brain effort was chosen as model input. Since brain effort is only known for maximal efforts, the model was later extended by Xia and Law [2008] by including a controller to account for the recruitment hierarchy of three different fiber types when matching the target force. A different modification of the original model [Liu et al., 2002] was implemented by Sih et al. [2012]. The authors expanded the model to four compartments and reformulated their equations to circumvent brain effort as input. In general, this allows the model to simulate arbitrary force profiles. Nevertheless, it is still defined branchwise.

Several authors have extended or modified the model of Xia and Law [2008]. Gede and Hubbard [2014] added a force-velocity dependence and generalized the model to task level. Furthermore, they removed the fast components of the model and changed the input to be the amount of active muscle which makes the model suitable for optimization [Gede, 2014]. However, because of the separate inputs for each fiber type, the model could only be validated for maximal efforts. Other modifications to the original model [Xia and Law, 2008], e.g. using time-variant [Sonne and Potvin, 2016] or contraction-specific [Looft, 2014] parameters, have been developed as well.

James and Green [2012] used a similar approach as Sih et al. [2012] but assumed that contractile properties vary as continuous functions of time and motor unit type. The power output of a single motor unit is defined non-smooth and the model does not account for force recovery. Callahan et al. [2013, 2016] built a

comprehensive model of torque generation. The model can be used to describe voluntary and externally stimulated contractions and uses a controller to match generated to target torque. Contessa and Luca [2013] developed a model focusing on motor units containing a feedback loop implemented to regulate the excitation and match target force.

Only the models proposed by Freund and Takala [2001] and Fayazi et al. [2013] fulfill our requirements and are thus examined further in this work. In Section 8.11.1, we show that these models can not capture the fast and slow dynamics of MVIC force observed in the literature [Carroll et al., 2017]. For this reason, a new model has to be developed.

8.4 Suitable models from the literature

During our literature search, we identified the models proposed by Freund and Takala [2001] and Fayazi et al. [2013] to be suitable for our intentions. Thus, we unify their notation and evaluate their performance by fitting them to a subset of the available data. Due to the later on discussed deficiencies, a new model had to be developed.

8.4.1 Freund and Takala model

Freund and Takala [2001] modeled fatigue and recovery of MVIC force as

$$\frac{\mathrm{d}}{\mathrm{d}t} x_{\mathrm{MVIC}}(t) = p_1(1 - x_{\mathrm{MVIC}}(t)) - p_2 u_{\mathrm{abs}}(t) \tag{8.1a}$$

$$h_{\mathrm{MVIC}}(t) = x_{\mathrm{MVIC}}(t). \tag{8.1b}$$

Here, the state variable

$$x_{\mathrm{MVIC}} : [0, T] \to \mathbb{R} \tag{8.1c}$$

is defined on the time interval $[0, T]$ and is equivalent to the current MVIC force capacity

$$h_{\mathrm{MVIC}}(t) = x_{\mathrm{MVIC}}(t). \tag{8.1d}$$

The absolute external isometric load

$$u_{\mathrm{abs}} : [0, T] \to [0, 1] \tag{8.1e}$$

represents the model input. The fatigue rate $p_2 u_{\mathrm{abs}}(t)$ depends linearly on u_{abs}. The recovery rate $p_1(1 - x_{\mathrm{MVIC}}(t))$ depends linearly on the difference between the current force capacity x_{MVIC} and the maximal force capacity. All states and inputs are normalized to baseline MVIC force and are thus dimensionless. The dimensionless parameters $p_1 \in [0, \infty)$ and $p_2 \in [0, \infty)$ determine the maximal speed of exponential recovery and fatigability of the muscle group. The initial condition

$$x_{\mathrm{MVIC}}(0) = x_0 \in [0, 1] \tag{8.1f}$$

describes the force capacity of the muscle group at $t = 0$. For an unfatigued muscle, one chooses $x_0 = 1$.

8.4.2 Fayazi et al. model

Based on the work of Ma et al. [2010], Fayazi et al. [2013] proposed dynamics similar to those of Freund and Takala [2001]. Keeping the notation introduced earlier, the model is given as as

$$\frac{\mathrm{d}}{\mathrm{d}t}x_{\mathrm{MVIC}}(t) = p_1(1 - x_{\mathrm{MVIC}}(t)) - p_2 u_{\mathrm{abs}}(t) x_{\mathrm{MVIC}}(t) \tag{8.2}$$

$$h_{\mathrm{MVIC}}(t) = x_{\mathrm{MVIC}}(t). \tag{8.3}$$

Thus, the difference to the model of Freund and Takala [2001] is an additional dependency of the fatigue rate on the current MVIC force. In the model of Ma et al. [2010], where fatigue and recovery are modeled separately, this factor ensures a sufficient decrease of fatigability during an MVIC effort.

8.5 Proposed nonlinear ordinary differential equation model

Based on the model of Freund and Takala [2001], we construct a new model given

$$\frac{\mathrm{d}}{\mathrm{d}t}x_{\mathrm{slow}}(t) = p_1(1 - x_{\mathrm{slow}}(t)) - p_2 u_{\mathrm{abs}}(t) \tag{8.4a}$$

$$\frac{\mathrm{d}}{\mathrm{d}t}x_{\mathrm{fast}}(t) = p_3(1 - u_{\mathrm{abs}}(t))^{p_4}(1 - x_{\mathrm{fast}}(t)) - p_5 u_{\mathrm{abs}}(t) \tag{8.4b}$$

$$h_{\mathrm{MVIC}}(t) = x_{\mathrm{slow}}(t) x_{\mathrm{fast}}(t), \tag{8.4c}$$

where

$$x : [0, T] \to \mathbb{R}^2 \tag{8.4d}$$

is defined on the time horizon $[0, T]$ and consists of two state variables x_{fast} and x_{slow}. Again, all states and inputs are normalized to baseline MVIC force and are thus dimensionless. The model furthermore contains five dimensionless parameters $p_j \in [0, \infty)$ for $j \in \{1, \ldots, 5\}$ and one input function

$$u_{\mathrm{abs}} : [0, T] \to [0, 1] \tag{8.4e}$$

representing the absolute external isometric load. The current MVIC force capacity is denoted by

$$h_{\mathrm{MVIC}} : [0, T] \to \mathbb{R} \tag{8.4f}$$

and the initial conditions for the states are given by

$$x(0) = x_0 \in [0, 1]^2. \tag{8.4g}$$

For an unfatigued muscle, one chooses $x_0 = (1, 1)^\top$.

A detailed explanation for choosing this model structure is given in Section 8.11. Table 8.1 summarizes the model components. To increase readability throughout the rest of this work, the arguments of the states and input functions are omitted whenever the dependencies are clear.

Table 8.1: Overview of the model components.

	Type	Interpretation
x_{slow}	State variable	Slow component
x_{fast}	State variable	Fast component
h_{MVIC}	Function	MVIC force
p_1	Parameter	Maximal recovery rate of x_{slow}
p_2	Parameter	Maximal fatigue rate of x_{slow}
p_3	Parameter	Maximal recovery rate of x_{fast}
p_4	Parameter	Influence of u_{abs} on recovery rate of x_{fast}
p_5	Parameter	Maximal fatigue rate of x_{fast}
u_{abs}	Input function	Absolute external load

8.6 Formulating a multi-stage variant of the model

To simulate maximum voluntary isometric contractions efforts, it is favorable to substitute

$$u_{\text{abs}}(t) = u_{\text{rel}}(t) h_{\text{MVIC}}(t) \tag{8.5a}$$

and use

$$u_{\text{rel}} : [0, T] \to [0, 1], \tag{8.5b}$$

the load relative to the current force capacity, as input. This substitution reflects the experimental settings of an MVIC effort, during which subjects are asked to contract maximally ($u_{\text{rel}} = 1$) instead of maintaining a certain target force u_{abs}. It furthermore allows to simulate MVIC efforts without an unnecessarily complex mathematical description of the non-constant input force u_{abs} and is necessary to model MVIC efforts for which no measurement values are given (e.g. in experiment E3a).

However, in contrast to using u_{abs} as input, this substitution only gives a prediction of the absolute external load at a certain level of effort u_{rel} by the model and not the actual absolute external load. Depending on whether the contraction is submaximal or maximal, we either used u_{abs} or u_{rel} to describe the experimental settings in this work.

We interpret this substitution as switching stages of a multi-stage model in order to model scenarios, where absolute and relative external force level are prescribed alternately. If such a switch occurs during an experiment, we denote this change by different right-hand side functions $f_{\text{abs}} : \mathbb{R}^2 \times \mathbb{R} \times \mathbb{R}^5 \to \mathbb{R}^2$ and $f_{\text{rel}} : \mathbb{R}^2 \times \mathbb{R} \times \mathbb{R}^5 \to \mathbb{R}^2$. We thus can summarize the dynamics of the ODE systems above as

$$\begin{aligned} \frac{\mathrm{d}}{\mathrm{d}t} x(t) &= f_{\text{abs}}(x(t), u_{\text{abs}}(t), p) \\ &= \begin{pmatrix} p_1(1 - x_{\text{slow}}(t)) - p_2 u_{\text{abs}}(t) \\ p_3(1 - u_{\text{abs}}(t))^{p_4}(1 - x_{\text{fast}}(t)) - p_5 u_{\text{abs}}(t) \end{pmatrix} \end{aligned} \tag{8.6a}$$

or

$$\begin{aligned}\frac{\mathrm{d}}{\mathrm{d}t}x(t) &= f_{\mathrm{rel}}(x(t), u_{\mathrm{rel}}(t), p) \\ &= \begin{pmatrix} p_1(1 - x_{\mathrm{slow}}(t)) - p_2 u_{\mathrm{rel}}(t) h_{\mathrm{MVIC}}(t) \\ p_3(1 - u_{\mathrm{rel}}(t) h_{\mathrm{MVIC}}(t))^{p_4}(1 - x_{\mathrm{fast}}(t)) - p_5 u_{\mathrm{rel}}(t) h_{\mathrm{MVIC}}(t) \end{pmatrix} \end{aligned} \tag{8.6b}$$

depending on the input function and right-hand side used. The transition of the states between the model stages is continuous. Note that during rest periods u_{rel} and u_{abs} are zero and thus both right-hand sides are identical

$$\begin{aligned}\frac{\mathrm{d}}{\mathrm{d}t}x(t) &= f_{\mathrm{rel}}(x(t), 0, p) \\ &= f_{\mathrm{abs}}(x(t), 0, p) \\ &= \begin{pmatrix} p_1(1 - x_{\mathrm{slow}}(t)) \\ p_3(1 - x_{\mathrm{fast}}(t)) \end{pmatrix}. \end{aligned} \tag{8.6c}$$

Remark. For most scenarios treated in this thesis, it is sufficient to choose one of the two stages. This choice is apparent from the the problem formulations and from the plots depicting either u_{abs} or u_{rel} as input. Scenarios where both stages are used are explicitly highlighted in the caption of the plots and can be furthermore distinguished by depicting both input functions u_{abs} and u_{rel}.

8.7 Available data

We use the mean values from several experiments examining muscle fatigue and recovery of the elbow flexors to evaluate the performance of the models under consideration. This is necessary, as to the best of our knowledge no study examined time courses of MVIC force for the same muscle group of a single subject under different loading schemes.

Data of the following experiments is used:

E1 Taylor et al. [1999] examined a 2 min MVIC effort and a recovery period lasting roughly 7 min for 8 subjects. Up to 30 MVIC force measurements are given per subject.

E2 Søgaard et al. [2006] examined a submaximal contraction at 15 % of baseline MVIC force lasting 43 min and 23 min of recovery for 9 subjects. 29 MVIC force measurements are given per subject.

E3a Taylor et al. [2000] examined intermittent MVIC efforts of 5 s contraction and 5 s rest and a 2 min recovery period for 9 subjects. Up to 18 MVIC force measurements are given per subject.

E3b Taylor et al. [2000] examined intermittent MVIC efforts of 15 s contraction and 10 s rest and a 4 min recovery period for 9 subjects. Up to 30 MVIC force measurements are given per subject.

E3c Taylor et al. [2000] examined intermittent MVIC efforts of 15 s contraction and 5 s rest and a 4 min recovery period for 8 subjects. Up to 30 MVIC force measurements are given per subject.

E3d Taylor et al. [2000] examined intermittent MVIC efforts of 30 s contraction and 5 s rest and a 3 min recovery period for 9 subjects. Up to 17 MVIC force measurements are given per subject.

E4 Gandevia et al. [1996] examined a 2 min MVIC effort and a subsequent 3 min recovery period for 8 subjects. 13 mean MVIC force values and standard errors of the means were extracted from the figures with the software Engauge Digitizer 10.0 [Mitchell et al.].

E5 Smith et al. [2007] examined a 70 min submaximal contraction at 5 % of baseline MVIC force and the following 29 min of recovery for 8 subjects. 52 MVIC force measurements are given per subject. As the measurement times are only given for one subject, we used those for the whole sample.

All experiments employed a similar setup (i.e. elbow flexed to 90 degrees, forearm vertical and supinated [Taylor et al., 1999; Søgaard et al., 2006; Taylor et al., 2000; Gandevia et al., 1996; Smith et al., 2007]), which justifies a comparison of these values. To the best of our knowledge, this is the most comprehensive set of data used to validate a model of the time course of MVIC force.

For each experiment $k \in \{\text{E1, E2, E3a, E3b, E3c, E3d, E4, E5}\}$, we use the mean values

$$\eta_l^k = \frac{1}{n^k} \sum_{i=1}^{n^k} \eta_{l,i}^k \tag{8.7}$$

of the n^k individual measurements $\eta_{l,i}^k$ to validate our model. The measurement errors ε_l^k are assumed to be additive, independent, and identically normally distributed with mean zero and standard deviation σ_l^k. We take σ_l^k to be the corrected sample standard deviation (SD) of the corresponding mean value η_l^k divided by the square root of the sample size n^k, i.e.

$$\sigma_l^k = \sqrt{\frac{1}{n^k(n^k-1)} \sum_{i=1}^{n^k} (\eta_{l,i}^k - \eta_l^k)^2}. \tag{8.8}$$

Thus, σ_k^l yields an approximation of the standard error of the mean. For experiment E4, the means and the corresponding standard errors were extracted directly from the figures. The test contractions interspersed during submaximal contractions and recovery are described to last 1 – 2 s [Taylor et al., 2000] or 2 – 3 s [Søgaard et al., 2006]. Therefore, we model those contractions to last 2 s.

8.8 Multi-experiment parameter estimation problems

We evaluate the models under consideration by fitting them to a subset of the available data. If a model performs satisfactorily, we furthermore validate it by using the calibrated model to predict the remaining data. As data of the available single experiments is not sufficient for a reliable model calibration, we formulate a multi-experiment parameter estimation problem:

$$\min_{p,x^{k,i}(\cdot)} \quad \frac{1}{2}\sum_{k\in K}\sum_{i=1}^{n_s^k}\sum_{j=1}^{n_m^{k,i}}\left(\frac{h_j^{k,i}(t_j^{k,i},x^{k,i}(t_j^{k,i}),p)-\eta_j^{k,i}}{\sigma_j^{k,i}}\right)^2 \tag{8.9a}$$

$$\text{s.t. for} \quad k\in K:$$

$$x^{k,1}(0)=x_0^{k,1} \tag{8.9b}$$

$$\text{and for} \quad k\in K \text{ and } i\in\{1,\dots,n_s^k-1\}:$$

$$x^{k,i+1}(0)=x^{k,i}(T^{k,i}) \tag{8.9c}$$

$$\text{and for} \quad k\in K,\ i\in S_{\text{abs}}^k, \text{ and } t\in[0,T^{k,i}]:$$

$$\frac{\mathrm{d}}{\mathrm{d}t}x^{k,i}(t)=f_{\text{abs}}^{k,i}(x^{k,i}(t),u_{\text{abs}}^{k,i}(t),p) \tag{8.9d}$$

$$\text{and for} \quad k\in K,\ i\in S_{\text{rel}}^k, \text{ and } t\in[0,T^{k,i}]:$$

$$\frac{\mathrm{d}}{\mathrm{d}t}x^{k,i}(t)=f_{\text{rel}}^{k,i}(x^{k,i}(t),u_{\text{rel}}^{k,i}(t),p). \tag{8.9e}$$

Here, the calibration set $K\subset\{\text{E1, E2, E3a, E3b, E3c, E3d, E4, E5}\}$ contains the experiments which are used for fitting the model. Furthermore, the sets S_{abs}^k and S_{rel}^k consist of the stages of experiment k which use either u_{abs} or u_{rel} as input (see Section 8.6).

To evaluate the models of Freund and Takala [2001] and Fayazi et al. [2013], we fit these models simultaneously to the data of E1 and E2. This subset is chosen as it contains a sustained maximal and a sustained submaximal contraction. To evaluate the proposed model, we furthermore add the data of E3a and E3c. This subset is chosen as it contains a sustained maximal, a sustained submaximal, and two intermittent maximal contractions and enables an identification of the parameters. The data of the remaining four experiments E3b, E3d, E4, and E5 is then used to test the predictive capability of the calibrated model.

8.9 Numerical solution via direct multiple shooting

To ensure a practical benefit of our approach, not only mathematical problem formulations but also the numerical solution methods need to be tailored to the real-life application. As we aim to calibrate the model for different trainees and muscle groups, an efficient and reliable solution is necessary. Therefore, we use specialized methods, which exploit the properties of the problems.

The optimization problem constrained by an ODE system (8.9) is solved by employing a first-discretize-then-optimize strategy. We use a direct multiple shooting approach to reduce the problem to a finite-dimensional form (see Bock [1987]). We employ three shooting nodes per experiment and use piecewise constant controls. We use DAESOL [Bauer, 1999] for integration of the ODE and sensitivity generation via internal numerical differentiation [Bock, 1981]. Relative and absolute integration tolerances are set to 10^{-8} and 10^{-7}. Maximum order is set to 6. Maximum step size is set to 1. The necessary derivatives of the model functions are computed via automatic differentiation with ADIFOR [Bischof et al., 1998]. The resulting structured nonlinear least-squares problem is solved with PAREMERA [Kircheis, 2015], an implementation of the reduced generalized Gauss-Newton method [Bock, 1987; Schlöder, 1988]. Termination criteria for PAREMERA is chosen to be $\epsilon = 10^{-3}$. Both packages are embedded in the optimum experimental design software VPLAN [Körkel, 2002].

Exemplarily, we give the dimensions of the PE problem used below to calibrate the proposed model. Several reformulations are necessary. With 35 to 91 control intervals and 18 to 30 shooting intervals per experiment, the resulting nonlinear program (NLP) has 221 variables and 208 equality constraints.

8.10 Numerical results

Remark. To increase readability, the plots in this thesis depict the (piecewise constant) input functions as continuous lines without markers. We emphasize that the thus resulting vertical lines do not bear any mathematical interpretation, but are merely included for visualization purposes.

8.10.1 Evaluation of suitable models from the literature

Figures 8.1 and 8.2 and Figures 8.3 and 8.4 illustrate the results of fitting each of the models of Freund and Takala [2001] and Fayazi et al. [2013] simultaneously to the data of E1 and E2. Table 8.2 lists the resulting parameter estimates and their estimated relative standard deviations for both models. The estimated common factor b^2 [Bock, 1987] for those fits is 7.45 for the model of Freund and Takala [2001] and 7.82 for the model of Fayazi et al. [2013]. Table 8.3 lists the mean absolute errors (MAE) and weighted residual sum of squares (WRSS) of both fits.

Table 8.2: Parameter estimates and their estimated relative standard deviations obtained by fitting the models of Freund and Takala [2001] and Fayazi et al. [2013] simultaneously to the data of E1 and E2. The common factors of these fits are estimated to be 7.45 and 7.82.

	p_1	± SD	p_2	± SD
Freund and Takala [2001]	$9.20 \cdot 10^{-3}$	± 3.75 %	$1.53 \cdot 10^{-2}$	± 3.56 %
Fayazi et al. [2013]	$8.66 \cdot 10^{-3}$	± 4.90 %	$2.24 \cdot 10^{-2}$	± 4.98 %

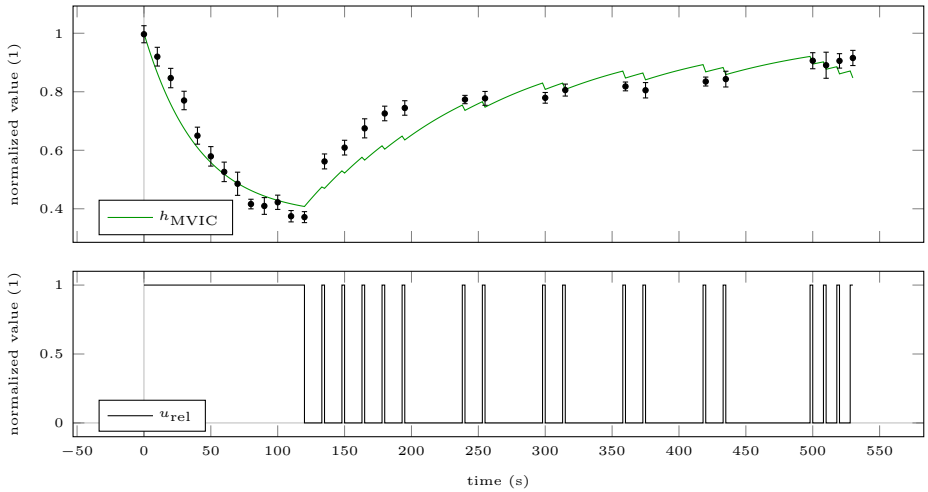

Figure 8.1: Model response obtained by fitting the model of Freund and Takala [2001] simultaneously to the data of E1 (shown here) and E2. The top row shows the mean values of the experiments plotted against the model response for the experimental setting. The error bars represent the standard errors of the means. Additionally, the relative force input is illustrated in the bottom row.

Table 8.3: Mean absolute errors and weighted residual sum of squares obtained by fitting the models of Freund and Takala [2001] and Fayazi et al. [2013] simultaneously to the data of E1 and E2.

	E1		E2	
	MAE	WRSS	MAE	WRSS
Freund and Takala [2001]	0.04	151.07	0.10	273.72
Fayazi et al. [2013]	0.05	210.97	0.09	234.80

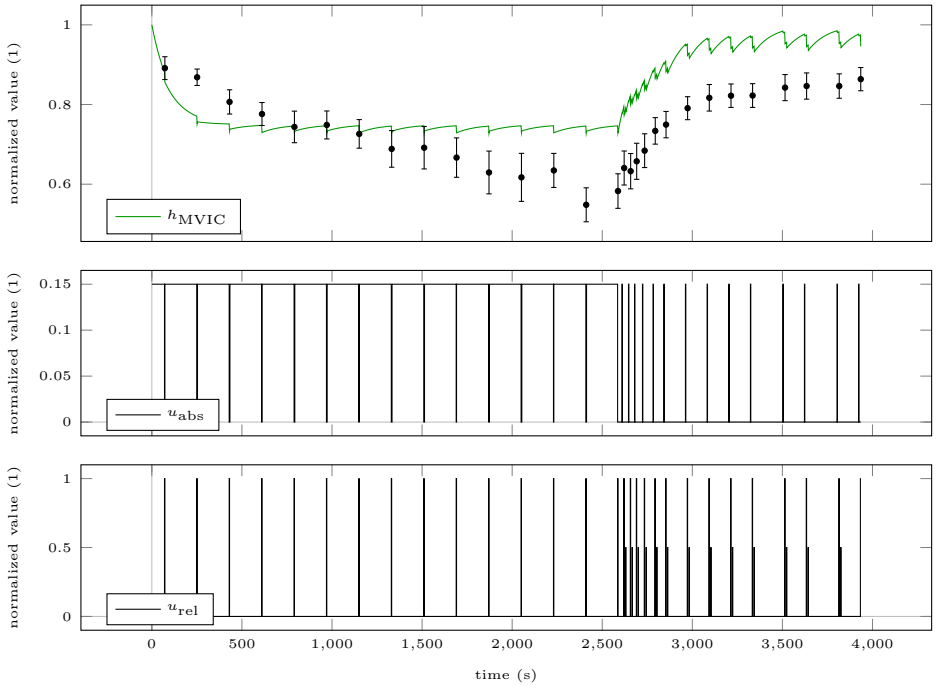

Figure 8.2: Model response obtained by fitting the model of Freund and Takala [2001] simultaneously to the data of E1 and E2 (shown here). The top row shows the mean values of the experiments plotted against the model response for the experimental setting. The error bars represent the standard errors of the means. Additionally, the absolute force input is illustrated in the middle row and the relative force input is illustrated in the bottom row. Note that these two input functions result from using the multi-stage formulation of the model as described in Section 8.6.

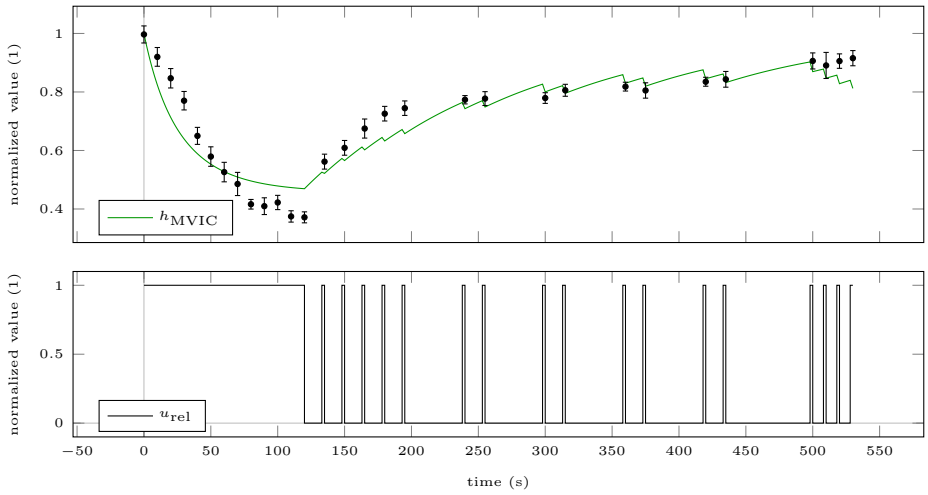

Figure 8.3: Model response obtained by fitting the model of Fayazi et al. [2013] simultaneously to the data of E1 (shown here) and E2. The top row shows the mean values of the experiments plotted against the model response for the experimental setting. The error bars represent the standard errors of the means. Additionally, the relative force input is illustrated in the bottom row.

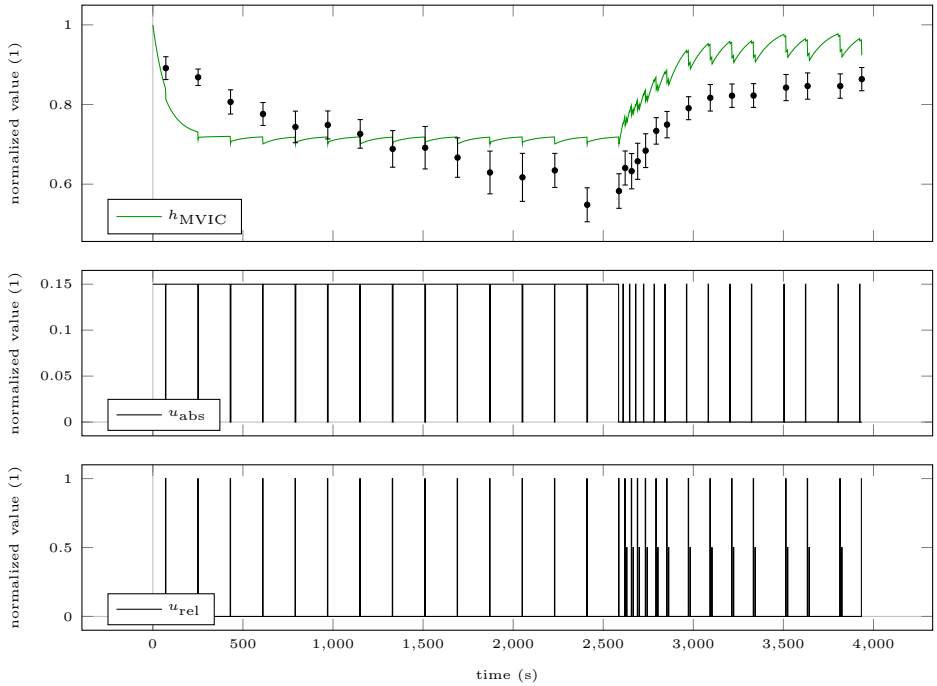

Figure 8.4: Model response obtained by fitting the model of Fayazi et al. [2013] simultaneously to the data of E1 and E2 (shown here). The top row shows the mean values of the experiments plotted against the model response for the experimental setting. The error bars represent the standard errors of the means. Additionally, the absolute force input is illustrated in the middle row and the relative force input is illustrated in the bottom row. Note that these two input functions result from using the multi-stage formulation of the model as described in Section 8.6.

8.10.2 Evaluation of proposed model

Figures 8.5, 8.6, 8.7, and 8.8 depict the results of fitting the proposed model simultaneously to the data of E1, E2, E3a, and E3c. Table 8.4 lists the resulting parameter estimates and their estimated relative standard deviations. The estimated common factor b^2 [Bock, 1987] for this fit is 1.87. Table 8.5 lists the mean absolute errors and weighted residual sum of squares of the fit.

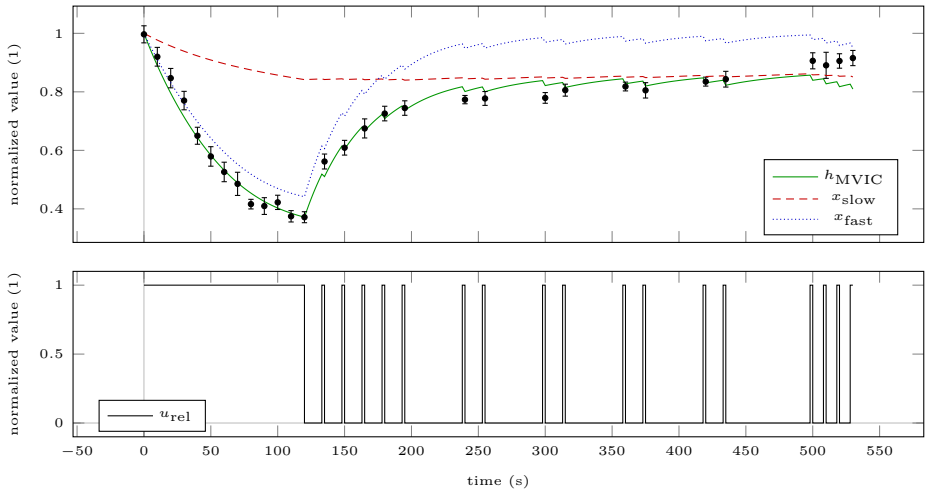

Figure 8.5: Model response obtained by fitting the proposed model simultaneously to the data of E1 (shown here), E2, E3a, and E3c. The top row shows the mean values of the experiments plotted against the model response for the experimental setting. The error bars represent the standard errors of the means. Additionally, the relative force input is illustrated in the bottom row.

Table 8.4: Parameter estimates and their estimated relative standard deviations obtained by fitting the proposed model simultaneously to the data of E1, E2, E3a, and E3c. The common factor for this fit is estimated to be 1.87.

	Interpretation	Estimate	± SD
p_1	Maximal recovery rate of x_{slow}	$1.20 \cdot 10^{-3}$	± 7.23 %
p_2	Maximal fatigue rate of x_{slow}	$2.46 \cdot 10^{-3}$	± 6.04 %
p_3	Maximal recovery rate of x_{fast}	$2.85 \cdot 10^{-2}$	± 6.44 %
p_4	Influence of u_{abs} on recovery rate of x_{fast}	3.99	± 11.84 %
p_5	Maximal fatigue rate of x_{fast}	$9.44 \cdot 10^{-3}$	± 2.99 %

Figures 8.9, 8.10, 8.11, and 8.12 illustrate the prediction of the calibrated model

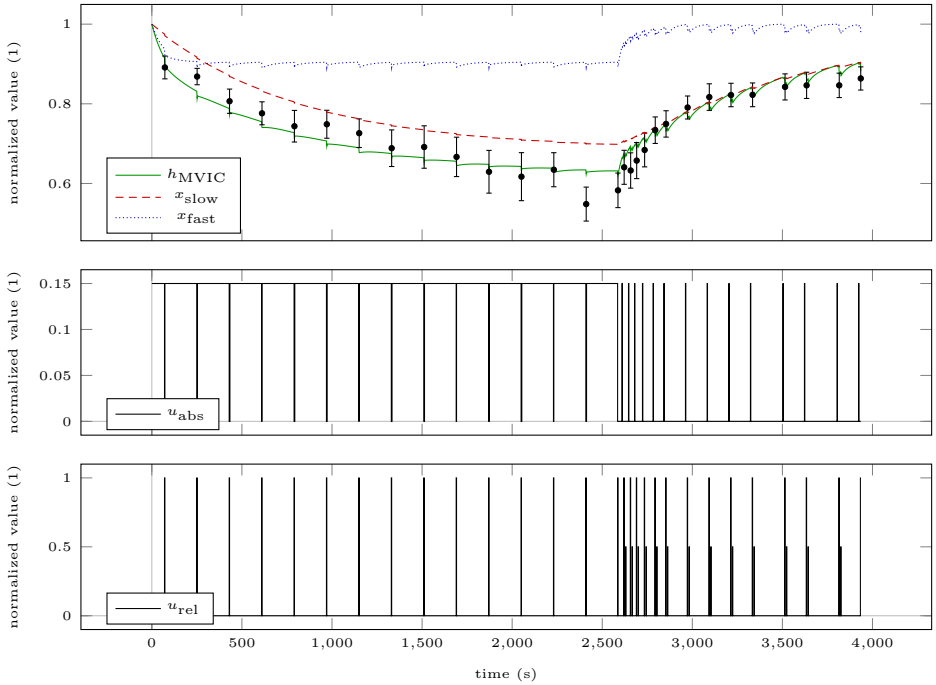

Figure 8.6: Model response obtained by fitting the proposed model simultaneously to the data of E1, E2 (shown here), E3a, and E3c. The top top row shows the mean values of the experiments plotted against the model response for the experimental setting. The error bars represent the standard errors of the means. Additionally, the absolute force input is illustrated in the middle row and the relative force input is illustrated in the bottom row. Note that these two input functions result from using the multi-stage formulation of the model as described in Section 8.6.

Table 8.5: Mean absolute errors and weighted residual sum of squares obtained by fitting the proposed model simultaneously to the data of E1, E2, E3a, and E3c.

	E1	E2	E3a	E3c
MAE	0.03	0.03	0.02	0.03
WRSS	66.68	25.82	17.17	80.83

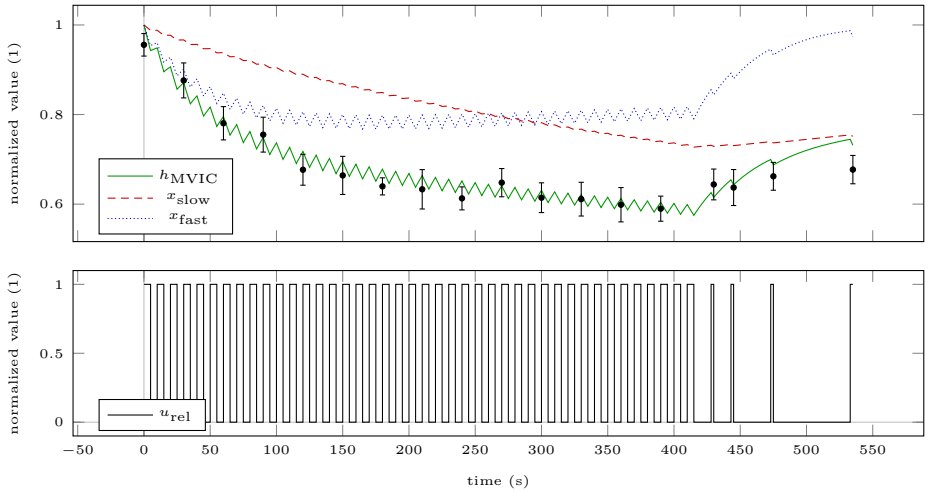

Figure 8.7: Model response obtained by fitting the proposed model simultaneously to the data of E1, E2, E3a (shown here), and E3c. The top row shows the mean values of the experiments plotted against the model response for the experimental setting. The error bars represent the standard errors of the means. Additionally, the relative force input is illustrated in the bottom row.

for the remaining four experiments E3b, E3d, E4, and E5. Table 8.6 lists the mean absolute errors and weighted residual sum of squares of the predictions.

Table 8.6: Mean absolute errors and weighted residual sum of squares obtained by using the calibrated model to predict the data of E3b, E3d, E4, and E5.

	E3b	E3d	E4	E5
MAE	0.04	0.03	0.03	0.03
WRSS	47.53	37.86	15.28	41.00

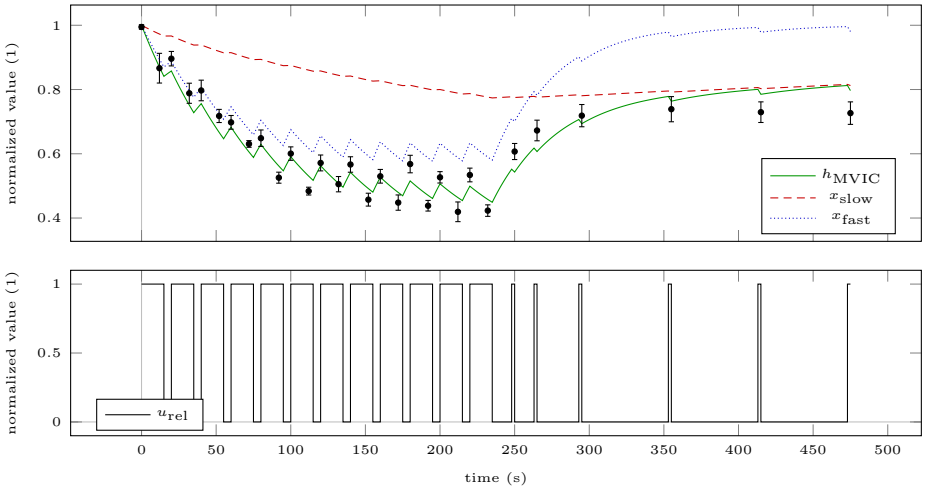

Figure 8.8: Model response obtained by fitting the proposed model simultaneously to the data of E1, E2, E3a, and E3c (shown here). The top row shows the mean values of the experiments plotted against the model response for the experimental setting. The error bars represent the standard errors of the means. Additionally, the relative force input is illustrated in the bottom row.

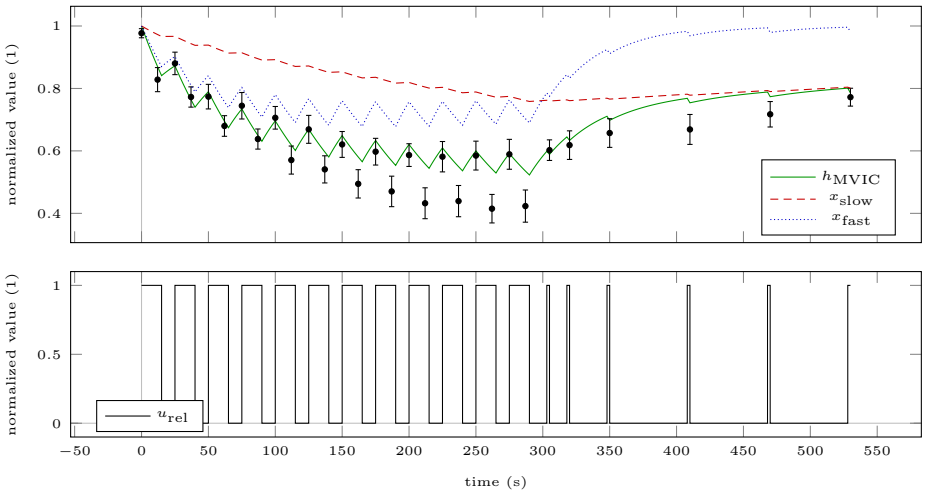

Figure 8.9: Model response obtained by simulating the calibrated model for the experimental settings of E3b. The top row shows the mean values of the experiments plotted against the model response for the experimental setting. The error bars represent the standard errors of the means. Additionally, the relative force input is illustrated in the bottom row.

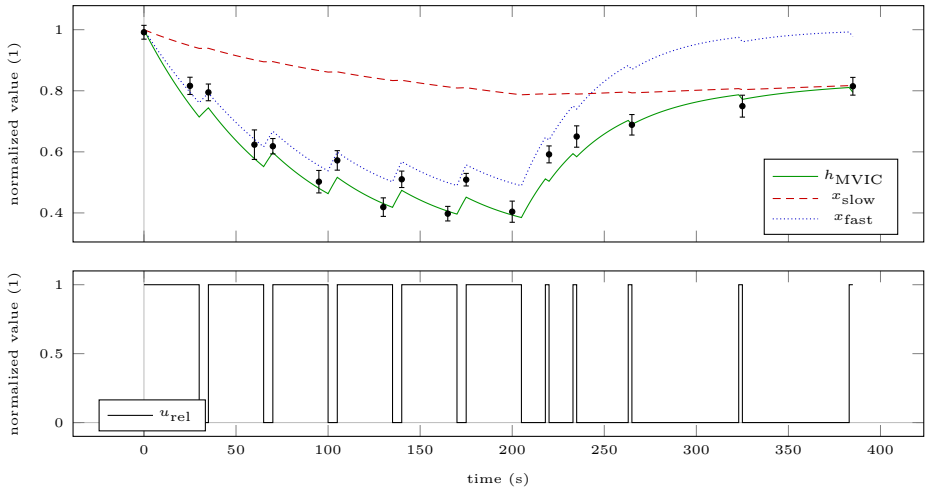

Figure 8.10: Model response obtained by simulating the calibrated model for the experimental settings of E3d. The top row shows the mean values of the experiments plotted against the model response for the experimental setting. The error bars represent the standard errors of the means. Additionally, the relative force input is illustrated in the bottom row.

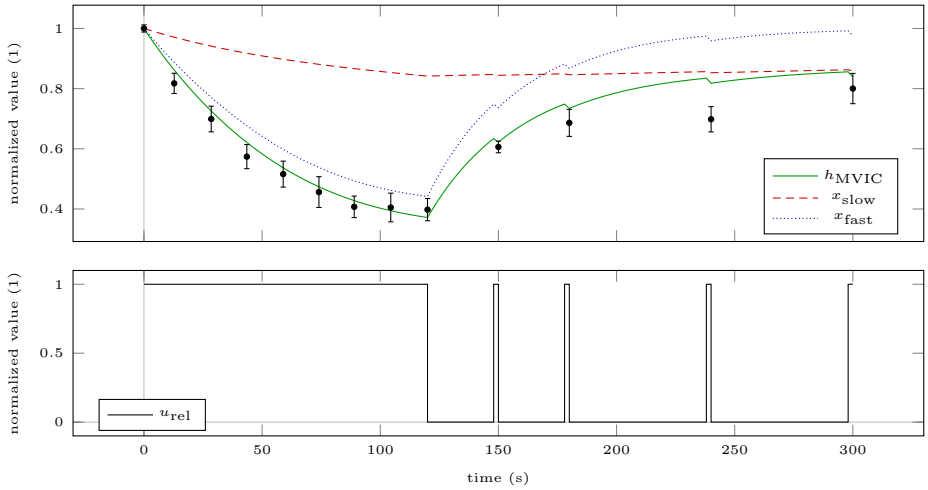

Figure 8.11: Model response obtained by simulating the calibrated model for the experimental settings of E4. The top row shows the mean values of the experiments plotted against the model response for the experimental setting. The error bars represent the standard errors of the means. Additionally, the relative force input is illustrated in the bottom row.

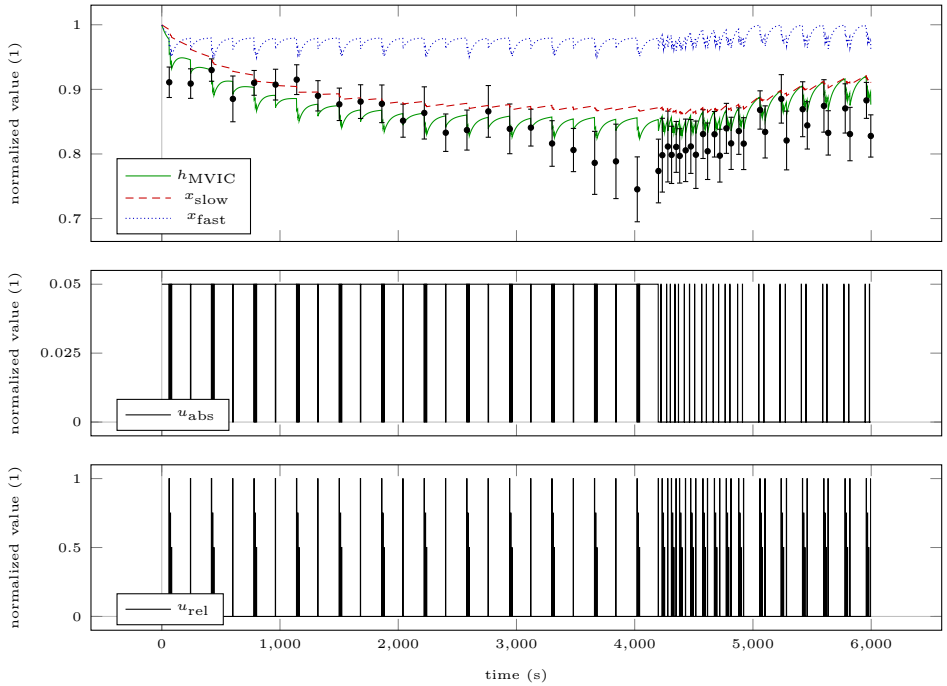

Figure 8.12: Model response obtained by simulating the calibrated model for the experimental settings of E5. The top row shows the mean values of the experiments plotted against the model response for the experimental setting. The error bars represent the standard errors of the means. Additionally, the absolute force input is illustrated in the middle row and the relative force input is illustrated in the bottom row. Note that these two input functions result from using the multi-stage formulation of the model as described in Section 8.6.

8.10.3 Information criteria for model selection

To analyze whether the performance of our proposed model outweighs the increased complexity, we compute the Akaike information criterion (AIC) and the AIC_c – a variant of the AIC adjusted to small sample sizes – for the fit of the three presented models to the data of the experiments E1 and E2. The AIC and the AIC_c are chosen since we are comparing unnested models. As we are only interested in comparing AIC and AIC_c between the models, we compute these quantities as

$$\mathrm{AIC} = n_m \ln(\mathrm{WRSS}) + 2n_p \tag{8.10}$$

and

$$\mathrm{AIC}_c = \mathrm{AIC} + \frac{2n_p(n_p+1)}{n_m - n_p - 1} \tag{8.11}$$

for our weighted nonlinear least-squares fit [Burnham and Anderson, 2002]. Here, n_m denotes the number of measurements, WRSS denotes the weighted residual sum of squares, and n_p denotes the number of parameters.

Table 8.7 shows the results. The minimum value indicates the preferred model. Note that the proposed model was actually fit simultaneously to the data of experiments E1, E2, E3a, and E3c compared to the models of Freund and Takala [2001] and Fayazi et al. [2013], which were fit simultaneously only to the data of experiments E1 and E2.

Table 8.7: AIC and AIC_c values for the fits of the three presented models to the data of experiments E1 and E2. The minimum value indicates the model to be preferred.

	Freund and Takala [2001]	Fayazi et al. [2013]	Proposed model
AIC	361.04	359.89	32.64
AIC_c	361.26	360.10	33.77

8.10.4 Cross-validation

To evaluate whether our results depend on the chosen subsets of the data, we cross-validate by repeating the above process for possible combinations without repetition which separate the data set into calibration and prediction set consisting of 4 experiments each.

To allow an identification of all parameters, we need to ensure that experiment E2 is part of the calibration set, as its data contains more valuable information on a submaximal contraction than the data of experiment E5. Furthermore, due to inconsistencies of the data of experiment E3b (see the discussion in Section 8.11), we always keep experiment E3b as part of the prediction set. This leaves 30 possible combinations to evaluate.

Table 8.8 and Figure 8.13 summarize the results of the cross-validation.

Table 8.8: Results of the cross-validation with 30 different combinations of calibration and prediction sets. The table gives the minimum (min), maximum (max), and median estimate of the parameters p_i and the weighted residual sum of squares (WRSS). The last column additionally gives the standard deviations (SD) normalized to the values obtained in Section 8.10.2.

	min	max	median	relative SD
p_1	$8.63 \cdot 10^{-4}$	$1.23 \cdot 10^{-3}$	$1.10 \cdot 10^{-3}$	10.60 %
p_2	$1.80 \cdot 10^{-3}$	$2.53 \cdot 10^{-3}$	$2.33 \cdot 10^{-3}$	9.69 %
p_3	$1.89 \cdot 10^{-2}$	$3.40 \cdot 10^{-2}$	$2.75 \cdot 10^{-2}$	12.89 %
p_4	1.95	4.34	3.59	17.00 %
p_5	$8.92 \cdot 10^{-3}$	$1.06 \cdot 10^{-2}$	$9.43 \cdot 10^{-3}$	3.95 %
WRSS	329.44	417.92	341.54	7.62 %

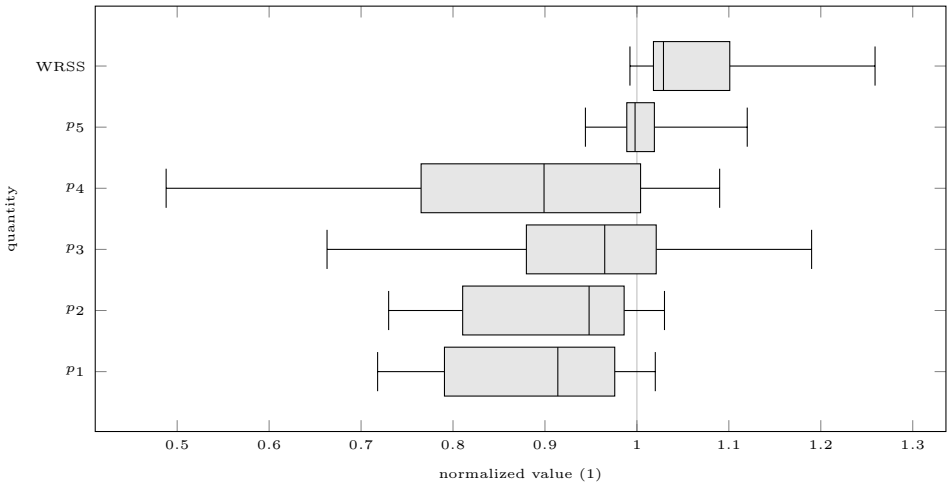

Figure 8.13: Results of the cross-validation with 30 different combinations of calibration and prediction sets. To visualize the deviations, the parameter estimates p_i and the WRSS are normalized to the values obtained in Section 8.10.2. The whiskers illustrate the minimum and maximum value. The boundaries of the box illustrate the first and the third quartiles. The line inside the box illustrates the median.

8.11 Discussion

8.11.1 Evaluation of suitable models from the literature

When evaluating the fits for the models of Freund and Takala [2001] and Fayazi et al. [2013] to the data of E1 and E2, the necessity of a new model becomes clear. The model of Freund and Takala [2001] captures the fatigue development during the MVIC effort of E1 correctly, whereas the model of Fayazi et al. [2013] underestimates it slightly. This is caused by combining the fatigue and recovery branches of Ma et al. [2010] linearly. Both models overestimate fatigue in the beginning of the submaximal contraction E2 and reach a steady-state too early. Furthermore, due to their mono-exponential recovery terms, they can not capture the initially faster recovery after cessation of the contractions.

8.11.2 Structure of the proposed model

Carroll et al. [2017] summarized the properties of the time courses of MVIC force during and after MVIC efforts and submaximal contractions as follows. During an MVIC effort, MVIC force usually drops below 50 % of baseline within 1 – 2 min. In the first 15 – 30 s after the contraction, MVIC force recovers quickly but only partially. Afterwards, recovery slows down, so that MVIC force reaches around 80 % of baseline after 4 – 5 min. During submaximal contractions, interspersed MVIC efforts reveal a slow decline of MVIC force depending on the contraction duration and intensity of the submaximal contraction. During the first minutes after the contraction, MVIC force recovers quickly but only partially. Further recovery depends on the duration and intensity of the preceding contraction as well and might take longer than 30 min.

From a mathematical point of view, this history dependence of recovery required a more complex model structure than that of Freund and Takala [2001] or of Fayazi et al. [2013]. Since no input is given to the model during recovery, information about the preceding contractions had to be either stored in the state variables or different branches for maximal or submaximal contractions had to be developed. As our focus was to keep the model suitable for derivative-based optimization methods, a branchwise definition was undesirable. Consequently, we duplicated the dynamics of Freund and Takala [2001] and modeled MVIC force as the product of two state variables x_{slow} and x_{fast}. The product was chosen to represent the chain of mechanisms leading to force generation. Yet, since this chain includes complex feedforward and feedback mechanisms, the strict separation is obviously an oversimplification. The choice of the product is furthermore supported by other authors who proposed using double-exponential functions to describe the time courses of fatigue [Deeb et al., 1992] and recovery [Clarke, 1962]. The inclusion of a second state enables the model to describe different time courses of recovery after contractions that decrease MVIC force to the same level (see for example Figures 9.3 and 9.4), while keeping the model structure suitable for our purpose.

The processes summarized in x_{slow} play a bigger role in contractions of long duration or repeated intermittent ones, as this state fatigues much slower and

takes longer to recover. Correlations to the Ca^{2+} sensitivity of the crossbrigdes, to the Ca^{2+} release of the sarcoplasmic reticulum [Allen et al., 2008], and to glycogen depletion [Sahlin et al., 1998] are likely. Furthermore, there is also a long lasting effect of reduced voluntary activation after prolonged contractions, the reason for which is currently unknown [Carroll et al., 2017].

x_{fast} pools a variety of mechanisms responsible for a quick onset of MVIC force reduction and a fast recovery. These mechanisms contribute to a larger degree during maximal and near maximal contractions and seem to be closely related to muscle perfusion [Carroll et al., 2017]. Possible factors include metabolite accumulation (e.g. inorganic phosphate) [Allen et al., 2008], firing of group III and IV afferents [Taylor et al., 2016], or energy deficiency [Sahlin et al., 1998]. Since studies have established a link between blood occlusion in the muscle (either through high-intensity contractions or artificially) and impeded recovery [Bigland-Ritchie et al., 1986; Kennedy et al., 2013], we added a dependency of the recovery rate on $(1 - u_{\text{abs}})^{p_4}$. The exponent p_4 determines the contraction intensity at which total occlusion occurs [Barnes, 1980; Sadamoto et al., 1983]. A similar dependency on activation was proposed by Riener et al. [1996] in the context of external stimulation. However, they assumed a linear relationship.

8.11.3 Validation of the proposed model

The fit of the proposed model to the data of the experiments E1 and E2 was improved substantially compared to the models of Freund and Takala [2001] and Fayazi et al. [2013]. Besides by visually inspecting the plots, this can also be seen by comparing the mean average errors and weighted residual sum of squares given in Table 8.3 and Table 8.5. Although more data was used for the entire fit of the proposed model, the MAE and the WRSS calculated for the experiments E1 and E2 were smaller than those obtained by fitting the models of Freund and Takala [2001] and Fayazi et al. [2013]. This was to be expected, as the proposed model employs five instead of two parameters. Yet, since all parameters could be estimated reasonably well, the model is not overparameterized and an experiment-wise comparison is justified. Our model is able to capture submaximal contractions, the initial fast recovery after cessation of a contraction, and the delayed recovery after prolonged contractions.

Due to the phenomenological nature of the model, most of the estimated parameter values do not allow a direct physiological interpretation. Nevertheless, we expect physiological characteristics like fiber type composition, capillarization, buffering capacity, muscle mass and strength, energy stores, and others to be reflected in the dimensionless parameter estimates. An inter-individual comparison of the estimates from the same muscle group or an intra-individual comparison of those from different muscle groups might provide interesting physiological insights. However, to evaluate this hypothesis, more data is needed.

Since the term $(1 - u_{\text{abs}})^{p_4}$ was specifically introduced to mimic blood occlusion during intense contractions, we compared the estimate of p_4 to the values given in literature. Sadamoto et al. [1983] determined that at a contraction intensity of

53 % of baseline MVIC force, muscle blood flow in the biceps was arrested. For the external load $u_{\text{abs}} = 0.53$, the estimated exponent $p_4 = 3.99$ would imply roughly 5 % of the induced blood flow reaching the elbow flexors and providing some kind of recovery. As we are not only considering the biceps but all elbow flexors, and as Barnes [1980] found a strength-dependency of the intensity necessary for total occlusion, this value seems to be consistent with the literature.

Using the estimated parameters, the model is able to predict the data of E3d, E4, and E5 satisfactorily. Nevertheless, it shows unexpected deficiencies when simulating experiment E3b. Namely, it can not capture the increasing fatigability of the subjects during the experiment. The exact reasons are unknown. However, this increasing fatigability can not be observed during the other experiments of Taylor et al. [2000]. Furthermore, this increase actually contradicts the size principle [Henneman et al., 1965] according to which primarily fatigue-resistant fibers should be used as the protocol progresses. Thus, fatigability should decrease during each contraction and a steady-state should be reached, as can be seen in the other experiments. Since this experiment additionally shows the largest inter-subject variability compared to other experiments from the study by Taylor et al. [2000], we suppose that motivational issues of some subjects were the cause of this phenomenon. We argue similarly concerning the force drops during the submaximal contractions E2 and E5 shortly before the end of the contraction, which are not captured by the model.

8.12 Limitations and future work

Currently, several aspects require further research before the model can be applied in the context of dynamic contractions, individual athletes, and different training goals.

To validate our model, we used the mean values of several experiments. This was necessary, as to the best of our knowledge no study examined time courses of MVIC force for the same muscle group of a single subject under different loading schemes. However, this implies that our work suffers the same drawbacks as all studies in physiology and sports sciences inferring conclusions from mean values. The observed fatigue and recovery patterns of the sample mean could be artifacts of data aggregation [Neyroud et al., 2016] and individual patterns could differ from the mean [Marina et al., 2014]. Thus, further research with data of individual subjects and other muscle groups has to be performed. To facilitate the necessary data acquisition, optimal experiments should be designed. We refer to Chapter 12 for details. Additional data might furthermore allow a more detailed physiological modeling, e.g. separating different fiber types or distinguishing between central and peripheral contributions.

The proposed model was specifically designed and validated for isometric contractions. We strongly discourage its use in combination with dynamic contractions without a thorough validation, as several phenomena which are not described by the model arise during concentric or eccentric contractions. These include,

among others, different fatigue and recovery patterns for specific contraction modes [Linnamo et al., 2000], force enhancement or force depression after preceding dynamic contractions [Herzog, 2004; Kosterina et al., 2012], or dependence of fatigue on joint angle [Place et al., 2005] and angular joint velocity [Morel et al., 2015]. Incorporating these effects into the model and validating these extensions is subject of future work.

To realize the full potential of the new model, suitable optimal control problems have to be developed and solved, e.g. to minimize the risk for work-related injuries or to maximize the benefits of resistance training. For the latter, current recommendations from the sports sciences about 'optimal' training with respect to maximizing strength, hypertrophy, power, or local muscular endurance have to be formulated mathematically (see Section 10). Currently, our model does not incorporate the concept of task failure [Enoka and Duchateau, 2008] except when MVIC force falls below target force. However, as Neyroud et al. [2013] and others have shown, task failure can occur even before this threshold is reached. Thus, to optimize training sessions in which other reasons for task failure than a lack of MVIC force may arise, a prediction of endurance time has to be incorporated into the model.

As soon as an extension of the model to dynamic contractions is given, the model and the suggested optimal control problems could be implemented into existing works on the optimization of dynamic movements. Eriksson [2008] and coworkers [Eriksson and Nordmark, 2011], for example, computed optimal movements for different cost functions with joint torques, muscle tensions, or neural stimulation as inputs. A combination of such works and ours could result in optimal training plans for the more commonly used dynamic constant external resistance training [Fleck and Kraemer, 2014].

8.13 Conclusion

Based on the model of Freund and Takala [2001], we developed a predictive ODE model of the time course of MVIC force which accounts for the fast and slow dynamics observed during fatiguing contractions and subsequent recovery [Carroll et al., 2017]. The model was validated with a comprehensive set of published data from the elbow flexors [Gandevia et al., 1996; Taylor et al., 1999, 2000; Søgaard et al., 2006; Smith et al., 2007] and shows promising results.

A special focus of this work was to keep the model suitable for derivative-based optimization methods. The newly developed model can readily be employed to optimize complex loading schemes, e.g. work shifts or resistance training plans (see Section 10). Our work allows to compare the influence of loading schemes on different muscle groups and individual subjects, once suitable data becomes available.

Chapter 9

Analyzing the time course of maximum voluntary isometric contraction force

In this chapter, we use the calibrated model to examine two observations from the literature regarding the fatigue and recovery patterns of maximum voluntary isometric contraction (MVIC) force. Since the model was validated with contraction intensities of 15 % of MVIC force and MVIC efforts, we use those for our simulations. In the first section, we describe the simulated scenarios – the influence of the force-time integral (FTI) on fatigue and the task-dependency of MVIC force recovery. In the second section, we present our results. In the third section, we discuss our results. In the fourth section, we draw conclusions for this chapter.

Remark. We emphasize that substantial parts of Herold et al. [2018] have been incorporated into this chapter either with only slight changes or without any changes.

9.1 Simulated scenarios

Rozand et al. [2015] observed that after sustained isometric contractions of the knee extensors with different intensities and similar force-time integral the induced level of fatigue did not differ. The FTI on the time interval $[0, T]$ is defined as

$$x_{\mathrm{FTI}} \stackrel{\mathrm{def}}{=} \int_0^T u_{\mathrm{abs}}(t)\mathrm{d}t \tag{9.1}$$

and often used as an analogue for work during isometric contractions, where no actual physical work is performed. To examine this observation with the calibrated model, we simulate a 60 s MVIC effort and a submaximal contraction at 15 % of baseline MVIC force lasting 292.40 s with the same FTI of 43.86.

Rashedi and Nussbaum [2017] observed that recovery was fatigue- and not task-dependent for intermittent isometric contractions of the index finger. Iguchi et al. [2008] noticed similar dependencies after sustained isometric contractions of the quadriceps. To examine this observation with the calibrated model, we simulate a 40 s MVIC effort and a submaximal contraction at 15 % of baseline MVIC force lasting 2310 s. Both contractions reduce MVIC force to 64.41 % of baseline and are followed by a 10 min recovery period.

9.2 Numerical results

Figures 9.1 and 9.2 show the model response obtained by simulating the calibrated model for a 60 s MVIC effort and a submaximal contraction at 15 % of baseline MVIC force lasting 292.40 s with the same FTI of 43.86. Both contractions end before a steady-state is reached. After the maximal contraction, MVIC force is reduced to 53.21 %. In contrast to this, MVIC force is reduced to 82.37 % after the submaximal contraction.

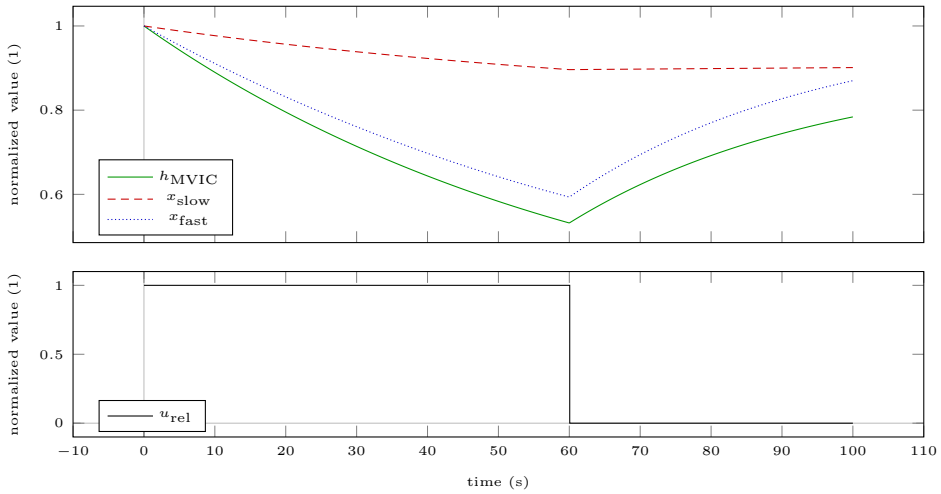

Figure 9.1: Model response obtained by simulating the calibrated model for an MVIC effort (shown here) and for a submaximal contraction with the same force-time integral. The top row shows the model response and the relative force input is illustrated in the bottom row.

Figures 9.3 and 9.4 shows the model response obtained by simulating the calibrated model for a 40 s MVIC effort and a submaximal contraction at 15 % of baseline MVIC force lasting 2310 s both reducing MVIC force to 64.41 % of baseline. Both contractions end before a steady-state is reached. At the end of the maximal scenario, MVIC force recovers to 96.25 %. In contrast to this, MVIC force recovers to 85.97 % at the end of the submaximal scenario.

9.3 Discussion

In the scenario motivated by Rozand et al. [2015], the induced fatigue is higher for the maximal contraction than for the submaximal contraction. We therefore can not reproduce their results for our settings.

In the scenario motivated by Rashedi and Nussbaum [2017], recovery from the MVIC effort is almost complete after 10 min, whereas recovery from the submax-

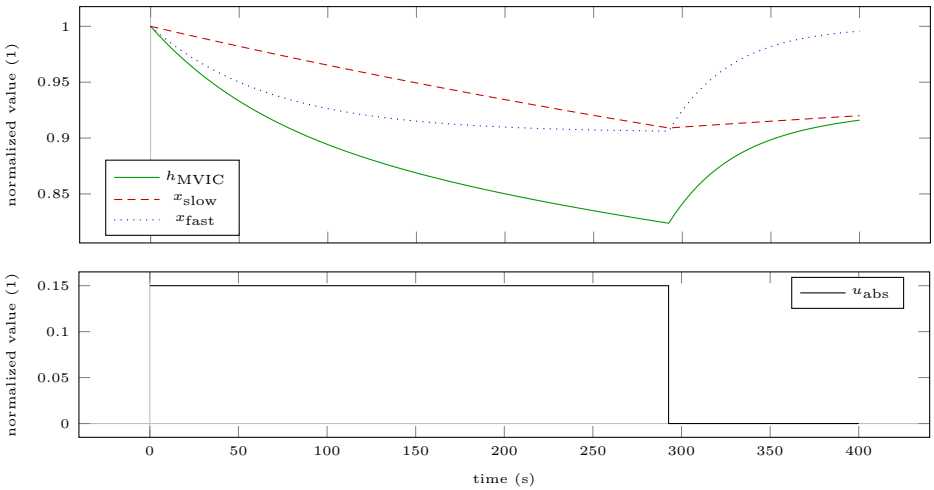

Figure 9.2: Model response obtained by simulating the calibrated model for an MVIC effort and for a submaximal contraction (shown here) with the same force-time integral. The top row shows the model response and the absolute force input is illustrated in the bottom row.

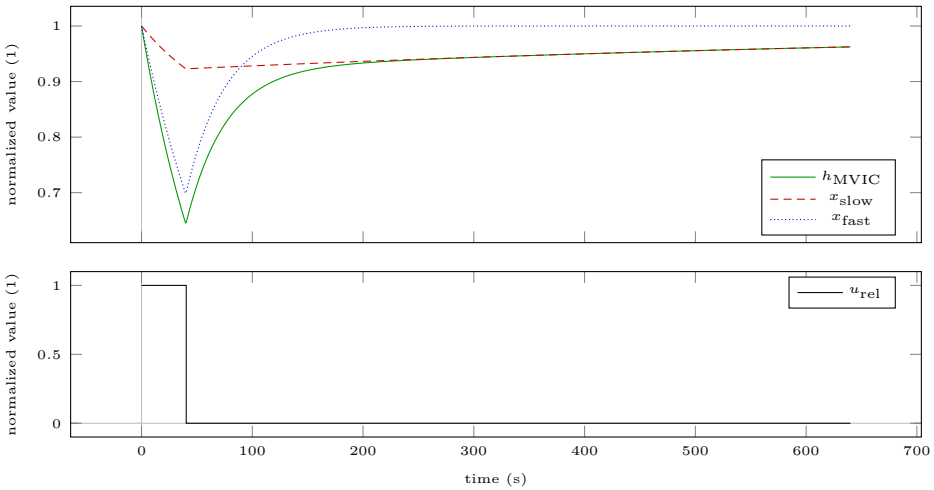

Figure 9.3: Model response obtained by simulating the calibrated model for an MVIC effort (shown here) and for a submaximal contraction inducing the same level of fatigue followed by 10 min of recovery. The top row shows the model response and the relative force input is illustrated in the bottom row. Recovery from the MVIC effort is almost complete after 10 min.

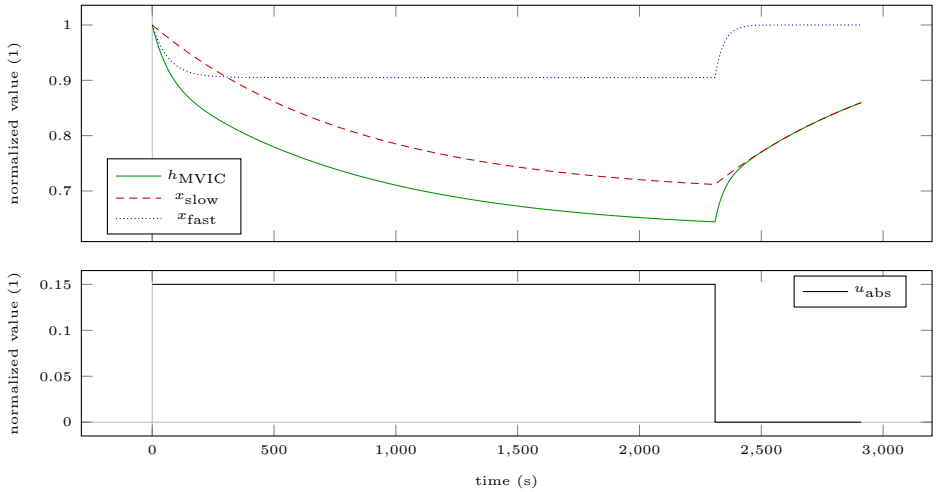

Figure 9.4: Model response obtained by simulating the calibrated model for an MVIC effort and for a submaximal contraction (shown here) inducing the same level of fatigue followed by 10 min of recovery. The top row shows the model response and the absolute force input is illustrated in the bottom row. Recovery from the submaximal contraction takes longer than 10 min.

imal contraction takes much longer. Thus, we can not reproduce their results for our settings either.

9.4 Conclusion

According to our simulations, it is therefore not advisable to plan loading schemes based on a generalization of either of these observations. Furthermore, these simulations emphasize the history dependence of fatigue and recovery patterns, which could become even more complex following dynamic contractions [Herzog, 2004; Kosterina et al., 2012]. Therefore, a good state estimation is crucial when working with muscles that have been active recently.

Chapter 10

Optimizing loading schemes for different training goals

In this chapter, we compute optimized loading schemes for different training goals. In the first section, we formulate the corresponding optimal control (OC) problems. In the second section, we describe the numerical solution of these problems. In the third section, we discuss the simulated scenarios. In the fourth section, we present our results. In the fifth section, we discuss our results. In the sixth section, we mention limitations and future work. In the seventh section, we give conclusions for this chapter.

Remark. We emphasize that substantial parts of Herold and Sommer [2020b] have been incorporated into this chapter either with only slight changes or without any changes.

10.1 Multi-stage optimal control problems

We use a multi-stage formulation on $n_s \geq 2$ stages – denoted by superscripts $i \in \{1, \dots, n_s\}$ – to model the resistance training sessions. To include metrics for the time-under-tension (TUT), the force-time-integral (FTI), and the accumulated fatigue, we extend the model by three states tracking these quantities $x_{\mathrm{TUT}}, x_{\mathrm{FTI}}$, and x_{fatigue}. The general multi-stage optimal control problem can then be formulated as

$$\max_{x^i(\cdot), u^i_{\mathrm{abs}}(\cdot), T^i} \quad \Phi(x^{n_s}(T^{n_s})) \tag{10.1a}$$

$$\text{s.t.} \quad x^1(0) = (1, 1, 0, 0, 0)^\top \tag{10.1b}$$

$$x^i(0) = x^{i-1}(T^{i-1}) \text{ for } i \in \{2, \dots, n_s\} \tag{10.1c}$$

$$\sum_{i=1}^{n_s} T^i = C_T \tag{10.1d}$$

$$x^{n_s}_{\mathrm{TUT}}(T^{n_s}) \leq C_{\mathrm{TUT}} \tag{10.1e}$$

$$x^{n_s}_{\mathrm{FTI}}(T^{n_s}) \leq C_{\mathrm{FTI}} \tag{10.1f}$$

$$\text{and for} \quad i \in \{1, 3, \dots, n_s - 2, n_s\} \text{ and } t \in [0, T^i]:$$

$$\frac{\mathrm{d}}{\mathrm{d}t} x^i{}_{\mathrm{slow}}(t) = p_1(1 - x^i_{\mathrm{slow}}(t)) - p_2 u^i_{\mathrm{abs}}(t) \tag{10.1g}$$

$$\frac{\mathrm{d}}{\mathrm{d}t}x^i{}_{\mathrm{fast}}(t) = p_3(1-u^i_{\mathrm{abs}}(t))^{p_4}(1-x^i_{\mathrm{fast}}(t)) - p_5 u^i_{\mathrm{abs}}(t) \tag{10.1h}$$

$$\frac{\mathrm{d}}{\mathrm{d}t}x^i{}_{\mathrm{FTI}}(t) = u^i_{\mathrm{abs}}(t) \tag{10.1i}$$

$$\frac{\mathrm{d}}{\mathrm{d}t}x^i{}_{\mathrm{TUT}}(t) = \begin{cases} 0 & \text{if } u^i_{\mathrm{abs}}(t) = 0 \\ 1 & \text{else} \end{cases} \tag{10.1j}$$

$$\frac{\mathrm{d}}{\mathrm{d}t}x^i{}_{\mathrm{fatigue}}(t) = 1 - h^i_{\mathrm{MVIC}}(t) \tag{10.1k}$$

$$u_{\mathrm{low}} \le u^i_{\mathrm{abs}}(t) \le h^i_{\mathrm{MVIC}}(t) \tag{10.1l}$$

and for $i \in \{2, 4, \ldots, n_s - 3, n_s - 1\}$ and $t \in [0, T^i]$:

$$\frac{\mathrm{d}}{\mathrm{d}t}x^i{}_{\mathrm{slow}}(t) = p_1(1-x^i_{\mathrm{slow}}(t)) \tag{10.1m}$$

$$\frac{\mathrm{d}}{\mathrm{d}t}x^i{}_{\mathrm{fast}}(t) = p_3(1-x^i_{\mathrm{fast}}(t)) \tag{10.1n}$$

$$\frac{\mathrm{d}}{\mathrm{d}t}x^i{}_{\mathrm{FTI}}(t) = 0 \tag{10.1o}$$

$$\frac{\mathrm{d}}{\mathrm{d}t}x^i{}_{\mathrm{TUT}}(t) = 0 \tag{10.1p}$$

$$\frac{\mathrm{d}}{\mathrm{d}t}x^i{}_{\mathrm{fatigue}}(t) = 0, \tag{10.1q}$$

with C_T being the total time and C_{TUT} and C_{FTI} the upper bounds on the total time-under-tension and the force-time integral. As described in Section 8.5, $h_{\mathrm{MVIC}} = x_{\mathrm{slow}}x_{\mathrm{fast}}$ describes the current maximum voluntary isometric contraction (MVIC) force. During odd numbered stages contractions with $u_{\mathrm{low}} \le u_{\mathrm{abs}}$ are possible. Even numbered stages are considered rest periods. The duration T^i of each stage is being optimized. We develop specific versions of this general optimal control problem in the following. If not mentioned otherwise, all sessions last 20 min, allow for $n_c = 25$ possible contractions, and have no restrictions on FTI or TUT. This implies $C_T = 1200$ s, $n_s = 49$ and neglecting Constraints (10.1e) and (10.1f). Table 10.1 gives an overview of the symbols used in the problem formulation.

10.2 Numerical solution via direct multiple shooting

As in Section 8.9, we need specialized methods to provide efficient and flexible solutions for different trainees and training goals.

To solve the problems numerically, we employ a first-discretize-then-optimize strategy. We use the optimal control software MUSCOD-II [Leineweber et al., 2003a,b], which originates from the work of Bock and Plitt [1984] and implements a direct multiple shooting approach. We employ four shooting nodes per stage and use piecewise constant controls. This discretization reflects the training reality and allows a direct interpretation of the solution for practitioners. Stage lengths are

Table 10.1: Overview of symbols used in the multi-stage OC problem (10.1).

Symbol	Interpretation
C_T	Total time
C_{FTI}	Upper bound on total FTI
C_{TUT}	Upper bound on total TUT
h^i_{MVIC}	MVIC force
i	Stage index
x^i_{TUT}	Time-under-tension
x^i_{FTI}	Force-time integral
x^i_{fatigue}	Accumulated fatigue
n_s	Number of stages
p_j	Parameters
Φ	Objective functional
t	Time
T^i	Stage duration
u^i_{abs}	External force
u_{low}	Lower bound on u_{abs}
x^i_{fast}	State variable
x^i_{slow}	State variable

initialized to be 5 s for contractions and 45 s for rests. The control u_{abs} is initialized to 0.8 when applicable. Furthermore, to approximately fulfill $u_{\mathrm{abs}} \leq h_{\mathrm{MVIC}}$ on the whole shooting interval and not only at the shooting node, we replace Constraint (10.1l) by the two constraints

$$u_{\mathrm{low}} \leq u^i_{\mathrm{abs}}(t) \tag{10.2a}$$

and

$$u^i_{\mathrm{abs}}(t) \leq h^i_{\mathrm{MVIC}}(t) + \frac{T^i}{4}\frac{\mathrm{d}}{\mathrm{d}t}h^i_{\mathrm{MVIC}}(t). \tag{10.2b}$$

The latter constraint includes a prediction of h_{MVIC} at the end of the shooting interval based on a linear extrapolation. We use a Runge-Kutta-Fehlberg integrator of order 4 with an error estimator of order 5 for integration of the ordinary differential equation (ODE) and sensitivity generation via internal numerical differentiation [Bock, 1981]. Integration tolerance is set to 10^{-8}. The necessary derivatives of the model functions are provided by finite difference approximations. The resulting nonlinear program (NLP) is then solved by a structure-exploiting trust-region sequential quadratic programming method with limited memory Broyden-Fletcher-Goldfarb-Shanno (BFGS) block updates of the Hessian. The termination criterion is set to a Karush-Kuhn-Tucker (KKT) tolerance of 10^{-6}.

Exemplarily, we give the dimensions of OC problem 'K' treated below. With 50 model stages and 4 shooting intervals on each stage, the resulting structured NLP has 1155 variables, 1001 equality constraints, and 2410 inequality constraints.

10.3 Optimized scenarios

In the following, we develop specific versions of the general optimal control problem (10.1) to model different real-life training sessions (labeled Session A to K). We refer to Tables 10.2 and 10.3 for a concise overview.

Table 10.2: Overview of sessions used in this work. If not mentioned otherwise, all sessions last 20 min and allow 25 possible contractions.

Session	Explanation	Objective	Constraints	Modified equations
FTI-based				
A	Maximize FTI	$\Phi(x) = x_{\mathrm{FTI}}$	$u_{\mathrm{low}} = 0$	-
$B_{70\%}$	Maximize FTI while ensuring a minimum threshold intensity	$\Phi(x) = x_{\mathrm{FTI}}$	$u_{\mathrm{low}} = 0.7$	-
$B_{90\%}$	Maximize FTI while ensuring a minimum threshold intensity	$\Phi(x) = x_{\mathrm{FTI}}$	$u_{\mathrm{low}} = 0.9$	-
C	Maximize FTI accumulated above a minimum threshold intensity	$\Phi(x) = x_{\mathrm{FTI}}$	$u_{\mathrm{low}} = 0$	$\frac{\mathrm{d}}{\mathrm{d}t} x^i{}_{\mathrm{FTI}}(t) = u^i_{\mathrm{abs}}(t) - 0.8$
D_5	Maximize FTI while ensuring a minimum threshold intensity with 5 possible contractions	$\Phi(x) = x_{\mathrm{FTI}}$	$u_{\mathrm{low}} = 0.8$	-
D_{50}	Maximize FTI while ensuring a minimum threshold intensity with 50 possible contractions	$\Phi(x) = x_{\mathrm{FTI}}$	$u_{\mathrm{low}} = 0.8$	-
E	Maximize a weighted version of FTI	$\Phi(x) = x_{\mathrm{FTI}}$	$u_{\mathrm{low}} = 0$	$\frac{\mathrm{d}}{\mathrm{d}t} x^i{}_{\mathrm{FTI}}(t) = (u^i_{\mathrm{abs}}(t))^2$
F	Maximize a weighted version of FTI	$\Phi(x) = x_{\mathrm{FTI}}$	$u_{\mathrm{low}} = 0.8$	$\frac{\mathrm{d}}{\mathrm{d}t} x^i{}_{\mathrm{FTI}}(t) = (u^i_{\mathrm{abs}}(t) - 0.8)^2$

Table 10.3: Overview of sessions used in this work. If not mentioned otherwise, all sessions last 20 min and allow 25 possible contractions.

Session	Explanation	Objective	Constraints	Modified equations
Fatigue-based				
G	Maximize fatigue	$\Phi(x) = x_{\text{fatigue}}$	$u_{\text{low}} = 0$	-
H	Maximize fatigue while ensuring a minimum threshold intensity	$\Phi(x) = x_{\text{fatigue}}$	$u_{\text{low}} = 0.8$	-
I	Minimize fatigue to reach a certain FTI	$\Phi(x) = -x_{\text{fatigue}}$	$u_{\text{low}} = 0$ $C_{\text{FTI}} = 150$	-
TUT-based				
J	Maximize TUT while ensuring a minimum threshold intensity	$\Phi(x) = x_{\text{TUT}}$	$u_{\text{low}} = 0.8$	-
K	Maximize a weighted version of TUT	$\Phi(x) = x_{\text{TUT}}$	$u_{\text{low}} = 0.8$	$\frac{\mathrm{d}}{\mathrm{d}t} x^i{}_{\text{TUT}}(t) = \begin{cases} 0 & \text{if } u^i_{\text{abs}}(t) = 0 \\ t & \text{else} \end{cases}$

10.3.1 FTI-based goals

Resistance training volume is an important determinant of long-term adaptations [Fleck and Kraemer, 2014]. For isometric contractions, where no actual physical work is performed, the force-time integral is an often used analogue of work [Rozand et al., 2015]. Thus, for Session A, we maximize the FTI accumulated during an RT session without imposing restrictions on the contraction intensity, i.e., $\Phi(x) = x_{\mathrm{FTI}}$ and $u_{\mathrm{low}} = 0$.

To increase maximum strength, high loads are recommended by some researchers, e.g., by the American College of Sports Medicine [2009]. Therefore, we compute an RT session, which maximizes the FTI and ensures that the contraction intensity is higher than a minimum threshold intensity. We examine how choosing a minimum threshold intensity of 70 % and 90 % of baseline MVIC force influences the solution. For Session $\mathrm{B}_{70\%}$, we set $\Phi(x) = x_{\mathrm{FTI}}$ and $u_{\mathrm{low}} = 0.7$. For Session $\mathrm{B}_{90\%}$, we set $\Phi(x) = x_{\mathrm{FTI}}$ and $u_{\mathrm{low}} = 0.9$.

As an alternative to the full FTI maximized in Session A, one can use the FTI accumulated above the minimum threshold intensity as an indicator of effective training volume. For Session C, we thus set $u_{\mathrm{low}} = 0$ and replace Equation (10.1i) with

$$\frac{\mathrm{d}}{\mathrm{d}t} x^i{}_{\mathrm{FTI}}(t) = u^i_{\mathrm{abs}}(t) - 0.8. \tag{10.3}$$

A similar measure has been used by Burnley [2009] when examining work capacity above critical torque.

For Session D, we examine the influence of the number of possible contractions on Session B and compute the solution for $n_c \in \{5, 6, \ldots, 49, 50\}$ possible contractions. This allows to investigate if more but expectedly shorter contractions allow to accumulate a higher FTI while ensuring a minimum threshold intensity of $u_{\mathrm{low}} = 0.8$ and if the additional possible contractions are actually realized in the solution.

Instead of choosing a minimum threshold intensity, we can emphasize higher loads by evaluating a weighting function on the integrand of the FTI. For demonstration purposes, we choose a quadratic weighting function for Session E. Therefore, we set $\Phi(x) = x_{\mathrm{FTI}}$ and replace Equation (10.1i) with

$$\frac{\mathrm{d}}{\mathrm{d}t} x^i{}_{\mathrm{FTI}}(t) = (u^i_{\mathrm{abs}}(t))^2. \tag{10.4}$$

u_{low} is set to 0. A similar approach has been used by Arandjelović [2013b] to describe the hypertrophy stimulus of a resistance training set, although he used a sigmoid function, which can be interpreted as a smoothing of the constraint $u_{\mathrm{low}} \leq u_{\mathrm{abs}}$ used in Session B.

A similar weighting can be applied to Session C by replacing Equation (10.1i) with

$$\frac{\mathrm{d}}{\mathrm{d}t} x^i{}_{\mathrm{FTI}}(t) = (u^i_{\mathrm{abs}}(t) - 0.8)^2 \tag{10.5}$$

and setting the objective functional to $\Phi(x) = x_{\mathrm{FTI}}$ for Session F. In contrast to Session C, $u_{\mathrm{low}} = 0.8$ is necessary here, as otherwise $u_{\mathrm{abs}} = 0$ would be the solution.

10.3.2 Fatigue-based goals

Effects of fatigue, e.g., metabolic stress or increased motor unit recruitment, have been attributed to trigger and/or positively influence muscle hypertrophy [Schoenfeld, 2010]. We examine which loading scheme maximizes fatigue, defined as the accumulated loss of MVIC force over time. Thus, for Session G, we choose $\Phi(x) = x_{\text{fatigue}}$ and $u_{\text{low}} = 0$.

For Session H, we maximize fatigue while ensuring a minimum threshold intensity of 80 % of baseline MVIC force. Therefore, we choose $\Phi(x) = x_{\text{fatigue}}$ and $u_{\text{low}} = 0.8$.

In contrast to maximizing fatigue, it might also be desired to accumulate a certain amount of work while minimizing fatigue, e.g., during the tapering period before a competition. For Session I, we exemplarily choose $\Phi(x) = -x_{\text{fatigue}}$ and $C_{\text{FTI}} = 150$ s.

10.3.3 TUT-based goals

Several authors have examined time-under-tension as a determinant of acute responses and long-term adaptations to RT (e.g., Burd et al. [2012] or Schott et al. [1995]). Therefore, for Session J, we maximize TUT while ensuring a minimum threshold intensity by choosing $\Phi(x) = x_{\text{TUT}}$ and $u_{\text{low}} = 0.8$.

Session J does not take into account the duration of the contractions used to accumulate the total TUT. However, some author have reported different adaptations to short and long duration contractions with greater hypertrophy occurring after long duration contractions [Schott et al., 1995]. Thus, to weight the duration of contractions quadratically, we replace Equation (10.1j) with

$$\frac{\mathrm{d}}{\mathrm{d}t} {x^i}_{\text{TUT}}(t) = \begin{cases} 0 & \text{if } u^i_{\text{abs}}(t) = 0 \\ t & \text{else} \end{cases} \tag{10.6}$$

for Session K. All other settings are kept as in Session J.

10.4 Numerical results

10.4.1 FTI-based goals

Figures 10.1 to 10.11 illustrates the model response obtained by simulating Sessions A to F. Figure 10.7 depicts the objective functional value in dependency of the number of possible contractions. Figures 10.8 and 10.9 depict the durations of contractions and rests in dependency of the number of possible contractions. For all sessions, all 25 possible contractions are realized.

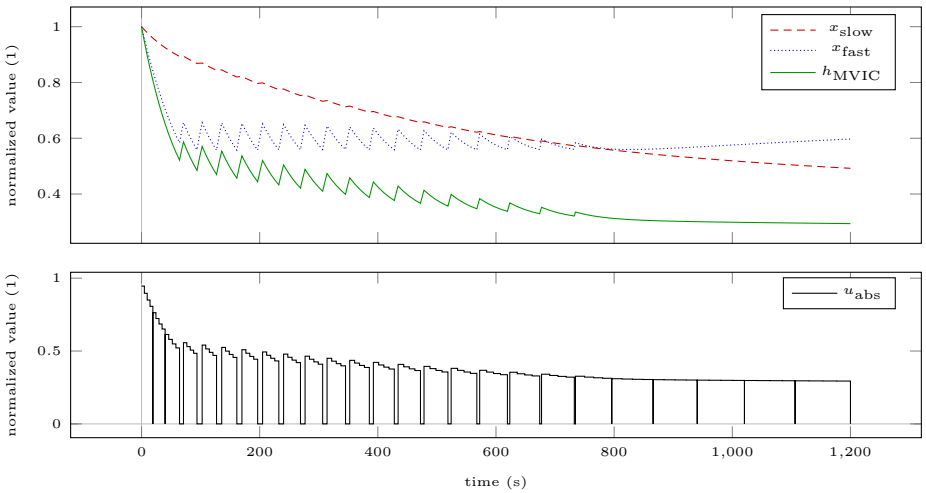

Figure 10.1: Model response obtained by simulating the calibrated model for Session A. The top row shows the model response and the absolute force input is illustrated in the bottom row.

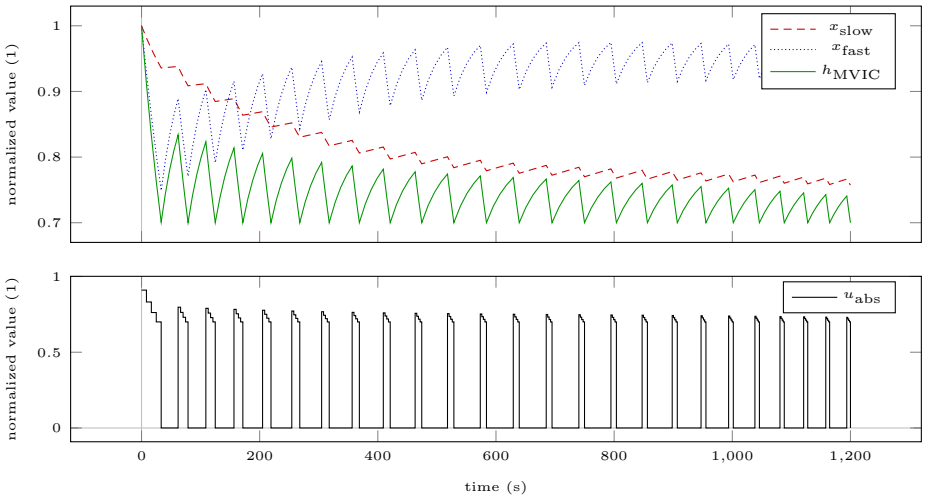

Figure 10.2: Model response obtained by simulating the calibrated model for Session $B_{70\%}$. The top row shows the model response and the absolute force input is illustrated in the bottom row.

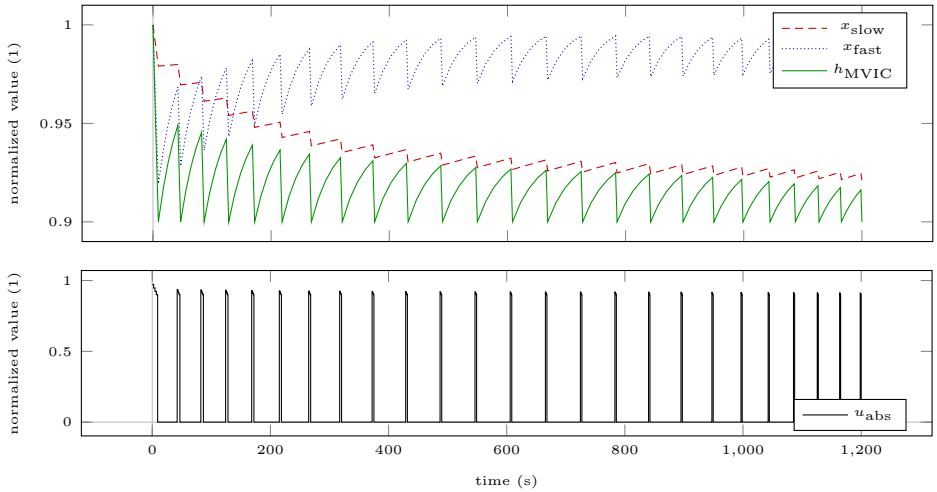

Figure 10.3: Model response obtained by simulating the calibrated model for Session $B_{90\%}$. The top row shows the model response and the absolute force input is illustrated in the bottom row.

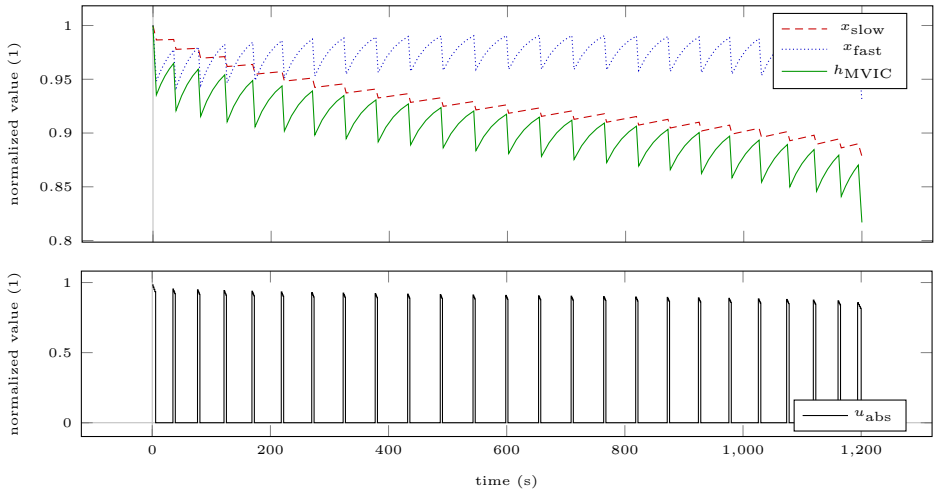

Figure 10.4: Model response obtained by simulating the calibrated model for Session C. The top row shows the model response and the absolute force input is illustrated in the bottom row.

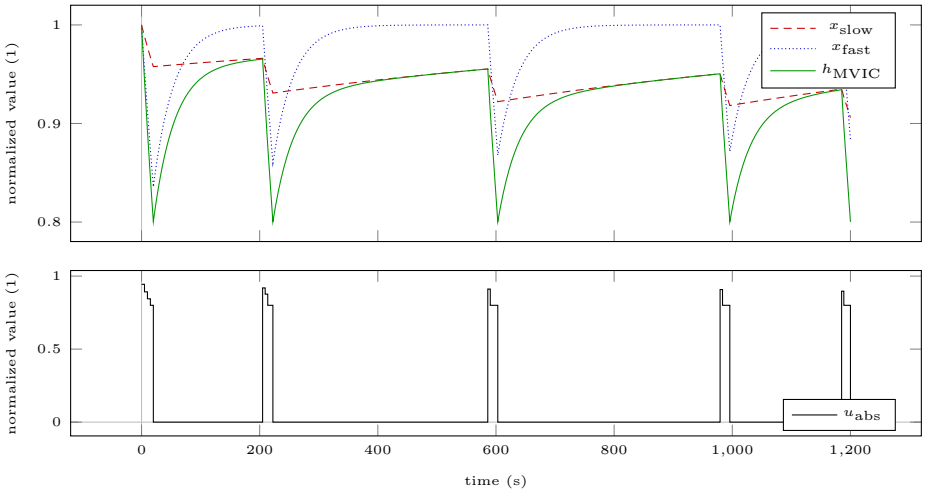

Figure 10.5: Model response obtained by simulating the calibrated model for Session D_5. The top row shows the model response and the absolute force input is illustrated in the bottom row.

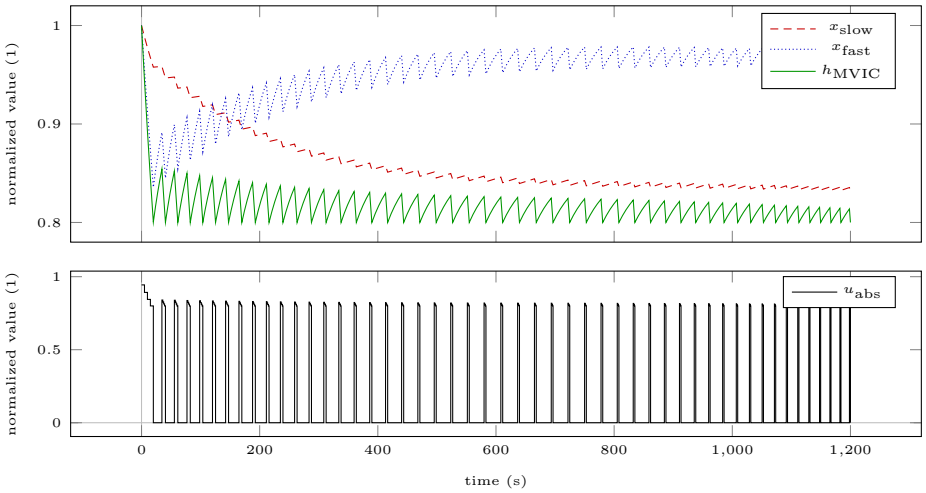

Figure 10.6: Model response obtained by simulating the calibrated model for Session D_{50}. The top row shows the model response and the absolute force input is illustrated in the bottom row.

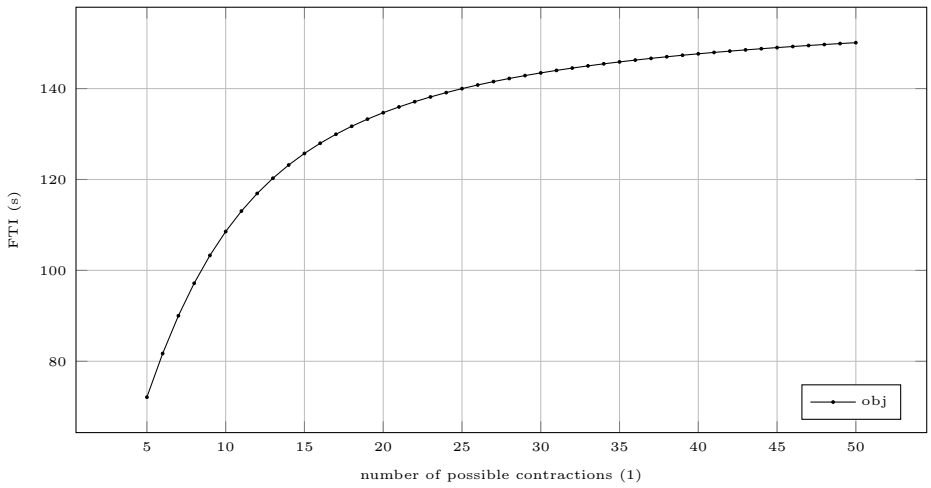

Figure 10.7: Dependency of the objective functional value on the number of possible contractions for Sessions D_5 to D_{50}. Increasing the number of possible contractions increases the FTI of the computed solution.

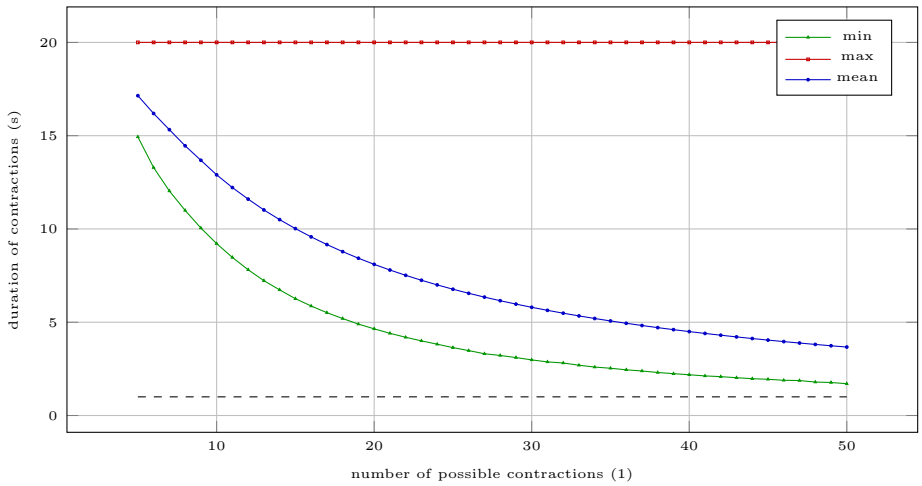

Figure 10.8: Dependency of the durations of contractions (a) and rests (b) on the number of possible contractions for Sessions D_5 to D_{50}. The horizontal dashed lines illustrate the 1 s mark. Increasing the number of possible contractions decreases the durations of contractions and rests of the computed solution.

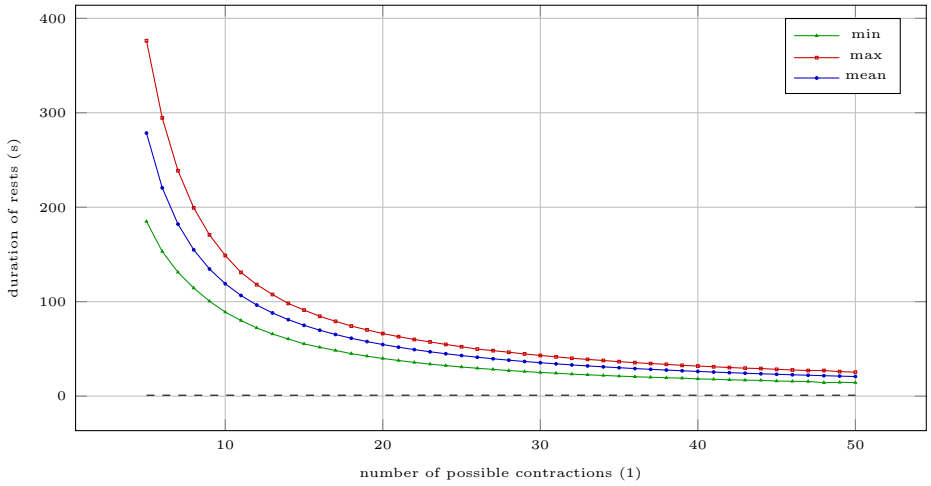

Figure 10.9: Dependency of the durations of contractions (a) and rests (b) on the number of possible contractions for Sessions D_5 to D_{50}. The horizontal dashed lines illustrate the 1 s mark. Increasing the number of possible contractions decreases the durations of contractions and rests of the computed solution.

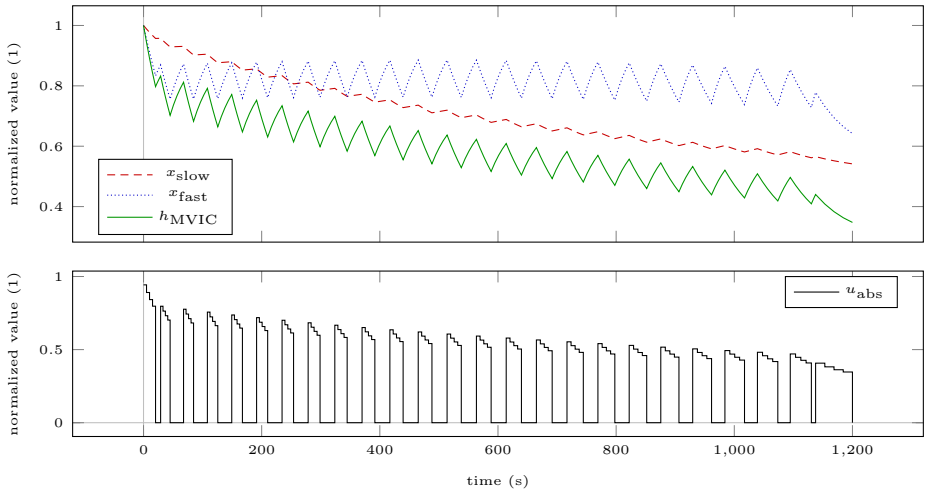

Figure 10.10: Model response obtained by simulating the calibrated model for Session E. The top row shows the model response and the absolute force input is illustrated in the bottom row.

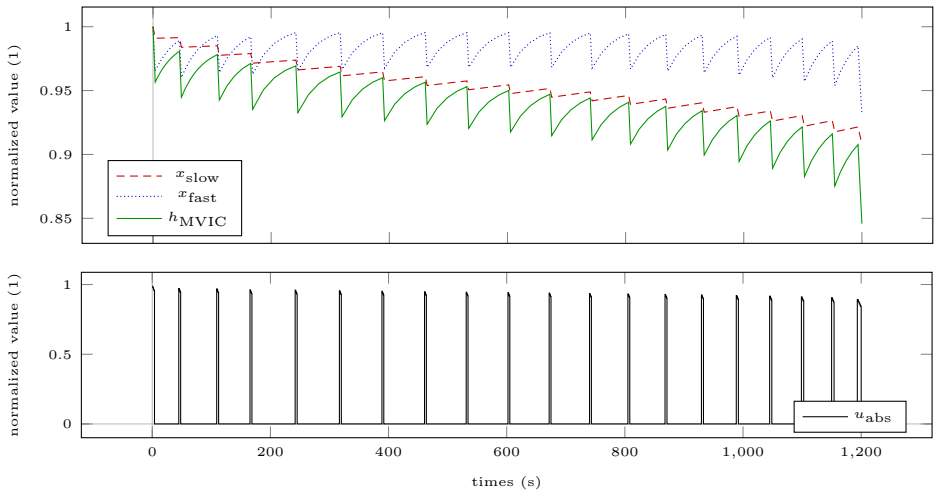

Figure 10.11: Model response obtained by simulating the calibrated model for Session F. The top row shows the model response and the absolute force input is illustrated in the bottom row.

10.4.2 Fatigue-based goals

Figures 10.12 to 10.14 illustrates the model response obtained by simulating Sessions G to I.

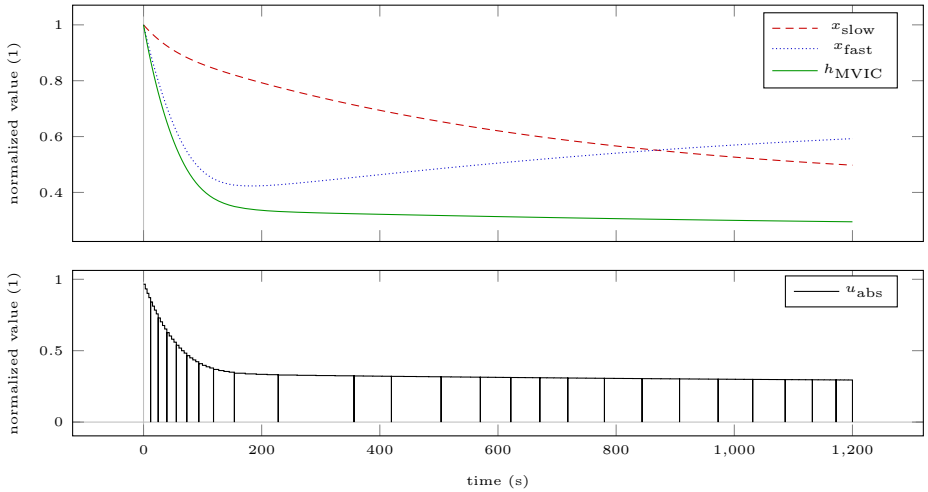

Figure 10.12: Model response obtained by simulating the calibrated model for Session G. The top row shows the model response and the absolute force input is illustrated in the bottom row.

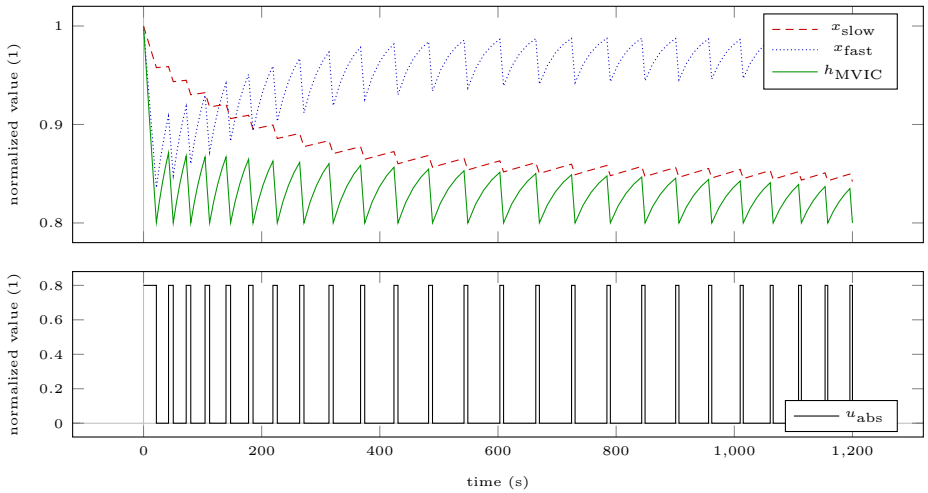

Figure 10.13: Model response obtained by simulating the calibrated model for Session H. The top row shows the model response and the absolute force input is illustrated in the bottom row.

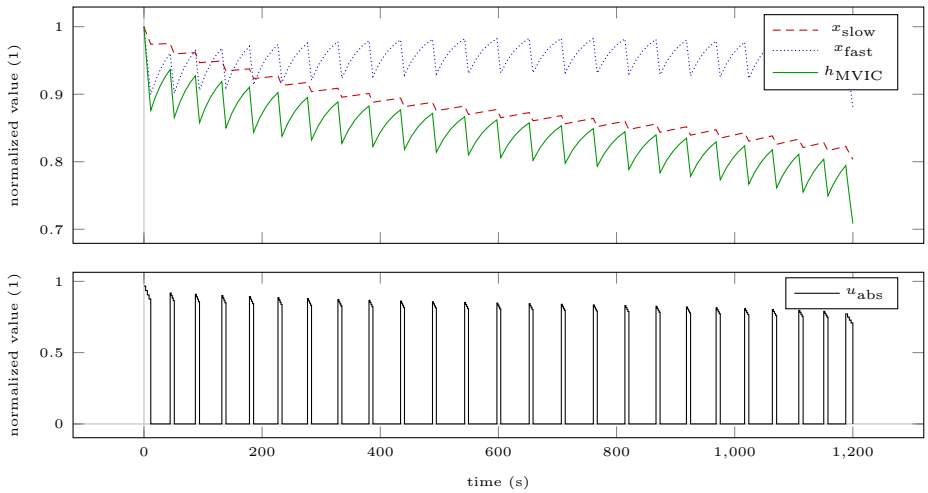

Figure 10.14: Model response obtained by simulating the calibrated model for Session I. The top row shows the model response and the absolute force input is illustrated in the bottom row.

10.4.3 TUT-based goals

Figures 10.15 and 10.16 illustrate the model response obtained by simulating Sessions J and K.

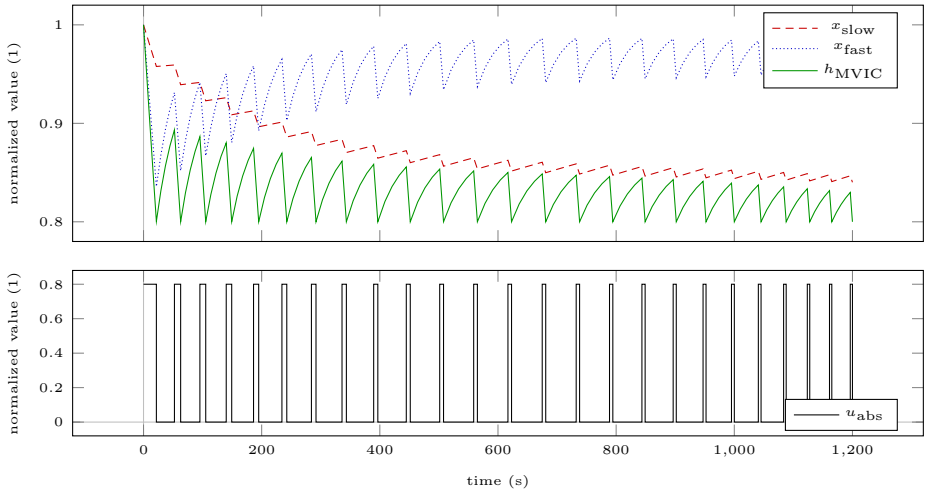

Figure 10.15: Model response obtained by simulating the calibrated model for Session J. The top row shows the model response and the absolute force input is illustrated in the bottom row.

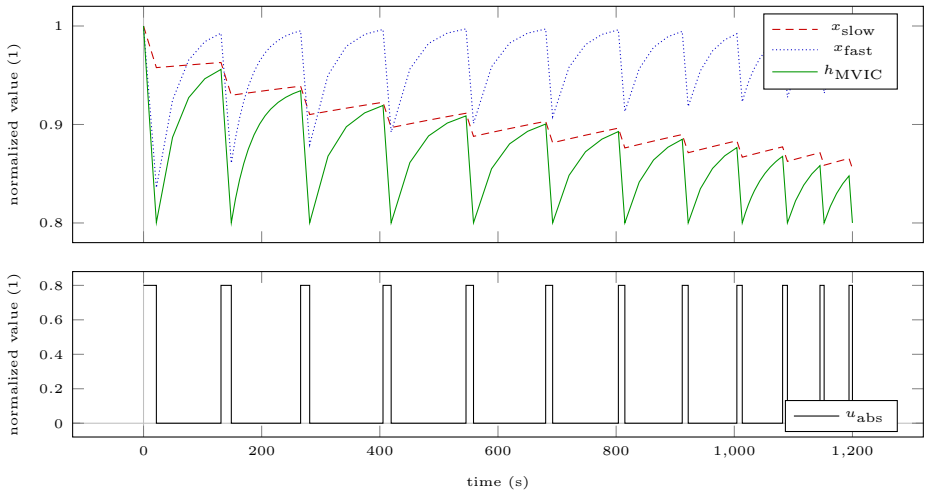

Figure 10.16: Model response obtained by simulating the calibrated model for Session K. The top row shows the model response and the absolute force input is illustrated in the bottom row.

10.4.4 Durations of contractions and rests

Table 10.4 contains the minimum, the maximum, and the mean durations of the contractions and rests for all sessions plotted. To a certain extent, this allows to examine the real-life feasibility of the computed sessions.

Table 10.4: Minimum, maximum, and mean durations of contractions δ_c and rests δ_r for all sessions plotted. To a certain extent, this data allows to examine the real-life feasibility of the computed sessions.

Session	$\min(\delta_c)$	$\max(\delta_c)$	$\text{mean}(\delta_c)$	$\min(\delta_r)$	$\max(\delta_r)$	$\text{mean}(\delta_r)$
A	19.21	465.46	60.54	1.96	8.76	6.49
$B_{70\%}$	6.24	33.28	11.41	28.63	45.64	38.11
$B_{90\%}$	1.62	9.13	3.04	33.02	56.96	46.83
C	3.71	6.06	4.11	28.90	51.81	45.72
D_5	14.94	20.00	17.14	184.96	376.31	278.57
D_{50}	1.70	20.00	3.67	14.38	25.36	20.75
E	16.10	62.36	26.06	7.15	25.63	22.86
F	3.08	6.54	3.52	39.36	73.22	59.45
G	1200.00	1200.00	1200.00	0.00	0.00	0.00
H	4.30	21.76	6.97	20.57	54.54	42.74
I	6.51	12.05	7.25	30.09	48.14	42.45
J	3.69	21.76	6.99	30.57	51.91	42.72
K	5.81	21.76	12.01	42.10	126.68	95.97

10.5 Discussion

10.5.1 Choice of training goals

In general, a model-based approach is limited by the predictive capability of the employed model and the available numerical solution methods. To enable a practically feasible approach, the proposed model offers a phenomenological description of muscular fatigue for different loading schemes. For this reason, we use optimality criteria for loading schemes identified in sports science to formulate the optimal control problems.

The three key performance indicators (KPIs) force-time integral, time-under-tension, and loss of MVIC force can readily be used in the optimal control problem formulations. Furthermore, we employ variants of these three KPIs to demonstrate how even slight modifications can change the structure of the solution. This highlights how important it is for exercise physiologists and sports scientists to identify the correct driving stimuli for adaptations in order to design optimized resistance training (RT) programs. Suitable physiological models would allow a more thorough search, e.g., by incorporating the build up of metabolites as hydrogen ions and inorganic phosphate or by describing the activation of different fiber types.

10.5.2 Structure of the computed RT sessions

While the resulting differences between the solutions might seem small at first, one should keep in mind that these differences accumulate during the course of an RT plan over weeks and months.

The results of Session D favor a higher number of contractions to accumulate more force-time integral in this scenario. This is in line with the solutions of most other sessions, in which all 25 possible contractions are realized. However, this is not the case for the solutions of Sessions A, F, G, and K. The results of Session A illustrate that the inclusion of rests is not beneficial during the beginning and the end of the session for this setting. To enable high contraction intensities, the solution of Session F consists of only 20 contractions. This is due to the fact that we weight the contraction intensities proportionally more than in the solution of Session C, where all 25 contractions are realized. The solution of Session G describes a sustained MVIC effort, which is caused by choosing the accumulated loss of MVIC force as training goal. The solution of Session K only realizes 12 contractions in order to enable longer contraction durations compared to the solution of Session J. This can be verified by comparing the mean contractions duration of Session J and K, i.e., 6.99 s and 12.01 s (see Table 10.4).

Except for the solutions of Sessions H, J, and K, all solutions consist exclusively of MVIC efforts. This was unexpected, as we anticipated that submaximal contractions might allow a greater accumulation of training volume due to them inducing less fatigue. It would be interesting to examine if such a behavior also occurs for dynamic constant external RT. The solution of Session H exhibits an interesting behavior as the inclusion of a minimum threshold intensity now favors submaximal contractions compared to the MVIC efforts of the solution of Session G. This is possibly caused by the longer contraction durations, which then contribute more to the accumulated fatigue. Session I exhibits the same behavior as the MVIC efforts reduce the time necessary to accumulate the desired FTI. The same holds for the solutions of Sessions J and K, where the submaximal contractions allow a greater time-under-tension. The submaximal contractions are all held until failure. In case this is not desired, this could be included into the optimization problem as a constraint. If a minimum threshold intensity was chosen, the MVIC efforts are held until this intensity is reached (see in particular Session B). Sessions C and F differ. Here, the contractions are terminated earlier as contractions with the minimum threshold intensity do not contribute to the chosen training goal. Session E demonstrates how a focus can be set on higher contraction durations without the use of a minimum threshold intensity.

A remark from a mathematical point of view: For all sessions, constraints limit the feasible region of the optimization problems and a large number of these constraints is active in the solutions, e.g., maximum or minimum contraction intensities are attained, which is expected in an optimal control context. All chosen constraints are solely physiologically motivated – no artificial constraints have been introduced. However, due to the discretization of the constraints within the multiple shooting approach, the algorithm only guarantees that the constraints are

met at the shooting nodes. In case of constraint violations between the shooting grid points, the grid can be refined easily to meet the requirements.

As already noticed during the model development, the grouping of repetitions into sets is not supported by our results. Instead, the contractions are spread more evenly over the whole time horizon to allow a greater accumulation of training volume, i.e., force-time integral. This is a similar approach to variants of so-called cluster sets [Tufano et al., 2017], which allow to increase training volume by breaking up the traditional set-repetition structure. Here, the algorithmic optimization of durations of contractions and rests provides a clear advantage over intuitive planning.

10.5.3 Real-life feasibility of the computed RT sessions

To ensure the real-life feasibility of the computed RT sessions, several aspects have to be taken into account. First, the duration of the contractions should not be too short, as the trainees need time to develop MVIC force. Second, the duration of the submaximal contractions should not be too long, as the concept of task failure or limited work capacity is currently not implemented into the model. Third, the rest periods between submaximal contractions should not be too short, as the model also does not account for a regeneration of work capacity.

Kawakami et al. [2000] examined 100 intermittent MVIC efforts lasting 1 s followed by 1 s rest of the triceps surae muscles and reported no problems in executing this task. Table 10.4 and Figures 10.8 and 10.9 show that our solutions do not propose durations shorter than 1 s for contractions and rests. Although a different muscle group was used in the study of Kawakami et al. [2000], their data demonstrates that such short intermittent contractions might be possible in general.

Yoon et al. [2007] examined endurance times for sustained isometric contractions of the elbow flexors at 90 degrees joint angle and at 80 % of MVIC force. Although the experimental setup differed slightly compared to that of the experiments used for the model validation (forearm horizontal versus forearm vertical to the ground), the mean endurance times of 25.0 s for men and 24.3 s for women are consistent with the maximum duration of 21.76 s of our solutions for Sessions H, J, and K (see Table 10.4). To the best of our knowledge, no prediction of endurance time or work capacity exists for MVIC efforts. Caffier et al. [1992], for example, examined MVIC efforts of several muscle groups lasting 10 min and reported no task failure among the subjects. Thus, it remains to be validated experimentally if the solutions of Session A, E, and G, which contain sustained MVIC efforts of long durations, can be realized in practice.

Although several authors have examined the recovery of endurance times (see, for example, the work of Stull and Kearney [1978] or Kroon and Naeije [1991]) and work capacity (see, for example, the review by [Jones and Vanhatalo, 2017]), to the best of our knowledge, no model of their time course exists that fulfills the prerequisites postulated for use in an optimization context. Furthermore, we are not aware of any experimental data that rejects the feasibility of the solutions

of Sessions H, J, and K due to too short rests. If this should be the case, lower bounds on the durations of the rests could be incorporated into the optimal control problem.

10.6 Limitations and future work

In the following, we discuss limitations of our work and motivate several directions of future research.

As no fully suitable mathematical model for the more commonly used dynamic constant external resistance (DCER) training is available, we are optimizing isometric RT sessions. Research shows that the transfer from isometric RT to dynamic performance is questionable [Oranchuk et al., 2019]. Therefore, we discourage direct transfer of our findings to DCER or other forms of training. However, an extension of our approach to DCER training is straightforward once suitable models become available. The same holds true for extensions to other indicators of muscle fatigue (e.g., power, contraction velocity, or muscular endurance), multiple exercises, or long-term planning.

Moreover, we are using parameters obtained from the elbow flexors, as so far those are the only ones available. For this reason, a comparison between muscle groups or subjects is not possible at the moment. It would be intriguing to calibrate the model to different muscle groups and subjects and then examine how the resulting parameters affect the optimized RT sessions. Lievens et al. [2020], for example, after analyzing fatigue and recovery patterns of MVIC torque of the knee extensors, conclude that individualizing training might be important to optimize performance. The authors used proton magnetic resonance spectroscopy to analyze muscle fiber typology of the gastrocnemius and then classify the subjects into a slow- and a fast-twitch group for which they expected different patterns. With a model-based approach, this classification could be formulated as a parameter estimation problem for which the necessary force measurements could be obtained in a single testing session. Afterwards, RT sessions could be optimized individually as proposed in this work.

Since we are using local optimization methods, modified initial guesses do not necessarily lead to identical results. Vanishing stages in the employed multi-stage formulation could lead to redundant discretized controls. Thus, the computed solutions are neither globally optimal nor unique. However, considering the fact that globally optimal solutions cannot be efficiently computed for problems of this type, starting from an initial (e.g., empirically derived) training design, the employed method generates an improved design that is locally optimal.

Last, we acknowledge that the model is validated with data from laboratory studies. Thus, we face the same problems as the original studies: the transfer from the laboratory to real-life RT needs to be verified experimentally. To this end, we outline two potential experimental setups in the following, which could be conducted together with interested practitioners from the sports sciences.

The first experiment is designed to verify if our model-based approach allows

to achieve a better objective functional value compared to an intuitive approach. For illustrative purposes, we choose Session B, which maximizes the FTI while ensuring a minimum threshold intensity using 25 contractions within 20 min. After the trainees have familiarized themselves with the dynamometer, a testing session is conducted to individually calibrate the model to the trainees' elbow flexors and obtain reliable parameter estimates [Herold and Sommer, 2020a]. After sufficient rest, the trainees are asked to intuitively perform a session, which they think to be optimal for the given task. An optimized session is then computed for each trainee and after resting sufficiently again, the trainees are asked to perform the optimized session. This order is chosen to prevent any learning effects. Afterwards, the data of the two sessions is analyzed and the objective functional values are compared. Furthermore, the real-life feasibility of the optimized sessions can be evaluated by computing the deviations of prescribed force and actual force.

After a successful first experiment, a second one could be conducted to examine whether the chosen objective functional is beneficial for our training goal. However, this can only be done in comparison to another objective functional. For illustrative purposes, we compare Sessions $B_{70\%}$ and $B_{90\%}$ with regard to increasing maximum strength. To this end, trainees with the same level of RT experience are randomly assigned to three groups – a control group, a group following optimized training protocols for Session $B_{70\%}$, and a group following optimized training protocols for Session $B_{90\%}$. At the beginning of the experiment, an MVIC force test is conducted. This test is repeated at the end of the experiment and the results are analyzed. We emphasize that in this work the sessions are optimized independently of each other. Therefore, long-term planning has to be determined by the experimenters. Nutrition and recovery should be adequate and comparable among the trainees. If desired, the model parameters and the optimized sessions could be updated at any desired point in time.

10.7 Conclusion

In this work, we demonstrate that a mathematical model-based approach could provide valuable impulses for practitioners and complement the predominant manual program design of loading schemes for RT. Although, the differences in the optimized sessions might seem small, one should keep in mind that those accumulate during the course of an RT plan over weeks and months.

With our approach, training protocols – either motivated by current practice or of a more exploratory and unconventional nature – could be examined at a large scale via forward simulations of the model. The flexible formulation of different training goals in terms of adjusted objective functions allows to evaluate the performance of training sessions in silico. Thus, training recommendations can be analyzed and rated w.r.t. their justification and efficiency without the tremendous testing efforts in actual trials.

As our approach is independent of the underlying model, we encourage researchers to develop and validate models, which are suitable for optimization and

which connect the training input of different RT types directly to training goals such as increasing strength and power, hypertrophy, or increasing local muscular endurance. This would extend the possibilities to set up the optimization problems and might furthermore help to identify the driving mechanisms for long-term adaptations. Then, we could exploit the full potential of our approach.

In addition to a large variety of application areas, e.g., biomechanical movement analysis or the design of sports equipment, our work underlines and demonstrates the enormous potential of quantitative mathematics to analyze and improve sports activities.

Chapter 11

Mathematical model-based estimation of critical torques

In this chapter, we present how the proposed model can be used to determine sports scientific key performance indicators at the example of critical torque (CT). In the first section, we give a definition of critical power (CP) and CT. In the second section, we formulate the estimation of CT as a nonlinear program. In the third section, we present our results. In the fourth section, we discuss our results. In the fifth section, we mention limitations and future work. In the sixth section, we draw conclusions for this chapter.

Remark. We emphasize that substantial parts of Herold and Sommer [2020a] have been incorporated into this chapter either with only slight changes or without any changes.

11.1 Critical power and critical torque

The power-endurance relationship of a constant power task can be described [Monod and Scherrer, 1965] by

$$T_{\text{lim}} = \frac{W'}{P - P_c} \tag{11.1}$$

or equivalently by

$$P = \frac{W'}{T_{\text{lim}}} + P_c, \tag{11.2}$$

where T_{lim} describes the endurance time of a task conducted at constant power P, W' describes the curvature constant, and P_c, the pole/asymptote of the function, is called CP. This relation is illustrated schematically in Figure 11.1. CP can be interpreted as the maximum power output at which a metabolic steady state can be obtained [Jones et al., 2019]. It constitutes an important fatigue threshold in exercise physiology and can be used to analyze, predict, or optimize performance [Craig et al., 2019]. Therefore, a reliable and economical estimation is of benefit for athletes, coaches, and exercise physiologists. Its equivalent for isometric or dynamic muscle contractions is the so-called CT, which we examine in this work.

Critical torque and the curvature constant W' are usually estimated from multiple submaximal constant torque tests to task failure spread over several days. Burnley et al. [2012], for example, used five trials to determine critical torque of

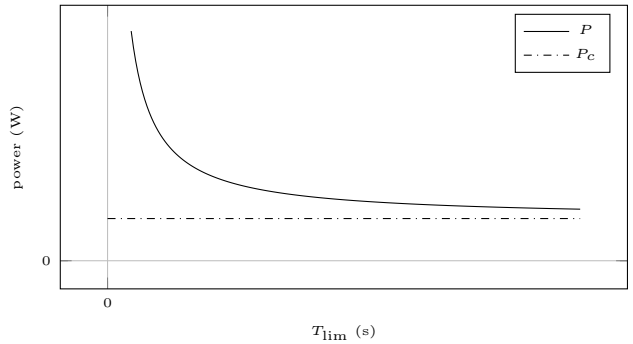

Figure 11.1: Schematic illustration of the power-endurance relationship of constant power tasks (11.2). The curvature of this relationship is determined by W' and its asymptote by P_c. The power that can be sustained for time T_{lim} can be obtained through $P = W'/T_{\mathrm{lim}} + P_c$.

the knee extensors. For intermittent contractions, CT furthermore depends on the work-rest ratio of the periodic loading scheme [Broxterman et al., 2014; Jones and Vanhatalo, 2017], which is commonly quantified by the so-called duty cycle. Thus, several CTs need to be estimated for an exercise to obtain a detailed description of the subject. This increases the experimental effort even further.

To reduce the experimental effort, all-out tests have been suggested. Burnley [2009] examined 5 min of maximum intermittent isometric contractions to determine critical torque of the knee extensors and showed that end-torque of these tests closely approximates CT. All-out tests have also been used for other exercises, e.g., for plantar flexion [Abdalla et al., 2018] or for handgrip exercise [Kellawan and Tschakovsky, 2014]. However, some authors have reported a possible overestimation of CP by the equivalent 3-min all-out test [Muniz-Pumares et al., 2018], which suggests that all-out tests might not be suitable for all subjects or might need to be adapted individually. Kellawan and Tschakovsky [2014], for example, used intermittent isometric contractions lasting 1 s with 2 s rest for 10 min, as they anticipated a longer time to plateau for their experimental setup.

11.2 A nonlinear program formulation of critical torque

Table 11.1 contains an overview of the simulation scenarios used in this chapter.

We compute the highest sustainable torque output of the elbow flexors by solving the nonlinear program

$$\max_{u_{\mathrm{abs}}, x_{\mathrm{slow}}, x_{\mathrm{fast}}} \quad u_{\mathrm{abs}} \tag{11.3a}$$

$$\text{s.t. } 0 = p_1(1 - x_{\mathrm{slow}}) - p_2 u_{\mathrm{abs}} \tag{11.3b}$$

$$0 = p_3(1 - u_{\mathrm{abs}})^{p_4}(1 - x_{\mathrm{fast}}) - p_5 u_{\mathrm{abs}} \tag{11.3c}$$

Table 11.1: Overview of simulation scenarios used in this chapter.

Scenario	Explanation
IC	Intermittent contractions lasting 3 s with 2 s rest
ICmax	Intermittent MVIC efforts lasting 3 s with 2 s rest
IC80	Intermittent contractions at 80 % of critical torque lasting 3 s with 2 s rest
IC120	Intermittent contractions at 120 % of critical torque lasting 3 s with 2 s rest
SC	Sustained contraction
SCmax	Sustained MVIC effort

$$u_{\text{abs}} \leq x_{\text{slow}} x_{\text{fast}} = h_{\text{MVIC}} \tag{11.3d}$$
$$0 \leq u_{\text{abs}}, x_{\text{slow}}, x_{\text{fast}} \leq 1. \tag{11.3e}$$

Here, we briefly abuse notation and let u_{abs}, x_{slow}, and x_{fast} denote real numbers in order to obtain the corresponding values of these functions when critical torque is reached. Constraints (11.3b) and (11.3c) ensure that maximum voluntary isometric contraction (MVIC) torque does not change further and Constraints (11.3d) and (11.3e) ensure that the input and the states are feasible.

Exemplarily, we solve the nonlinear program (11.3) for a sustained contraction (Scenario SC) and for intermittent contractions lasting 3 s with 2 s rest (Scenario IC) as conducted by Burnley [2009] for the knee extensors. For Scenario IC, we use

$$0 = 3(p_1(1 - x_{\text{slow}}) - p_2 u_{\text{abs}}) + 2(p_1(1 - x_{\text{slow}})) \tag{11.4a}$$
$$0 = 3(p_3(1 - u_{\text{abs}})^{p_4}(1 - x_{\text{fast}}) - p_5 u_{\text{abs}}) + 2(p_3(1 - x_{\text{fast}})) \tag{11.4b}$$

instead of Constraints (11.3b) and (11.3c). This choice approximates that during one contraction-rest cycle MVIC torque does not change further. The nonlinear program is solved numerically the sequential least-squares programming algorithm by Kraft [1988] provided in SciPy 1.2.1 [Virtanen et al., 2020].

We verify our results by simulating the model for a sustained MVIC effort (Scenario SCmax) and intermittent MVIC efforts lasting 3 s with 2 s rest (Scenario ICmax) until a plateau of MVIC torque is reached. These simulations correspond to all-out tests proposed by Burnley [2009]. Thus, the end-test torques provide estimates of CTs. To terminate our simulations during Scenario SCmax because a plateau is reached, we demand $|\frac{\mathrm{d}}{\mathrm{d}t} x_{\text{slow}}| \leq 10^{-6}$ and $|\frac{\mathrm{d}}{\mathrm{d}t} x_{\text{fast}}| \leq 10^{-6}$. To terminate our simulations during Scenario ICmax because a plateau is reached, we demand that the torque at the beginning of two adjacent contractions does not differ more than 10^{-6}. These thresholds are low enough to ensure that a steady state has been obtained, but do not require excessive computation times. Afterwards, we compare the computed steady states to the end-test torques of simulated 5-min all-out tests for both scenarios.

To illustrate that the thus determined steady states separate domains of contraction intensity, we recreate the experimental setting of Burnley et al. [2012] for the elbow flexors. We simulate intermittent contractions lasting 3 s with 2 s rest at 80 % (Scenario IC80) and at 120 % (Scenario IC120) of the previously determined critical torque on a time horizon of 60 min or until MVIC torque drops below target torque.

Finally, to demonstrate the full potential of our approach, we compute the highest sustainable torque output of the elbow flexors for intermittent contractions depending on the duty cycle. The duty cycle is defined as the ratio $t_c/(t_c+t_r)$, where t_c denotes the duration of a contraction and t_r denotes the inter-repetition rest. Therefore, we solve the nonlinear program (11.3) for 100 duty cycles distributed uniformly in $[0, 1]$ and plot the results.

11.3 Numerical results

For Scenario SC, our model-based estimation of CT yields 27.99 % of baseline MVIC torque. For Scenario IC, the solution is 41.01 % of baseline MVIC torque.

Figures 11.2 and 11.3 show the model response obtained by simulating Scenarios SCmax and ICmax for 5 min. For both scenarios, a steady state according to our definition in the previous section is not obtained after 5 min. End-test torques are 32.59 % of baseline MVIC torque for the sustained contraction and 54.72 % of baseline MVIC torque for the intermittent contractions. Simulating the scenarios on a time horizon of 60 min results in steady states. The sustained contraction levels off at 28.01 % of baseline MVIC torque. The intermittent contractions level off at 40.89 % of baseline MVIC torque. Both solutions are similar to the results obtained by solving the optimization problem 11.3. To illustrate the discrepancy to the end-test torques obtained by the 5-min all-out test, these steady states are depicted as dash-dotted lines in Figures 11.2 and 11.3.

Figures 11.4 and 11.5 show the model response obtained by simulating Scenarios IC80 and IC120. During Scenario IC80, MVIC torque approaches a steady state above the target torque at 52.60 % of baseline MVIC torque. During Scenario IC120, MVIC torque falls below target torque at $t = 773$ s.

Figure 11.6 depicts the highest sustainable torque output of the elbow flexors for intermittent contractions depending on the duty cycle.

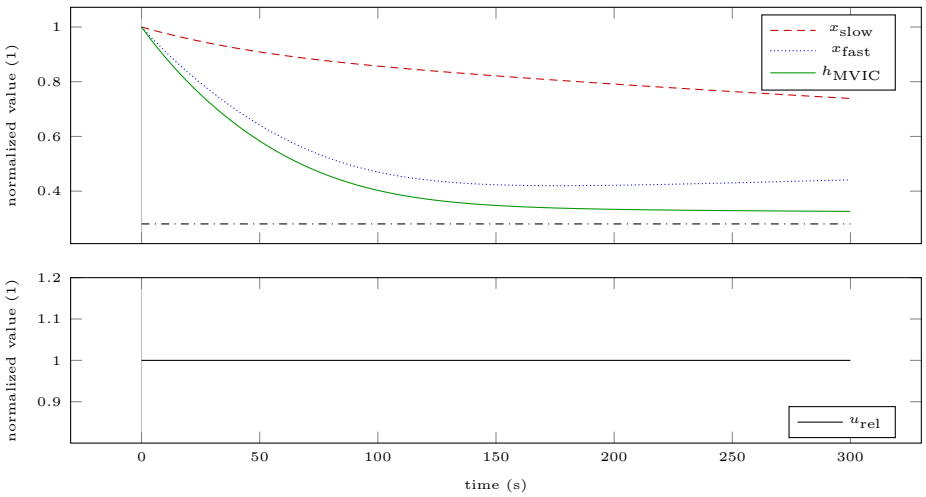

Figure 11.2: Model response obtained by simulating Scenario SCmax for 5 min. The bottom row illustrates the relative torque input. The dash-dotted lines represent the steady states obtained by simulating the scenario until a plateau of MVIC torque is reached.

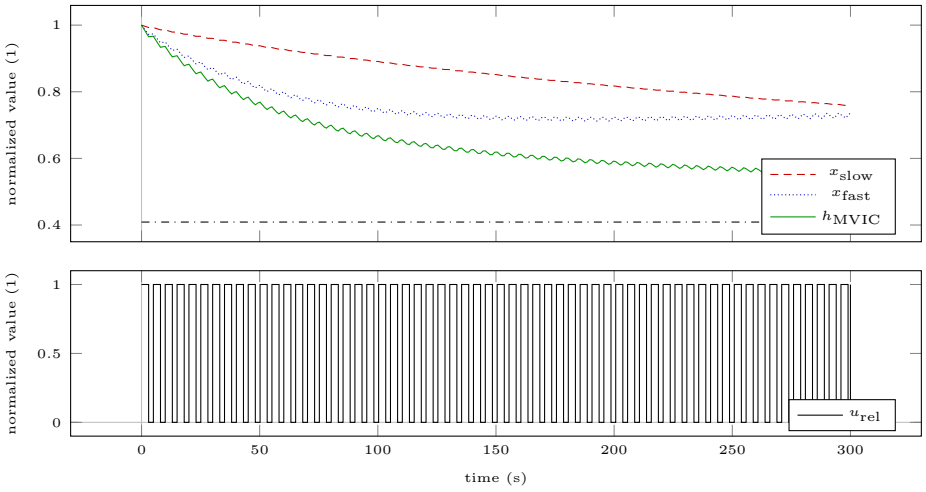

Figure 11.3: Model response obtained by simulating Scenario ICmax for 5 min. The bottom row illustrates the relative torque input. The dash-dotted lines represent the steady states obtained by simulating the scenario until a plateau of MVIC torque is reached.

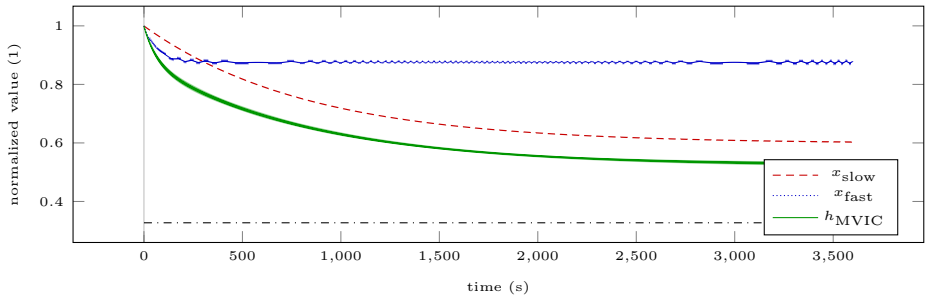

Figure 11.4: Model response obtained by simulating Scenario IC80 for 60 min. The dash-dotted lines represent the target torques of the intermittent contractions. The torque input has been omitted for this plot as due to the high number of intermittent contractions the plot would become illegible.

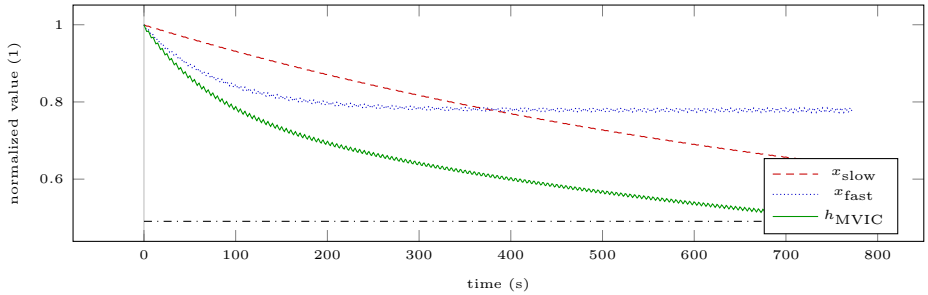

Figure 11.5: Model response obtained by simulating Scenario IC120 until MVIC torque drops below target torque. The dash-dotted lines represent the target torques of the intermittent contractions. The torque input has been omitted for this plot as due to the high number of intermittent contractions the plot would become illegible.

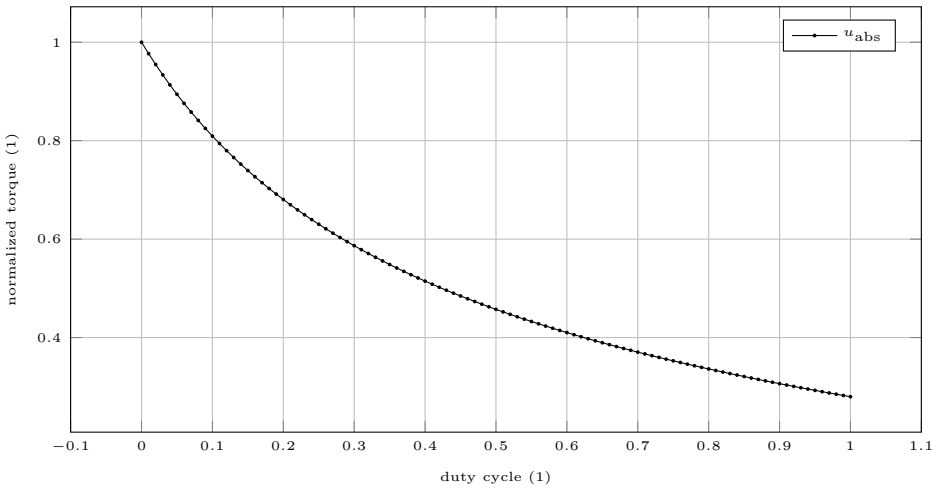

Figure 11.6: Highest sustainable torque output of the elbow flexors for intermittent contractions depending on the duty cycle. The duty cycle denotes the ratio $t_c/(t_c + t_r)$, where t_c denotes the duration of a contraction and t_r denotes the inter-repetition rest.

11.4 Discussion

Our results show that our approach yields similar estimates for CTs as the all-out tests proposed by Burnley [2009], if those are conducted for a sufficiently long duration. On the one hand, this verifies our model-based approach from a practical point of view. On the other hand, this augments the theoretical justification of the all-out tests, as the optimization problem 11.3 arises purely from the definition of CT as the highest sustainable torque output.

Using the experimental setup of Burnley et al. [2012], we can illustrate that the determined steady states indeed separate domains of contraction intensity. This is remarkable, as the concept of critical torque was not specifically implemented into the model but rather emerges naturally. These results underline the importance of critical torque as an important fatigue threshold in exercise physiology.

Our results also show that the durations needed to actually attain a steady state for the elbow flexors are longer than the 5 min proposed by Burnley [2009] for the knee extensors. Yet, durations of 60 min can not be used in real experiments. Therefore, to a certain degree, an overestimation of critical torque is probable when using all-out tests. This is in line with other authors who found that the equivalent 3-min all-out tests might overestimate critical power [Muniz-Pumares et al., 2018]. In our simulations, this overestimation is more pronounced for the intermittent contractions than for the sustained contraction. Thus, we propose that the durations of all-out tests are adjusted to the subject and the exercise if conventional methods for the estimation of critical torque are used. However, we emphasize that these adjustments are not necessary when using our model-based approach.

Previous studies have shown the knee extensors to be more fatigable than the elbow flexors. For examples, we refer to Vernillo et al. [2017] for a comparison of MVIC efforts and to Frey-Law and Avin [2010] for an analysis of endurance times. Our results are consistent with these findings, as the estimated critical torques of the elbow flexors are higher than the corresponding ones for the knee extensors. Burnley et al. [2012], for example, report a mean critical torque of the knee extensors of 34 % of baseline MVIC torque for intermittent isometric contractions lastings 3 s with 2 s rest. For the same contraction scheme, our computations yield a critical torque of 41 % of baseline MVIC torque for the elbow flexors. Moreover, Hendrix et al. [2009a] give a mean critical torque of 17.6 % of baseline MVIC torque for sustained contractions of the knee extensors. For the same contraction scheme, our computations yield a critical torque of 28 % of baseline MVIC torque for the elbow flexors.

Different experimental conditions (e.g., joint angles) complicate a straightforward comparison of our results to other studies examining critical torques of the elbow flexors. Furthermore, deducing a clear trend from the considered studies proves to be challenging. Hendrix et al. [2009b], for instance, report a mean critical torque of 17.6 % of baseline MVIC torque for sustained contractions of the elbow flexors, compared to a mean value of 26.3 % by Hendrix et al. [2010]. In contrast, for a continuous isometric contraction of the elbow flexors that can be

sustained for 60 min, Hagberg [1981] gives a mean contraction intensity of only 8.2 % of baseline MVIC torque and Sato et al. [1984] give only 10.3 % of baseline MVIC torque. For intermittent isometric contractions lasting 2 s with 2 s rest that can be sustained for 60 min, Hagberg [1981] reports a mean value of 25.1 % of baseline MVIC torque. The high variability of reported values points out the need for further research, as it is unclear whether those result from inter-individual or from methodological differences.

11.5 Limitations and future work

In the following, we discuss limitations of our work and motivate several directions of future research.

First, we do not formally prove that the solutions of the optimization problem (11.3) are approached and obtained during an all-out test for all periodic loading schemes and parameter values, as this is beyond the scope of this work. Rather this has to be ensured individually, as we did for the two scenarios examined here.

Second, we can not provide an estimate of the curvature parameter W'. The intuitive connection to impulse above end-test torque could not be verified by Burnley [2009]. Thus, at the moment, if an estimate of W' is desired, conventional submaximal constant power tests to failure have to be employed.

Third, due to the phenomenological nature of the model it does not provide insight into the metabolic or systemic profile of the subject and the tested muscles. Therefore, it remains to be examined experimentally which mechanisms are responsible for the model calibrated to the elbow flexors reaching its steady state later than the knee extensors examined by Burnley [2009].

Fourth, the model is currently limited to isometric contractions only. It would be interesting to see if a similar steady state behavior emerges naturally after the model has been extended to isokinetic contractions or contractions with dynamic constant external resistance. Thus, incorporating a velocity-dependency into the model could save additional experimental effort when dealing with these contractions. Morel et al. [2019], for example, showed that the asymptote of MVIC torque during an isokinetic all-out test depends on the contraction velocity. Intriguingly, during all-out tests, the time course of power bears strong resemblance with the time course of torque (see, for example, Figure 1 in Vanhatalo et al. [2007]). This might indicate a possible application of the model in power-measured exercises. Eriksson et al. [2016] already demonstrated that a model-based approach is also feasible for whole-body exercise. The authors developed a mathematical model of fatigue during whole-body exercise and qualitatively showed that their model can be used to determine critical power.

Last, we only consider unfatigued muscles. Yet, it is also possible to use our approach for prefatigued muscles by treating the initial values x_0 as additional parameters during the parameter estimation. Then, studies investigating the influence of fatigue on CT similar to those of Vanhatalo and Jones [2009] or Clark et al. [2018] are possible. This might provide further understanding and quantifi-

cation of the interaction of fatigue and fatigability.

11.6 Conclusion

We are able to estimate CTs for sustained and intermittent isometric contractions with a model-based approach in a single testing session. This reduces the experimental effort considerably compared to conventional testing.

Chapter 12

Optimizing testing sessions for model calibration

In this chapter, we compute optimized testing sessions to reduce the experimental effort when calibrating the proposed model. In the first section, we describe the experimental setting. In the second section, we formulate the corresponding optimum experimental design (OED) problems. In the third section, we discuss their numerical solution. In the fourth section, we describe the simulated scenarios. In the fifth section, we present our results. In the sixth section, we discuss our results. In the seventh section, we give conclusions for this chapter.

Remark. We emphasize that substantial parts of Herold and Sommer [2020a] have been incorporated into this chapter either with only slight changes or without any changes.

12.1 Experimental setting

Allen et al. [1995] report a mean empirical coefficient of variation of 3.78 % for individual 2 – 3 s maximum voluntary isometric contraction (MVIC) torque measurements of the elbow flexors in the unfatigued state. The experimental setup was similar to that used for the model development. To account for the increased torque variability observed during fatigue [Contessa et al., 2009], we use this value as absolute standard deviation of the measurement errors. The measurement error ε of a 2 s MVIC relative torque measurement is thus assumed to be additive, independent, and identically normally distributed with mean zero and standard deviation $\sigma_{2\mathrm{s}} = 0.0378$. The subscript denotes the duration of the contraction.

State of the art force transducers can provide high frequency measurement data. Hence, we may assume that measurements of MVIC torque can be obtained continuously if the subject can accurately estimate the applied torque u_{abs} in relation to its current torque capacity h_{MVIC}, i.e., if the subject can accurately estimate

$$u_{\mathrm{rel}}(t) = \frac{u_{\mathrm{abs}}(t)}{h_{\mathrm{MVIC}}(t)}. \tag{12.1}$$

This yields the measurement function

$$h(t) = u_{\mathrm{rel}}(t) h_{\mathrm{MVIC}}(t). \tag{12.2}$$

However, estimating u_{rel} for submaximal contractions is a challenging task [Banister, 1979], which is additionally influenced by fatigue [Jones and Hunter, 1983].

Therefore, we increase the standard deviation of measurements taken at submaximal contractions according to

$$\sigma(t) = \sigma_{2\mathrm{s}}(2 - u_{\mathrm{rel}}(t)). \tag{12.3}$$

For maximum contractions ($u_{\mathrm{rel}} = 1$), we again obtain the uncertainty observed by Allen et al. [1995].

To allow a numerical treatment of the continuous measurements [Janka, 2015], we choose a sufficiently fine measurement grid $(t_j)_{j\in\{1,\dots,n_m\}}$ and approximate the corresponding discretized standard deviations by

$$\sigma_j = \sigma_{2\mathrm{s}}(2 - u_{\mathrm{rel}}(t_j))\sqrt{\frac{2}{\Delta t_j}}, \quad j \in \{1, \dots, n_m\}. \tag{12.4}$$

Here, Δt_j denotes the duration of the measurement following the grid point t_j. The weighting $\sqrt{\frac{2}{\Delta t_j}}$ is necessary to take into account the coarseness of the measurement grid. For example, doubling Δt_j would then correspond to weighting the measurement taken at t_j twice. This furthermore allows us to treat measurements of any duration.

Moreover, we introduce a measure of the total time-under-tension (TUT)

$$I_{\mathrm{TUT}}(t) = \int_0^t \begin{cases} 0 & \text{if } u_{\mathrm{rel}}(\tau) = 0 \\ 1 & \text{else} \end{cases} \mathrm{d}\tau \tag{12.5}$$

to allow a fair comparison between different loading schemes. If we verify $u_{\mathrm{rel}} \in \{0, 1\}$ for our solutions, we can use

$$I_{\mathrm{TUT}}(t) = \int_0^t u_{\mathrm{rel}}(\tau)\mathrm{d}\tau \tag{12.6}$$

as an equivalent measure.

12.2 Multi-stage optimum experimental design problems

We use a multi-stage formulation on $n_s \geq 2$ stages – denoted by superscripts $i \in \{1, \dots, n_s\}$ – to model the loading schemes. We define

$$J = \begin{pmatrix} J_1^1 \\ J_2^1 \\ \dots \\ J_1^2 \\ J_2^2 \\ \dots \end{pmatrix} \in \mathbb{R}^{n_m \times n_p}, \tag{12.7a}$$

with $n_m = \sum_{i=1}^{n_s} n_m^i$ and

$$J_j^i = \frac{1}{\sigma_j^i} \left(\frac{\partial h^i}{\partial x^i} x_p^i(t_j^i) + \frac{\partial h^i}{\partial p}(t_j^i) \right) \Bigg|_{p=\hat{p}} \in \mathbb{R}^{n_p}, \tag{12.7b}$$

where the sensitivities of the model states w.r.t. the parameters are denoted by $G_p^i(t) = \frac{\mathrm{d}x^i}{\mathrm{d}p}(t)$ and the measurement times on stage i are denoted by t_j^i. To track TUT, we introduce an additional state I_{TUT} defined as in Equation (12.5). The multi-stage OED problem can then be formulated as

$$\min_{\substack{x^i(\cdot), G_p^i(\cdot), I_{\mathrm{TUT}}^i(\cdot) \\ u_{\mathrm{rel}}^i(\cdot), T^i}} \quad \frac{1}{5}\mathrm{tr}((J^\top J)^{-1}) \tag{12.7c}$$

$$\text{s.t.} \quad 0.01\ \mathrm{s} \leq T^i \text{ for } i \in \{1, \dots, n_s\} \tag{12.7d}$$

$$\sum_{i=1}^{n_s} T^i \leq C_T \tag{12.7e}$$

$$I_{\mathrm{TUT}}^{n_s}(T^{n_s}) \leq C_{\mathrm{TUT}} \tag{12.7f}$$

$$x^0(0) = (1,1)^\top \tag{12.7g}$$

$$G_p^0(0) = (0,0)^\top \tag{12.7h}$$

$$I_{\mathrm{TUT}}^0(0) = 0 \tag{12.7i}$$

$$\text{and for} \quad i \in \{2, \dots, n_s\}:$$

$$x^i(0) = x^{i-1}(T^{i-1}) \tag{12.7j}$$

$$G_p^i(0) = G_p^{i-1}(T^{i-1}) \tag{12.7k}$$

$$I_{\mathrm{TUT}}^i(0) = I_{\mathrm{TUT}}^{i-1}(T^{i-1}) \tag{12.7l}$$

$$\text{and for} \quad i \in \{1, 3, \dots, n_s - 2, n_s\} \text{ and } t \in [0, T^i]:$$

$$\frac{\mathrm{d}}{\mathrm{d}t}x^i(t) = f_{\mathrm{rel}}(x^i(t), u_{\mathrm{rel}}^i(t), p) \tag{12.7m}$$

$$\frac{\mathrm{d}}{\mathrm{d}t}G_p^i(t) = \frac{\partial f_{\mathrm{rel}}}{\partial x^i}G_p^i(t) + \frac{\partial f_{\mathrm{rel}}}{\partial p} \tag{12.7n}$$

$$\frac{\mathrm{d}}{\mathrm{d}t}I_{\mathrm{TUT}}^i(t) = u_{\mathrm{rel}}^i(t) \tag{12.7o}$$

$$0 \leq u_{\mathrm{rel}}^i(t) \leq 1 \tag{12.7p}$$

$$\text{and for} \quad i \in \{2, 4, \dots, n_s - 3, n_s - 1\} \text{ and } t \in [0, T^i]:$$

$$\frac{\mathrm{d}}{\mathrm{d}t}x^i(t) = f_{\mathrm{rel}}(x^i(t), 0, p) \tag{12.7q}$$

$$\frac{\mathrm{d}}{\mathrm{d}t}G_p^i(t) = \frac{\partial f_{\mathrm{rel}}}{\partial x^i}G_p^i(t) + \frac{\partial f_{\mathrm{rel}}}{\partial p} \tag{12.7r}$$

$$\frac{\mathrm{d}}{\mathrm{d}t}I_{\mathrm{TUT}}^i(t) = 0, \tag{12.7s}$$

with C_T being the upper bound on the sum of all stage durations T^i and C_{TUT} being the upper bound on the sum of all stage-wise TUTs. The lower bounds on the stage durations T^i (12.7d) are necessary to avoid a division by zero in Equation (12.4), as the stage durations are being optimized. As described in Section 8.5, $h_{\mathrm{MVIC}} = x_{\mathrm{slow}}x_{\mathrm{fast}}$ describes the current MVIC torque and f_{rel} denotes the right-

hand side of the chosen model stage. Minimizing the trace of $(J^\top J)^{-1}$ corresponds to minimizing the average variance of the parameter estimates [Pukelsheim, 1993]. To weight the parameters equally, we scale all parameters to 1 beforehand. Table 12.1 gives an overview of the symbols used in the problem formulation.

Table 12.1: Overview of symbols used in OED problem (12.7).

Symbol	Interpretation
C_T	Upper bound on total time
C_{TUT}	Upper bound on total TUT
f_{rel}	Right-hand side of ODE system
G_p^i	Sensitivities of states
h^i	Measurement function
h^i_{MVIC}	MVIC torque
i	Stage index
I^i_{TUT}	Time-under-tension
J^i	Jacobian
n_s	Number of stages
p	Parameters
$\hat{p}$	Current parameter guess
σ^i_j	Standard deviation of measurement error
t	Time
T^i	Stage duration
t^i_j	Measurement time
tr	Trace of matrix
u^i_{rel}	External torque relative to current MVIC torque
x^i	State variables

12.3 Numerical solution via direct single shooting

As in Sections 8.9 and 10.2, we need specialized methods to provide efficient and flexible solutions for different trainees with individual features.

To solve the problem, we employ a first-discretize-then-optimize strategy. We use a direct single shooting approach to reduce the problem to a finite-dimensional form. We use piecewise constant controls, as this discretization reflects the training reality and allows a direct interpretation of the solution for practitioners. We use 100 measurements per stage. We employ DAESOL [Bauer, 1999] for integration of the ordinary differential equation system (ODE) and sensitivity generation via internal numerical differentiation [Bock, 1981]. Relative and absolute integration tolerances are set to 10^{-8} and 10^{-7}. Maximum order is set to 6. Maximum step size is set to 1. The necessary derivatives of the model functions are computed via automatic differentiation with ADIFOR [Bischof et al., 1998]. The resulting nonlinear program is then solved with the line search sequential quadratic programming method SNOPT [Gill et al., 2005]. Major optimality tolerance for SNOPT is

set to 10^{-6}. The intuitive testing session is used as initial guess. We use the software package VPLAN [Körkel, 2002] to carry out all steps. Several reformulations are necessary to fit the multi-stage setting into the VPLAN framework.

Exemplarily, we give the dimensions of OED problem 'OTS200' treated below. Several reformulations are necessary, which yield 2 control functions discretized on 21 control intervals. On 11 of these intervals 100 discrete measurements are used to approximate the continuous data acquisition. The resulting nonlinear program (NLP) has 1142 nonlinear variables, 2 nonlinear constraints, and 1101 linear constraints.

12.4 Optimized scenarios

To illustrate the benefits of OED, we compare the uncertainties of the parameters resulting from an intuitive testing session (Scenario ITS) with those resulting from algorithmically designed optimized testing sessions (Scenarios OTS200 and OTS400). Scenario ITS consists of a 3 min MVIC effort followed by 2 s MVIC efforts at 10 s, 30 s, 1 min, 2 min, 5 min, 10 min, 15 min, 20 min, 25 min, and 30 min after cessation of the sustained MVIC effort to check the time course of recovery. Thus, it lasts 1982 s in total, of which 200 s are TUT. This loading scheme is motivated by comparable sessions conducted to examine fatigue and recovery of skeletal muscle [Gandevia et al., 1996; Søgaard et al., 2006].

The optimized sessions are computed as described above with Scenario ITS as initial guess. For Scenario OTS200, to allow a fair comparison, we limit the maximum number of contractions to 11 (which implies $n_s = 21$), the total time to $C_T = 1982$ s, and the time-under-tension to $C_{\mathrm{TUT}} = 200$ s as in the intuitive testing session. On each odd numbered model stage, we use constant controls and employ $n_m^i = 100$ discrete measurements to approximate the continuous measurements of the force transducer. Even numbered stages are considered rest periods. For Scenario OTS400, we use the same setup but increase the limit of the time-under-tension to $C_{\mathrm{TUT}} = 400$ s.

Additionally, we demonstrate how the uncertainties of the parameters propagate through the model. As no measurement data is available, we assume that the intuitive and the optimized testing sessions resulted in the same parameter estimates p but with different standard deviations σ_p. We then draw 10000 random samples from $\mathcal{N}(p, \sigma_p^2)$ and simulate two different scenarios with these perturbed parameters. We redraw realizations with negative parameters, since the model is not evaluable for those. The probability for which is 0.5 % when using the standard deviations resulting from the intuitive testing session and 0 % when using those resulting from the optimized testing sessions. First, we simulate Scenario ICmax for 60 min, as we have done to estimate critical torque. Second, we simulate a possible resistance training session consisting of 5 sets of 5 maximum contractions lasting 5 s with 5 s inter-repetition rest and 120 s inter-set rest (Scenario RTS). For both scenarios, we then analyze the differences of end-MVIC torque of the perturbed settings to the nominal setting p. The kernel density estimates used for this

analysis were obtained using the gaussian_kde function of SciPy 1.2.1 [Virtanen et al., 2020] with Scott's rule of thumb for bandwidth selection.

Table 12.2 contains an overview of the simulation scenarios used in this chapter.

Table 12.2: Overview of simulation scenarios used in this chapter.

Scenario	Explanation
ITS	Intuitive testing session consisting of a 3 min MVIC effort followed by 2 s MVIC efforts at 10 s, 30 s, 1 min, 2 min, 5 min, 10 min, 15 min, 20 min, 25 min, and 30 min after cessation of the sustained MVIC effort to check the time course of recovery
OTS200	Optimized testing session lasting 1982 s in total with 200 s time-under-tension and a maximum of 11 contractions
OTS400	Optimized testing session lasting 1982 s in total with 400 s time-under-tension and a maximum of 11 contractions
RTS	Resistance training session consisting of 5 sets of 5 MVIC efforts lasting 5 s with 5 s inter-repetition rest and 120 s inter-set rest

12.5 Numerical results

Figures 12.1, 12.2, and 12.3 illustrate the loading schemes and the model response of the intuitive and the optimized testing sessions. Figure 12.4 illustrates the estimated standard deviations of the model parameters and the trace of the variance-covariance matrix resulting from these sessions.

The loading scheme of Scenario RTS is illustrated in Figure 12.5. Figures 12.6 and 12.7 show the kernel density estimates of the differences of end-MVIC torque of the perturbed settings to the nominal setting p for both scenarios. Figure 12.4 illustrates the standard deviations of those differences.

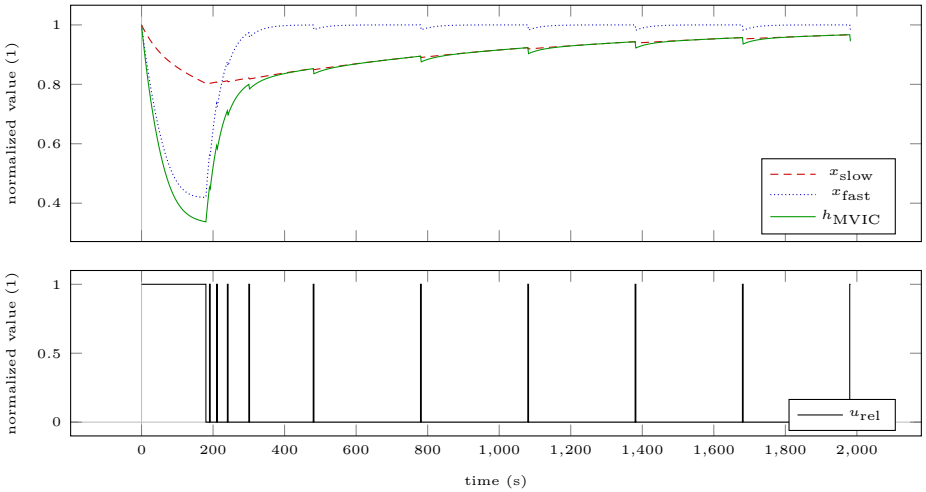

Figure 12.1: Model response obtained by simulating the intuitive testing session ITS. The bottom row illustrates the relative torque input. All contractions are maximal.

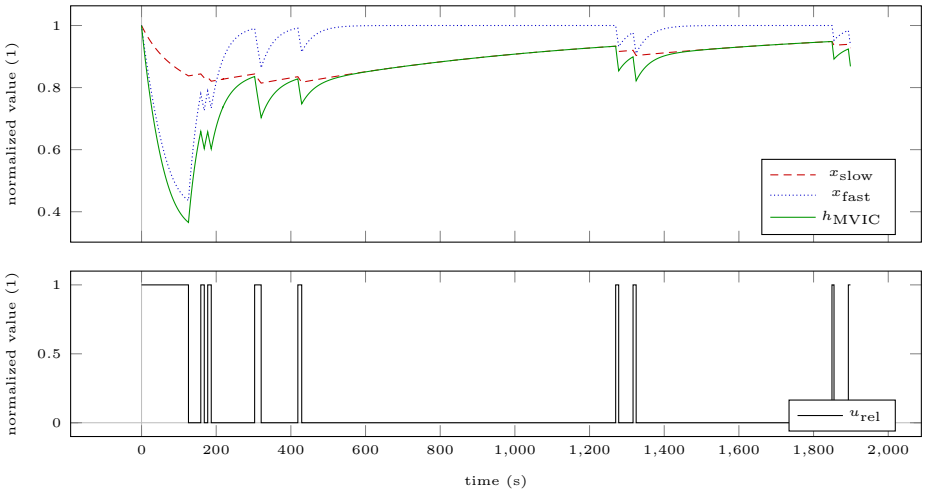

Figure 12.2: Model response obtained by simulating the optimized testing session OTS200. The bottom row illustrates the relative torque input. All contractions are maximal.

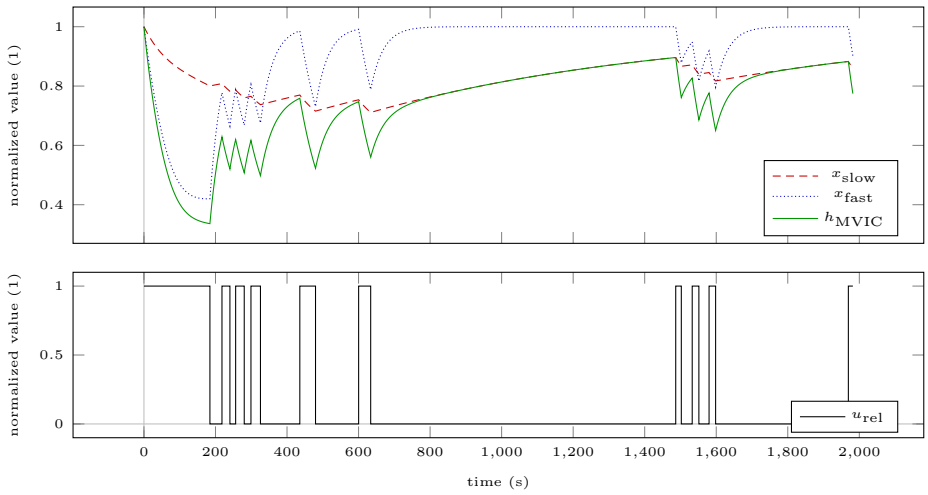

Figure 12.3: Model response obtained by simulating the optimized testing session OTS400. The bottom row illustrates the relative torque input. All contractions are maximal.

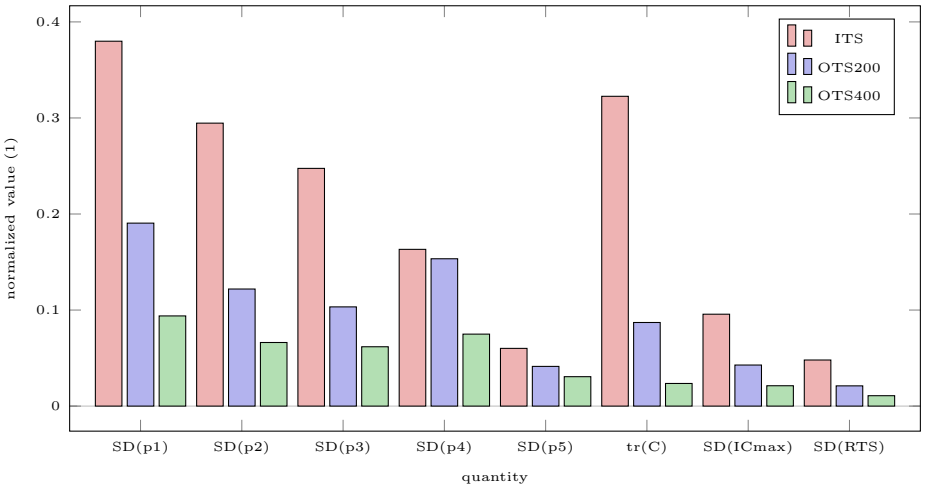

Figure 12.4: Estimated standard deviations of the model parameters SD(p) and trace tr(C) of the variance-covariance matrix resulting from the intuitive (Scenario ITS) and the optimized testing sessions (Scenarios OTS200 and OTS400). All parameters were scaled to 1 for the OED computations. Furthermore, SD(ICmax) and SD(RTS) denote the standard deviations of the differences of end-MVIC torque of the 10000 perturbed settings from the nominal setting p using the parameter uncertainties resulting from the intuitive testing session (ITS) and from the optimized testing sessions (OTS200 and OTS400).

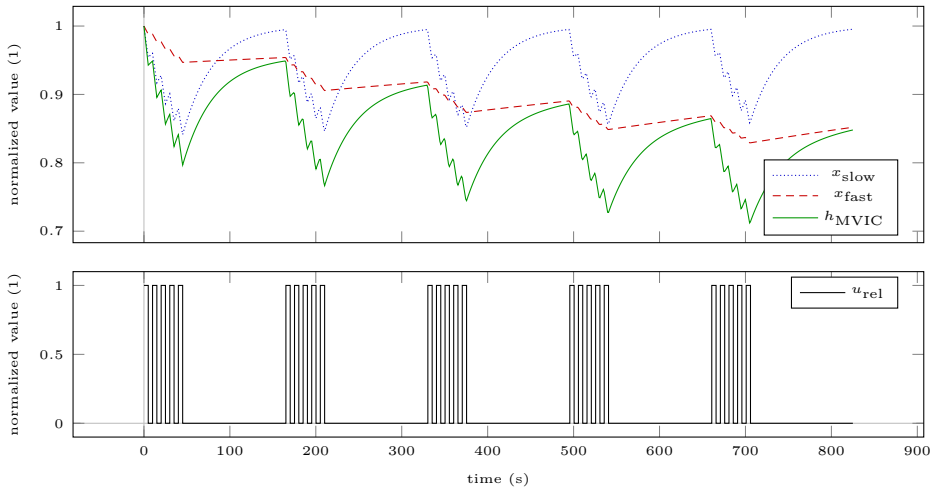

Figure 12.5: Model response obtained by simulating Scenario RTS. The bottom row illustrates the relative torque input. This is one of two scenarios used to examine how the parameter uncertainties propagate through the model.

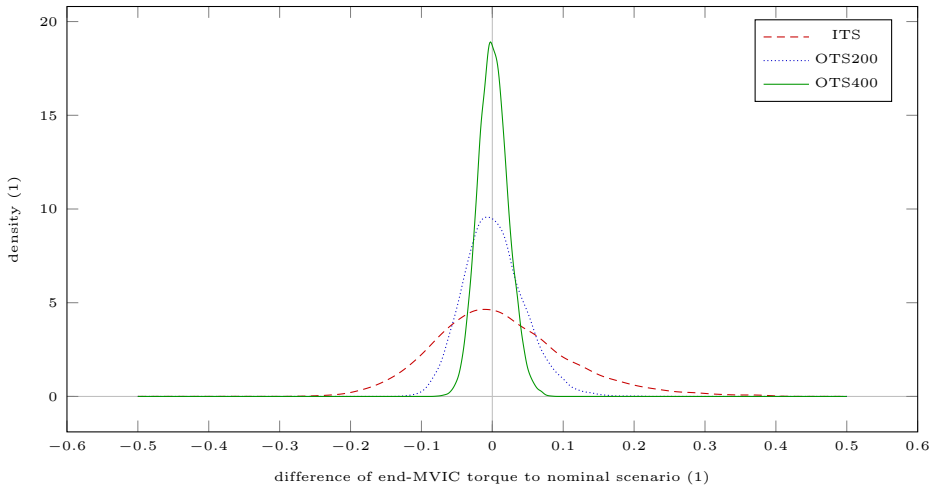

Figure 12.6: Kernel density estimates obtained by analyzing the differences of end-MVIC torque of the 10000 perturbed settings from the nominal setting p using the parameter uncertainties resulting from the intuitive testing session (ITS) and from the optimized testing sessions (OTS200 and OTS400). This plot shows the results for Scenario ICmax. The parameter uncertainties of the optimized testing sessions result in sharper peaks around the mean value 0.

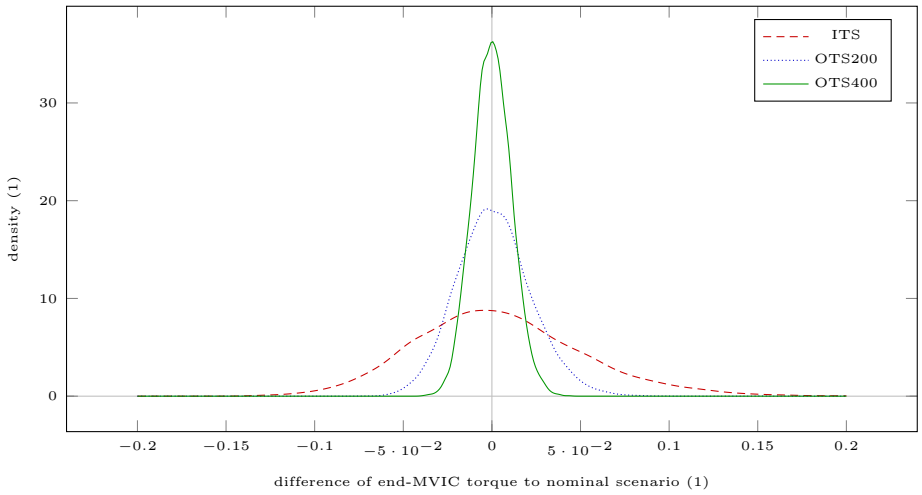

Figure 12.7: Kernel density estimates obtained by analyzing the differences of end-MVIC torque of the 10000 perturbed settings from the nominal setting p using the parameter uncertainties resulting from the intuitive testing session (ITS) and from the optimized testing sessions (OTS200 and OTS400). This plot shows the results for Scenario RTS. The parameter uncertainties of the optimized testing sessions result in sharper peaks around the mean value 0.

12.6 Discussion

Figure 12.4 illustrates that the optimized testing session OTS200 decreases the uncertainties of all parameters substantially compared to the intuitive session ITS. Scenario OTS200 consists of a prolonged MVIC effort in the beginning and 8 MVIC efforts afterwards. Those are of slightly longer duration and distributed differently than in the intuitive testing session. However, the constraints imposed on the total time and on the time-under-tension seem to be too restrictive to allow an actual identification of the parameters.

Therefore, we increase the limit on TUT for the OED problem OTS400. Here, all parameters can be identified with reasonable accuracy (SD $\leq$ 10 %). We acknowledge that a testing session lasting more than 30 min with almost 7 min of maximum contractions is taxing on the subjects. Nevertheless, we are certain that the benefit of calibrating the model in a single session outweighs this aspect. In case a testing session has to be stopped, the measurement data does not have to be discarded but can be used in a multi-experiment setting [Schlöder and Bock, 1983] for subsequent parameter estimations. This is a further advantage of our approach.

These scenarios serve as representative real-world examples and the improvements in Figure 12.4 demonstrate what an optimization-based approach to designing experiments is capable of. Depending on the preferences of the experimenters and the subjects, further experiments could be designed in a straightforward manner reducing the experimental effort considerably.

As the parameters of the model do not bear a direct physiological meaning, designing specific experiments to reduce their uncertainties might seem unnecessary to practitioners. It is important to keep in mind that the uncertainties of the parameter estimates propagate through the model and influence other quantities of interest. Our simulations of the perturbed settings illustrate this influence on the estimate of critical torque and end-MVIC torque of a potential resistance training session. Scenario RTS was chosen as a further illustrative example since the model was designed to optimize such scenarios. The standard deviations in Figure 12.4 and the kernel density estimates of Figures 12.6 and 12.7 demonstrate clearly how reduced parameter uncertainties improve the model prediction.

12.7 Conclusion

We are able to estimate the model parameters with satisfying accuracy in a single optimized testing session. This reduces the experimental effort considerably when calibrating the model to the trainee.

Conclusion and outlook

In this thesis, we developed a novel mathematical approach to model, simulate, and optimize loading schemes for resistance training. Our approach allows to work with small amounts of data, which is common in sports science or exercise physiology. Using data from the elbow flexors as example, we demonstrated the full process of collecting data, modeling, calibrating the model by estimating parameters, analyzing simulations, computing optimal loading schemes for different training goals, and designing optimal experiments for model calibration. Along this process, we highlighted and tackled the arising mathematical challenges and transferred our results to resistance training practice.

Our work underlines the possibilities which can arise by fostering interdisciplinary cooperations between sports scientists and applied mathematicians and creates the foundation for further research once suitable data and models become available. This includes the validation of the model for individual subjects and other muscle groups, but also other contraction modes and long-term adaptations should be taken into account by researchers building on our work. We expect these extensions to yield significant contributions to the fields of scientific computing on the one hand and sports science and exercise physiology on the other hand.

Danksagung

Diese Arbeit wäre ohne eine Vielzahl von Personen nicht möglich gewesen, denen allen ich zu tiefstem Dank verpflichtet bin. Aus meinem Arbeitsumfeld seien eine wenige im Folgenden explizit erwähnt.

Mein besonderer Dank gilt Hans Georg Bock und Johannes Schlöder dafür, dass sie mir in ihrer Arbeitsgruppe „Simulation und Optimierung“ am Interdisziplinären Zentrum für Wissenschaftliches Rechnen (IWR) der Universität Heidelberg die finanziellen Möglichkeiten und wissenschaftlichen Freiheiten zur Verfügung gestellt haben, um diese Arbeit zu verwirklichen.

Bei meinen Koautoren Johannes Schlöder, Christian Kirches und Andreas Sommer möchte ich mich für die gemeinsamen Publikationen im Zusammenhang mit dieser Arbeit bedanken und dafür, dass sie sich die Zeit genommen haben meine Ideen zu diskutieren und in die richtigen Bahnen zu lenken. In diesem Zusammenhang sei auch den Editoren und Reviewern unserer Publikationen zu danken – für hilfreiche Kommentare und die Möglichkeit neue Nicht-Standard-Ansätze innerhalb der Sportwissenschaften zu veröffentlichen.

Für die Finanzierung eines Stipendiums bedanke ich mich bei der Heidelberg Graduate School of Mathematical and Computational Methods for the Sciences (GSC 220), die durch die Deutsche Forschungsgemeinschaft (DFG) im Rahmen der Exzellenzinitiative finanziert wurde. Weiterhin bedanke ich mich bei der DFG für Finanzierung im Rahmen des Projekts „Wissenschaftliches Rechnen (ZUK 5.4)“ innerhalb des Zukunftskonzepts der Universität Heidelberg. Beim Bundesministerium für Bildung und Forschung (BMBF) bedanke ich mich für Finanzierung im Rahmen des Projekts „Modellierung, Optimierung und Regelung von Netzwerken heterogener Energiesysteme mit volatiler erneuerbarer Energieerzeugung (MOReNet, 05M18VHA)“.

Weiterhin möchte ich mich bedanken ...
... bei Janet Taylor dafür, dass sie mir ohne große Umschweife die Daten ihrer Publikationen zur Verfügung gestellt und erklärt hat,
... bei Matt Millard für einige entscheidende Hinweise zur Planung dieser Arbeit,
... bei Stefan Körkel, Klaus Roth, Sebastian Walter und Markus Buchner für das Initiieren des Projekts und die Betreuung in der Anfangsphase,
... bei Abir Al-Laham, Anja Vogel, Anastasia Walter und Jeannette Walsch für die administrative Hilfe innerhalb der Arbeitsgruppe,
... bei Thomas Kloepfer für seine Hilfe bei jeglichen technischen Angelegenheiten,

Danksagung

. . . bei Anne Paulski für die Zusammenarbeit in ZUK 5.4,
. . . bei Ramona Ludwig für die Zusammenarbeit in MOReNet,
. . . bei meinen Koautoren und Jürgen Gutekunst für das Korrekturlesen,
. . . und bei meinen Kollegen für die sehr angenehme und interessante Zeit.

Heidelberg, 2020

Bibliography

L. H. P. Abdalla, B. S. Denadai, N. M. Bassan, and C. C. Greco. Exercise tolerance during muscle contractions below and above the critical torque in different muscle groups. *Applied Physiology, Nutrition, and Metabolism*, 43(2): 174–179, 2018. doi: 10.1139/apnm-2017-0381. URL `https://doi.org/10.1139/apnm-2017-0381`.

J. Albersmeyer. Adjoint based algorithms and numerical methods for sensitivity generation and optimization of large scale dynamic systems. Dissertation, Heidelberg University, 2010. URL `https://doi.org/10.11588/heidok.00011651`. doi: 10.11588/heidok.00011651.

D. G. Allen, G. D. Lamb, and H. Westerblad. Skeletal Muscle Fatigue: Cellular Mechanisms. *Physiological Reviews*, 88(1):287–332, 2008. doi: 10.1152/physrev.00015.2007. URL `https://doi.org/10.1152/physrev.00015.2007`.

G. M. Allen, S. C. Gandevia, and D. K. McKenzie. Reliability of measurements of muscle strength and voluntary activation using twitch interpolation. *Muscle & Nerve*, 18(6):593–600, 1995. doi: 10.1002/mus.880180605. URL `https://doi.org/10.1002/mus.880180605`.

American College of Sports Medicine. American College of Sports Medicine Position Stand. Progression Models in Resistance Training for Healthy Adults. *Medicine & Science in Sports & Exercise*, 41(3):687, 2009. doi: 10.1249/MSS.0b013e3181915670. URL `https://doi.org/10.1249/MSS.0b013e3181915670`.

American College of Sports Medicine. ACSM Information On Resistance Training for Health and Fitness, 2013. URL `https://www.prescriptiontogetactive.com/static/pdfs/resistance-training-ACSM.pdf`. Accessed on 2020-04-21.

O. Arandjelović. A mathematical model of neuromuscular adaptation to resistance training and its application in a computer simulation of accommodating loads. *European Journal of Applied Physiology*, 110(3):523–538, 2010. doi: 10.1007/s00421-010-1526-3. URL `https://doi.org/10.1007/s00421-010-1526-3`.

O. Arandjelović. Optimal effort investment for overcoming the weakest point: new insights from a computational model of neuromuscular adaptation. *European Journal of Applied Physiology*, 111(8):1715–1723, Aug 2011. doi: 10.1007/s00421-010-1814-y. URL `https://doi.org/10.1007/s00421-010-1814-y`.

O. Arandjelović. Common Variants of the Resistance Mechanism in the Smith Machine: Analysis of Mechanical Loading Characteristics and Application to Strength-Oriented and Hypertrophy-Oriented Training. *The Journal of*

Strength & Conditioning Research, 26(2):350–363, 2012. doi: 10.1519/JSC.0b013e318220e6d2. URL https://doi.org/10.1519/JSC.0b013e318220e6d2.

O. Arandjelović. Computer simulation based parameter selection for resistance exercise. *arXiv preprint arXiv:1306.4724*, 2013a. URL https://arxiv.org/abs/1306.4724.

O. Arandjelović. Does cheating pay: the role of externally supplied momentum on muscular force in resistance exercise. *European Journal of Applied Physiology*, 113(1):135–145, Jan 2013b. doi: 10.1007/s00421-012-2420-y. URL https://doi.org/10.1007/s00421-012-2420-y.

O. Arandjelović. Computer-Aided Parameter Selection for Resistance Exercise Using Machine Vision-Based Capability Profile Estimation. *Augmented Human Research*, 2(1):4, Jul 2017. doi: 10.1007/s41133-017-0007-1. URL https://doi.org/10.1007/s41133-017-0007-1.

G. Atkinson, O. Peacock, and L. Passfield. Variable versus constant power strategies during cycling time-trials: Prediction of time savings using an up-to-date mathematical model. *Journal of Sports Sciences*, 25(9):1001–1009, 2007. doi: 10.1080/02640410600944709. URL https://doi.org/10.1080/02640410600944709.

E. W. Banister. The perception of effort: An inductive approach. *European Journal of Applied Physiology and Occupational Physiology*, 41(2):141–150, Jun 1979. doi: 10.1007/BF00421661. URL https://doi.org/10.1007/BF00421661.

E. W. Banister, T. W. Calvert, M. V. Savage, and T. M. Bach. A system model of training for athletic performance. *Australian Journal of Sports Medicine*, 7 (3):57–61, 1975.

Y. Bard. *Nonlinear Parameter Estimation*. Academic Press, 1974.

W. S. Barnes. The relationship between maximum isometric strength and intramuscular circulatory occlusion. *Ergonomics*, 23(4):351–357, 1980. doi: 10.1080/00140138008924748. URL https://doi.org/10.1080/00140138008924748.

I. Bauer. Numerische Verfahren zur Lösung von Anfangswertaufgaben und zur Generierung von ersten und zweiten Ableitungen mit Anwendungen bei Optimierungsaufgaben in Chemie und Verfahrenstechnik. Dissertation, Heidelberg University, January 1999. URL https://doi.org/10.11588/heidok.00001513. doi: 10.11588/heidok.00001513.

S. Benzekry, C. Lamont, A. Beheshti, A. Tracz, J. M. L. Ebos, L. Hlatky, and P. Hahnfeldt. Classical Mathematical Models for Description and Prediction of Experimental Tumor Growth. *PLOS Computational Biology*, 10(8):1–19, 08 2014. doi: 10.1371/journal.pcbi.1003800. URL https://doi.org/10.1371/journal.pcbi.1003800.

B. R. Bigland-Ritchie, N. J. Dawson, R. S. Johansson, and O. C. Lippold. Reflex origin for the slowing of motoneurone firing rates in fatigue of human voluntary contractions. *The Journal of Physiology*, 379(1):451–459, 1986. doi: 10.1113/jphysiol.1986.sp016263. URL https://doi.org/10.1113/jphysiol.1986.sp016263.

S. P. Bird, K. M. Tarpenning, and F. E. Marino. Designing Resistance Training Programmes to Enhance Muscular Fitness: A Review of the Acute Programme Variables. *Sports Medicine*, 35(10):841–851, 2005. doi: 10.2165/00007256-200535100-00002. URL https://doi.org/10.2165/00007256-200535100-00002.

C. Bischof, A. Carle, P. Hovland, P. Khademi, and A. Mauer. ADIFOR 2.0 Users' Guide (Revision D). Technical report, Mathematics and Computer Science Division Technical Memorandum No. 192 and Center for Research on Parallel Computation Technical Report CRPC-95516-S, 1998. URL https://doi.org/10.2172/93483. doi: 10.2172/93483.

H. G. Bock. Numerical Treatment of Inverse Problems in Chemical Reaction Kinetics. In K. H. Ebert, P. Deuflhard, and W. Jäger, editors, *Modelling of Chemical Reaction Systems: Proceedings of an International Workshop, Heidelberg, Fed. Rep. of Germany, September 1–5, 1980*, pages 102–125. Springer Berlin Heidelberg, 1981. doi: 10.1007/978-3-642-68220-9_8. URL https://doi.org/10.1007/978-3-642-68220-9_8.

H. G. Bock. Randwertproblemmethoden zur Parameteridentifizierung in Systemen nichtlinearer Differentialgleichungen. Dissertation, Rheinische Friedrich-Wilhelms-Universität Bonn, 1987.

H. G. Bock and K.-J. Plitt. A Multiple Shooting Algorithm for Direct Solution of Optimal Control Problems. In *Proceedings of the 9th IFAC World Congress*, pages 1603–1608. Pergamon Press, Oxford, 1984. doi: 10.1016/s1474-6670(17)61205-9. URL https://doi.org/10.1016/s1474-6670(17)61205-9.

H. G. Bock, E. Kostina, and J. P. Schlöder. On the Role of Natural Level Functions to Achieve Global Convergence for Damped Newton Methods. In M. J. D. Powell and S. Scholtes, editors, *System Modelling and Optimization: Methods, Theory and Applications. 19th IFIP TC7 Conference on System Modelling and Optimization July 12–16, 1999, Cambridge, UK*, pages 51–74, 2000. doi: 10.1007/978-0-387-35514-6_3. URL http://dx.doi.org/10.1007/978-0-387-35514-6_3.

H. G. Bock, E. Kostina, and J. P. Schlöder. Numerical Methods for Parameter Estimation in Nonlinear Differential Algebraic Equations. *GAMM-Mitteilungen*, 30(2):376–408, 2007. doi: 10.1002/gamm.200790024. URL https://doi.org/10.1002/gamm.200790024.

H. G. Bock, S. Körkel, and J. P. Schlöder. Parameter Estimation and Optimum Experimental Design for Differential Equation Models. In H. G. Bock, T. Carraro, W. Jäger, S. Körkel, R. Rannacher, and J. P. Schlöder, editors, *Model Based Parameter Estimation: Theory and Applications*, pages 1–30. Springer Berlin Heidelberg, 2013. doi: 10.1007/978-3-642-30367-8_1. URL https://doi.org/10.1007/978-3-642-30367-8_1.

L. E. Brown and J. P. Weir. ASEP Procedures Recommendation I: Accurate Assessment Of Muscular Strength And Power. *Journal of Exercise Physiology*, 4(11), 2001. URL https://www.asep.org/asep/asep/Brown2.pdf. Accessed on 2020-06-06.

N. Brown, D. Bubeck, D. F. B. Haeufle, J. Weickenmeier, E. Kuhl, W. Alt, and S. Schmitt. Weekly Time Course of Neuro-Muscular Adaptation to Intensive Strength Training. *Frontiers in Physiology*, 8:329, 2017. doi: 10.3389/fphys.2017.00329. URL https://doi.org/10.3389/fphys.2017.00329.

R. Broxterman, C. Ade, S. Wilcox, S. Schlup, J. Craig, and T. Barstow. Influence of duty cycle on the power-duration relationship: Observations and potential mechanisms. *Respiratory Physiology & Neurobiology*, 192:102–111, 2014. doi: 10.1016/j.resp.2013.11.010. URL https://doi.org/10.1016/j.resp.2013.11.010.

N. A. Burd, R. J. Andrews, D. W. West, J. P. Little, A. J. Cochran, A. J. Hector, J. G. Cashaback, M. J. Gibala, J. R. Potvin, S. K. Baker, and S. M. Phillips. Muscle time under tension during resistance exercise stimulates differential muscle protein sub-fractional synthetic responses in men. *The Journal of Physiology*, 590(2):351–362, 2012. doi: 10.1113/jphysiol.2011.221200. URL https://doi.org/10.1113/jphysiol.2011.221200.

K. P. Burnham and D. R. Anderson. *Model Selection and Multimodel Inference*. Springer New York, 2002. doi: 10.1007/b97636. URL https://doi.org/10.1007/b97636.

M. Burnley. Estimation of critical torque using intermittent isometric maximal voluntary contractions of the quadriceps in humans. *Journal of Applied Physiology*, 106(3):975–983, 2009. doi: 10.1152/japplphysiol.91474.2008. URL https://doi.org/10.1152/japplphysiol.91474.2008.

M. Burnley, A. Vanhatalo, and A. M. Jones. Distinct profiles of neuromuscular fatigue during muscle contractions below and above the critical torque in humans. *Journal of Applied Physiology*, 113(2):215–223, 2012. doi: 10.1152/japplphysiol.00022.2012. URL https://doi.org/10.1152/japplphysiol.00022.2012.

T. Busso, K. Häkkinen, A. Pakarinen, C. Carasso, J. R. Lacour, P. V. Komi, and H. Kauhanen. A systems model of training responses and its relationship to

hormonal responses in elite weight-lifters. *European Journal of Applied Physiology and Occupational Physiology*, 61(1):48–54, 1990. doi: 10.1007/BF00236693. URL https://doi.org/10.1007/BF00236693.

T. Busso, K. Häkkinen, A. Pakarinen, H. Kauhanen, P. V. Komi, and J. R. Lacour. Hormonal adaptations and modelled responses in elite weightlifters during 6 weeks of training. *European Journal of Applied Physiology and Occupational Physiology*, 64(4):381–386, Jul 1992. doi: 10.1007/BF00636228. URL https://doi.org/10.1007/BF00636228.

G. Caffier, H. Rehfeldt, H. Kramer, and R. Mucke. Fatigue during sustained maximal voluntary contraction of different muscles in humans: dependence on fibre type and body posture. *European Journal of Applied Physiology and Occupational Physiology*, 64(3):237–243, May 1992. doi: 10.1007/BF00626286. URL https://doi.org/10.1007/BF00626286.

D. M. Callahan, B. R. Umberger, and J. A. Kent-Braun. A Computational Model of Torque Generation: Neural, Contractile, Metabolic and Musculoskeletal Components. *PLOS ONE*, 8(2):1–11, 02 2013. doi: 10.1371/journal.pone.0056013. URL https://doi.org/10.1371/journal.pone.0056013.

D. M. Callahan, B. R. Umberger, and J. A. Kent. Mechanisms of in vivo muscle fatigue in humans: investigating age-related fatigue resistance with a computational model. *The Journal of Physiology*, 594(12):3407–3421, 2016. doi: 10.1113/JP271400. URL https://doi.org/10.1113/JP271400.

T. W. Calvert, E. W. Banister, M. V. Savage, and T. Bach. A Systems Model of the Effects of Training on Physical Performance. *IEEE Transactions on Systems, Man, and Cybernetics*, (2):94–102, 1976. doi: 10.1109/tsmc.1976.5409179. URL https://doi.org/10.1109/tsmc.1976.5409179.

G. E. Campos, T. J. Luecke, H. K. Wendeln, K. Toma, F. C. Hagerman, T. F. Murray, K. E. Ragg, N. A. Ratamess, W. J. Kraemer, and R. S. Staron. Muscular adaptations in response to three different resistance-training regimens: specificity of repetition maximum training zones. *European Journal of Applied Physiology*, 88(1):50–60, 2002. doi: 10.1007/s00421-002-0681-6. URL https://doi.org/10.1007/s00421-002-0681-6.

T. J. Carroll, J. L. Taylor, and S. C. Gandevia. Recovery of central and peripheral neuromuscular fatigue after exercise. *Journal of Applied Physiology*, 122(5):1068–1076, 2017. doi: 10.1152/japplphysiol.00775.2016. URL https://doi.org/10.1152/japplphysiol.00775.2016.

I. E. Clark, A. Vanhatalo, S. J. Bailey, L. J. Wylie, B. S. Kirby, B. W. Wilkins, and A. M. Jones. Effects of Two Hours of Heavy-Intensity Exercise on the Power-Duration Relationship. *Medicine & Science in Sports & Exercise*, 50(8):1658–1668, 2018. doi: 10.1249/MSS.0000000000001601. URL https://doi.org/10.1249/MSS.0000000000001601.

D. C. Clarke and P. F. Skiba. Rationale and resources for teaching the mathematical modeling of athletic training and performance. *Advances in Physiology Education*, 37(2):134–152, 2013. doi: 10.1152/advan.00078.2011. URL https://doi.org/10.1152/advan.00078.2011.

D. H. Clarke. Strength Recovery from Static and Dynamic Muscular Fatigue. *Research Quarterly. American Association for Health, Physical Education and Recreation*, 33(3):349–355, 1962. doi: 10.1080/10671188.1962.10616463. URL https://doi.org/10.1080/10671188.1962.10616463.

P. Contessa and C. J. D. Luca. Neural control of muscle force: indications from a simulation model. *Journal of Neurophysiology*, 109(6):1548–1570, 2013. doi: 10.1152/jn.00237.2012. URL https://doi.org/10.1152/jn.00237.2012.

P. Contessa, A. Adam, and C. J. De Luca. Motor unit control and force fluctuation during fatigue. *Journal of Applied Physiology*, 107(1):235–243, 2009. doi: 10.1152/japplphysiol.00035.2009. URL https://doi.org/10.1152/japplphysiol.00035.2009.

J. C. Craig, A. Vanhatalo, M. Burnley, A. M. Jones, and D. C. Poole. Chapter 8 - Critical Power: Possibly the Most Important Fatigue Threshold in Exercise Physiology. In J. A. Zoladz, editor, *Muscle and Exercise Physiology*, pages 159–181. Academic Press, 2019. doi: 10.1016/B978-0-12-814593-7.00008-6. URL https://doi.org/10.1016/B978-0-12-814593-7.00008-6.

B. Crewther, J. Cronin, and J. Keogh. Possible Stimuli for Strength and Power Adaptation. *Sports Medicine*, 35(11):967–989, Nov 2005. doi: 10.2165/00007256-200535110-00004. URL https://doi.org/10.2165/00007256-200535110-00004.

J. M. Deeb, C. G. Drury, and D. R. Pendergast. An exponential model of isometric muscular fatigue as a function of age and muscle groups. *Ergonomics*, 35(7-8):899–918, 1992. doi: 10.1080/00140139208967370. URL https://doi.org/10.1080/00140139208967370.

J. L. Dideriksen, D. Farina, M. Baekgaard, and R. M. Enoka. An integrative model of motor unit activity during sustained submaximal contractions. *Journal of Applied Physiology*, 108(6):1550–1562, 2010. doi: 10.1152/japplphysiol.01017.2009. URL https://doi.org/10.1152/japplphysiol.01017.2009.

K. El ahrache, D. Imbeau, and B. Farbos. Percentile values for determining maximum endurance times for static muscular work. *International Journal of Industrial Ergonomics*, 36(2):99–108, 2006. doi: 10.1016/j.ergon.2005.08.003. URL https://doi.org/10.1016/j.ergon.2005.08.003.

R. M. Enoka and J. Duchateau. Muscle fatigue: what, why and how it influences muscle function. *The Journal of Physiology*, 586(1):11–23, 2008. doi: 10.1113/jphysiol.2007.139477. URL https://doi.org/10.1113/jphysiol.2007.139477.

A. Eriksson. Optimization in target movement simulations. *Computer Methods in Applied Mechanics and Engineering*, 197(49):4207 – 4215, 2008. doi: 10.1016/j.cma.2008.04.017. URL https://doi.org/10.1016/j.cma.2008.04.017.

A. Eriksson and A. Nordmark. Activation dynamics in the optimization of targeted movements. *Computers & Structures*, 89(11):968 – 976, 2011. doi: 10.1016/j.compstruc.2011.01.019. URL https://doi.org/10.1016/j.compstruc.2011.01.019.

A. Eriksson, H.-C. Holmberg, and H. Westerblad. A numerical model for fatigue effects in whole-body human exercise. *Mathematical and Computer Modelling of Dynamical Systems*, 22(1):21–38, 2016. doi: 10.1080/13873954.2015.1083592. URL https://doi.org/10.1080/13873954.2015.1083592.

J. W. Evans. Periodized Resistance Training for Enhancing Skeletal Muscle Hypertrophy and Strength: A Mini-Review. *Frontiers in Physiology*, 10:13, 2019. doi: 10.3389/fphys.2019.00013. URL https://doi.org/10.3389/fphys.2019.00013.

S. A. Fayazi, N. Wan, S. Lucich, A. Vahidi, and G. Mocko. Optimal pacing in a cycling time-trial considering cyclist's fatigue dynamics. In *2013 American Control Conference*, pages 6442–6447, June 2013. doi: 10.1109/ACC.2013.6580849. URL https://doi.org/10.1109/ACC.2013.6580849.

S. J. Fleck and W. Kraemer. *Designing Resistance Training Programs, 4E*. Human Kinetics, 2014. URL https://books.google.com/books?id=CczZAgAAQBAJ.

J. Freund and E.-P. Takala. A dynamic model of the forearm including fatigue. *Journal of Biomechanics*, 34(5):597–605, 2001. doi: 10.1016/S0021-9290(01)00009-4. URL https://doi.org/10.1016/S0021-9290(01)00009-4.

L. A. Frey-Law and K. G. Avin. Endurance time is joint-specific: A modelling and meta-analysis investigation. *Ergonomics*, 53(1):109–129, 2010. doi: 10.1080/00140130903389068. URL https://doi.org/10.1080/00140130903389068.

A. J. Fuglevand, D. A. Winter, and A. E. Patla. Models of recruitment and rate coding organization in motor-unit pools. *Journal of Neurophysiology*, 70(6):2470–2488, 1993. doi: 10.1152/jn.1993.70.6.2470. URL https://doi.org/10.1152/jn.1993.70.6.2470.

J. P. Gacesa, T. Ivancevic, N. Ivancevic, F. P. Paljic, and N. Grujic. Nonlinear dynamics in muscle fatigue and strength model during maximal self-perceived elbow extensors training. *Journal of Biomechanics*, 43(12):2440 – 2443, 2010. doi: 10.1016/j.jbiomech.2010.04.034. URL https://doi.org/10.1016/j.jbiomech.2010.04.034.

S. C. Gandevia. Spinal and Supraspinal Factors in Human Muscle Fatigue. *Physiological Reviews*, 81(4):1725–1789, 2001. doi: 10.1152/physrev.2001.81.4.1725. URL https://doi.org/10.1152/physrev.2001.81.4.1725.

S. C. Gandevia, G. M. Allen, J. E. Butler, and J. L. Taylor. Supraspinal factors in human muscle fatigue: evidence for suboptimal output from the motor cortex. *The Journal of Physiology*, 490(2):529–536, 1996. doi: 10.1113/jphysiol.1996.sp021164. URL https://doi.org/10.1113/jphysiol.1996.sp021164.

C. J. Gatti, J. Scibek, O. Svintsitski, J. E. Carpenter, and R. E. Hughes. An Integer Programming Model for Optimizing Shoulder Rehabilitation. *Annals of Biomedical Engineering*, 36(7):1242–1253, Jul 2008. doi: 10.1007/s10439-008-9491-2. URL https://doi.org/10.1007/s10439-008-9491-2.

G. Gede. *Optimal Pacing Strategies for Cyclist Time Trials*. PhD thesis, University of California, Davis, 2014. URL https://search.proquest.com/docview/1665571951.

G. Gede and M. Hubbard. A bioenergetic model for simulating athletic performance of intermediate duration. *Journal of Biomechanics*, 47(14):3448 – 3453, 2014. doi: 10.1016/j.jbiomech.2014.09.017. URL https://doi.org/10.1016/j.jbiomech.2014.09.017.

P. E. Gill, W. Murray, and M. A. Saunders. User's Guide for QPOPT 1.0: A Fortran Package for Quadratic Programming. Technical report, 1995.

P. E. Gill, W. Murray, and M. A. Saunders. SNOPT: An SQP Algorithm for Large-Scale Constrained Optimization. *SIAM Review*, 47(1):99–131, 2005. doi: 10.1137/S0036144504446096. URL https://doi.org/10.1137/S0036144504446096.

P. E. Gill, M. A. Saunders, and E. Wong. On the Performance of SQP Methods for Nonlinear Optimization. In B. Defourny and T. Terlaky, editors, *Modeling and Optimization: Theory and Applications*, pages 95–123, Cham, 2015. Springer International Publishing. doi: 10.1007/978-3-319-23699-5_5. URL https://doi.org/10.1007/978-3-319-23699-5_5.

K. P. Granata and P. Gottipati. Fatigue influences the dynamic stability of the torso. *Ergonomics*, 51(8):1258–1271, 2008. doi: 10.1080/00140130802030722. URL https://doi.org/10.1080/00140130802030722.

J. Grgic, P. Mikulic, H. Podnar, and Z. Pedisic. Effects of linear and daily undulating periodized resistance training programs on measures of muscle hypertrophy: a systematic review and meta-analysis. *PeerJ*, 5:e3695, 2017. doi: 10.7717/peerj.3695. URL https://doi.org/10.7717/peerj.3695.

J. Grgic, B. Lazinica, P. Mikulic, and B. Schoenfeld. Should resistance training programs aimed at muscular hypertrophy be periodized? A systematic review of periodized versus non-periodized approaches. *Science & Sports*, 33(3):e97 – e104, 2018a. doi: 10.1016/j.scispo.2017.09.005. URL https://doi.org/10.1016/j.scispo.2017.09.005.

J. Grgic, B. J. Schoenfeld, T. B. Davies, B. Lazinica, J. W. Krieger, and Z. Pedisic. Effect of Resistance Training Frequency on Gains in Muscular Strength: A Systematic Review and Meta-Analysis. *Sports Medicine*, 48(5):1207–1220, 2018b. doi: 10.1007/s40279-018-0872-x. URL https://doi.org/10.1007/s40279-018-0872-x.

J. Grgic, B. J. Schoenfeld, M. Skrepnik, T. B. Davies, and P. Mikulic. Effects of Rest Interval Duration in Resistance Training on Measures of Muscular Strength: A Systematic Review. *Sports Medicine*, 48(1):137–151, 2018c. doi: 10.1007/s40279-017-0788-x. URL https://doi.org/10.1007/s40279-017-0788-x.

A. Griewank and A. Walther. *Evaluating Derivatives: Principles and Techniques of Algorithmic Differentiation*. SIAM, 2nd edition, 2008. doi: 10.1137/1.9780898717761. URL https://doi.org/10.1137/1.9780898717761.

M. Hagberg. Muscular endurance and surface electromyogram in isometric and dynamic exercise. *Journal of Applied Physiology*, 51(1):1–7, 1981. doi: 10.1152/jappl.1981.51.1.1. URL https://doi.org/10.1152/jappl.1981.51.1.1.

E. Hairer and G. Wanner. *Solving Ordinary Differential Equations II*, volume 14 of *Springer Series in Computational Mathematics*. Springer, Berlin, 2nd edition, 1996. doi: 10.1007/978-3-642-05221-7. URL https://doi.org/10.1007/978-3-642-05221-7.

E. Hairer, S. P. Nørsett, and G. Wanner. *Solving Ordinary Differential Equations I*, volume 8 of *Springer Series in Computational Mathematics*. Springer, Berlin, 2nd edition, 1993. doi: 10.1007/978-3-540-78862-1. URL https://doi.org/10.1007/978-3-540-78862-1.

S. K. Harries, D. R. Lubans, and R. Callister. Systematic Review and Meta-analysis of Linear and Undulating Periodized Resistance Training Programs on Muscular Strength. *The Journal of Strength & Conditioning Research*, 29(4):1113–1125, 2015. doi: 10.1519/jsc.0000000000000712. URL https://doi.org/10.1519/jsc.0000000000000712.

K. Hatz. Efficient numerical methods for hierarchical dynamic optimization with application to cerebral palsy gait modeling. Dissertation, Heidelberg University, 2014. URL https://doi.org/10.11588/heidok.00016803. doi: 10.11588/heidok.00016803.

D. Hawkins and M. Hull. Muscle force as affected by fatigue: Mathematical model and experimental verification. *Journal of Biomechanics*, 26(9):1117–1128, 1993. doi: 10.1016/S0021-9290(05)80010-7. URL https://doi.org/10.1016/S0021-9290(05)80010-7.

D. A. Hawkins. *A cellular-based muscle model: Formulation and application for studying muscle mechanics*. PhD thesis, University of California, Davis, 1990. URL https://search.proquest.com/docview/303823538.

C. R. Hendrix, T. J. Housh, G. O. Johnson, M. Mielke, C. L. Camic, J. M. Zuniga, and R. J. Schmidt. Comparison of Critical Force to EMG Fatigue Thresholds during Isometric Leg Extension. *Medicine & Science in Sports & Exercise*, 41(4):956–964, 2009a. doi: 10.1249/MSS.0b013e318190bdf7. URL https://doi.org/10.1249/MSS.0b013e318190bdf7.

C. R. Hendrix, T. J. Housh, G. O. Johnson, J. P. Weir, T. W. Beck, M. H. Malek, M. Mielke, and R. J. Schmidt. A comparison of critical force and electromyographic fatigue threshold for isometric muscle actions of the forearm flexors. *European Journal of Applied Physiology*, 105(3):333–342, 2009b. doi: 10.1007/s00421-008-0895-3. URL https://doi.org/10.1007/s00421-008-0895-3.

C. R. Hendrix, T. J. Housh, C. L. Camic, J. M. Zuniga, G. O. Johnson, and R. J. Schmidt. Comparing electromyographic and mechanomyographic frequency-based fatigue thresholds to critical torque during isometric forearm flexion. *Journal of Neuroscience Methods*, 194(1):64 – 72, 2010. doi: 10.1016/j.jneumeth.2010.07.006. URL https://doi.org/10.1016/j.jneumeth.2010.07.006.

E. Henneman, G. Somjen, and D. O. Carpenter. Functional significance of cell size in spinal motoneurons. *Journal of Neurophysiology*, 28(3):560–580, 1965. doi: 10.1152/jn.1965.28.3.560. URL https://doi.org/10.1152/jn.1965.28.3.560.

J. L. Herold and A. Sommer. A model-based estimation of critical torques reduces the experimental effort compared to conventional testing. *European Journal of Applied Physiology*, Apr. 2020a. doi: 10.1007/s00421-020-04358-w. URL https://doi.org/10.1007/s00421-020-04358-w.

J. L. Herold and A. Sommer. A mathematical model-based approach to optimize loading schemes of isometric resistance training sessions. *Sports Engineering*, 2020b. doi: 10.1007/s12283-020-00337-8. URL https://doi.org/10.1007/s12283-020-00337-8.

J. L. Herold, C. Kirches, and J. P. Schlöder. A phenomenological model of the time course of maximal voluntary isometric contraction force for optimization of complex loading schemes. *European Journal of Applied Physiology*, 118(12):2587–2605, Dec 2018. doi: 10.1007/s00421-018-3983-z. URL https://doi.org/10.1007/s00421-018-3983-z.

W. Herzog. History dependence of skeletal muscle force production: Implications for movement control. *Human Movement Science*, 23(5):591 – 604, 2004. doi: 10.1016/j.humov.2004.10.003. URL https://doi.org/10.1016/j.humov.2004.10.003.

C. Hoffmann, C. Kirches, A. Potschka, S. Sager, and L. Wirsching. *MUSCOD-II User Manual*. Interdisciplinary Center for Scientific Computing (IWR), Heidelberg University, Germany, 2014.

M. Iguchi, K. Baldwin, C. Boeyink, C. Engle, M. Kehoe, A. Ganju, A. J. Messaros, and R. K. Shields. Low frequency fatigue in human quadriceps is fatigue dependent and not task dependent. *Journal of Electromyography and Kinesiology*, 18(2):308–316, 2008. doi: 10.1016/j.jelekin.2006.09.010. URL https://doi.org/10.1016/j.jelekin.2006.09.010.

A. James and S. Green. A phenomenological model of muscle fatigue and the power-endurance relationship. *Journal of Applied Physiology*, 113(10):1643–1651, 2012. doi: 10.1152/japplphysiol.00800.2012. URL https://doi.org/10.1152/japplphysiol.00800.2012.

D. Janka. Sequential quadratic programming with indefinite Hessian approximations for nonlinear optimum experimental design for parameter estimation in differential–algebraic equations. Dissertation, Heidelberg University, 2015. URL https://doi.org/10.11588/heidok.00019170. doi: 10.11588/heidok.00019170.

A. M. Jones and A. Vanhatalo. The 'Critical Power' Concept: Applications to Sports Performance with a Focus on Intermittent High-Intensity Exercise. *Sports Medicine*, 47(1):65–78, Mar 2017. doi: 10.1007/s40279-017-0688-0. URL https://doi.org/10.1007/s40279-017-0688-0.

A. M. Jones, M. Burnley, M. I. Black, D. C. Poole, and A. Vanhatalo. The maximal metabolic steady state: redefining the 'gold standard'. *Physiological Reports*, 7(10):e14098, 2019. doi: 10.14814/phy2.14098. URL https://doi.org/10.14814/phy2.14098.

D. A. Jones, O. M. Rutherford, and D. F. Parker. Physiological changes in skeletal muscle as a result of strength training. *Quarterly Journal of Experimental Physiology*, 74(3):233–256, May 1989. doi: 10.1113/expphysiol.1989.sp003268. URL https://doi.org/10.1113/expphysiol.1989.sp003268.

L. Jones and I. Hunter. Effect of fatigue on force sensation. *Experimental Neurology*, 81(3):640–650, 1983. doi: 10.1016/0014-4886(83)90332-1. URL https://doi.org/10.1016/0014-4886(83)90332-1.

Y. Kawakami, K. Amemiya, H. Kanehisa, S. Ikegawa, and T. Fukunaga. Fatigue responses of human triceps surae muscles during repetitive maximal isometric contractions. *Journal of Applied Physiology*, 88(6):1969–1975, 2000. doi: 10.1152/jappl.2000.88.6.1969. URL https://doi.org/10.1152/jappl.2000.88.6.1969.

J. M. Kellawan and M. E. Tschakovsky. The Single-Bout Forearm Critical Force Test: A New Method to Establish Forearm Aerobic Metabolic Exercise Intensity and Capacity. *PLOS ONE*, 9(4):1–10, 04 2014. doi: 10.1371/journal.pone.0093481. URL https://doi.org/10.1371/journal.pone.0093481.

D. S. Kennedy, C. J. McNeil, S. C. Gandevia, and J. L. Taylor. Firing of antagonist small-diameter muscle afferents reduces voluntary activation and torque of elbow flexors. *The Journal of Physiology*, 591(14):3591–3604, 2013. doi: 10.1113/jphysiol.2012.248559. URL https://doi.org/10.1113/jphysiol.2012.248559.

M. W. Keyserling, G. D. Herrin, and D. B. Chaffin. Isometric Strength Testing as a Means of Controlling Medical Incidents on Strenuous Jobs. *Journal of Occupational and Environmental Medicine*, 22(5):332–336, 1980. doi: 10.1097/00043764-198005000-00006. URL https://doi.org/10.1097/00043764-198005000-00006.

R. Kircheis. Structure Exploiting Parameter Estimation and Optimum Experimental Design Methods and Applications in Microbial Enhanced Oil Recovery. Dissertation, Heidelberg University, 2015. URL https://doi.org/10.11588/heidok.00022098. doi: 10.11588/heidok.00022098.

C. Kirches. A Numerical Method for Nonlinear Robust Optimal Control with Implicit Discontinuities and an Application to Powertrain Oscillations. Diploma thesis, Heidelberg University, 2006. URL http://mathopt.de/PUBLICATIONS/Kirches2006.pdf.

C. Kirches, H. G. Bock, J. P. Schlöder, and S. Sager. Complementary Condensing for the Direct Multiple Shooting Method. In *Modeling, Simulation and Optimization of Complex Processes*, pages 195–206. Springer Berlin Heidelberg, 2012. doi: 10.1007/978-3-642-25707-0_16. URL https://doi.org/10.1007/978-3-642-25707-0_16.

C. Kisner, L. A. Colby, and J. Borstad. *Therapeutic exercise: foundations and techniques*. F.A. Davis Company, Philadelphia, USA, 7th edition, 2017. URL https://books.google.com/books?id=yZc6DwAAQBAJ.

N. Kosterina, H. Westerblad, and A. Eriksson. History effect and timing of force production introduced in a skeletal muscle model. *Biomechanics and Modeling in Mechanobiology*, 11(7):947–957, Sep 2012. doi: 10.1007/s10237-011-0364-5. URL https://doi.org/10.1007/s10237-011-0364-5.

D. Kraft. A software package for sequential quadratic programming. *Forschungsbericht. Deutsche Forschungs- und Versuchsanstalt für Luft- und Raumfahrt*, 1988. URL https://books.google.com/books?id=4rKaGwAACAAJ.

J. W. Krieger. Single vs. Multiple Sets of Resistance Exercise for Muscle Hypertrophy: A Meta-Analysis. *The Journal of Strength & Conditioning Research*, 24(4):1150–1159, 2010. doi: 10.1519/jsc.0b013e3181d4d436. URL https://doi.org/10.1519/jsc.0b013e3181d4d436.

G. W. Kroon and M. Naeije. Recovery of the human biceps electromyogram after heavy eccentric, concentric or isometric exercise. *European Journal of*

Applied Physiology and Occupational Physiology, 63(6):444–448, Nov 1991. doi: 10.1007/BF00868076. URL https://doi.org/10.1007/BF00868076.

S. Körkel. Numerische Methoden für Optimale Versuchsplanungsprobleme bei nichtlinearen DAE-Modellen. Dissertation, Heidelberg University, 2002. URL https://doi.org/10.11588/heidok.00002980. doi: 10.11588/heidok.00002980.

D. T. Leetun, M. L. Ireland, J. D. Willson, B. T. Ballantyne, and I. M. Davis. Core Stability Measures as Risk Factors for Lower Extremity Injury in Athletes. *Medicine & Science in Sports & Exercise*, 36(6):926–934, 2004. doi: 10.1249/01.mss.0000128145.75199.c3. URL https://doi.org/10.1249/01.mss.0000128145.75199.C3.

D. B. Leineweber. Efficient Reduced SQP Methods for the Optimization of Chemical Processes Described by Large Sparse DAE Models. Dissertation, Heidelberg University, 1999.

D. B. Leineweber, I. Bauer, H. G. Bock, and J. P. Schlöder. An efficient multiple shooting based reduced SQP strategy for large-scale dynamic process optimization. Part 1: theoretical aspects. *Computers & Chemical Engineering*, 27(2):157–166, 2003a. doi: 10.1016/S0098-1354(02)00158-8. URL https://doi.org/10.1016/S0098-1354(02)00158-8.

D. B. Leineweber, A. Schäfer, H. G. Bock, and J. P. Schlöder. An efficient multiple shooting based reduced SQP strategy for large-scale dynamic process optimization. Part II: Software aspects and applications. *Computers & Chemical Engineering*, 27(2):167–174, 2003b. doi: 10.1016/S0098-1354(02)00195-3. URL https://doi.org/10.1016/S0098-1354(02)00195-3.

E. Lievens, M. Klass, T. Bex, and W. Derave. Muscle fiber typology substantially influences time to recover from high-intensity exercise. *Journal of Applied Physiology*, 2020. doi: 10.1152/japplphysiol.00636.2019. URL https://doi.org/10.1152/japplphysiol.00636.2019.

V. Linnamo, R. Bottas, and P. Komi. Force and EMG power spectrum during and after eccentric and concentric fatigue. *Journal of Electromyography and Kinesiology*, 10(5):293 – 300, 2000. doi: 10.1016/S1050-6411(00)00021-3. URL https://doi.org/10.1016/S1050-6411(00)00021-3.

J. Z. Liu, R. W. Brown, and G. H. Yue. A Dynamical Model of Muscle Activation, Fatigue, and Recovery. *Biophysical Journal*, 82(5):2344–2359, 2002. doi: 10.1016/S0006-3495(02)75580-X. URL https://doi.org/10.1016/S0006-3495(02)75580-X.

J. M. Looft. *Adaptation and validation of an analytical localized muscle fatigue model for workplace tasks*. PhD thesis, The University of Iowa, 2014. URL https://doi.org/10.17077/etd.up9amoqs.

D. Lum and T. M. Barbosa. Brief Review: Effects of Isometric Strength Training on Strength and Dynamic Performance. *International journal of sports medicine*, 2019. doi: 10.1055/a-0863-4539. URL https://doi.org/10.1055/a-0863-4539.

L. Ma, D. Chablat, F. Bennis, and W. Zhang. A new simple dynamic muscle fatigue model and its validation. *International Journal of Industrial Ergonomics*, 39(1): 211–220, 2009. doi: 10.1016/j.ergon.2008.04.004. URL https://doi.org/10.1016/j.ergon.2008.04.004.

L. Ma, D. Chablat, F. Bennis, W. Zhang, and F. Guillaume. A new muscle fatigue and recovery model and its ergonomics application in human simulation. *Virtual and Physical Prototyping*, 5(3):123–137, 2010. doi: 10.1080/17452759.2010.504056. URL https://doi.org/10.1080/17452759.2010.504056.

L. Ma, W. Zhang, S. Wu, and Z. Zhang. A new simple local muscle recovery model and its theoretical and experimental validation. *International Journal of Occupational Safety and Ergonomics*, 21(1):86–93, 2015. doi: 10.1080/10803548.2015.1017961. URL https://doi.org/10.1080/10803548.2015.1017961.

A. Mader. A transcription-translation activation feedback circuit as a function of protein degradation, with the quality of protein mass adaptation related to the average functional load. *Journal of Theoretical Biology*, 134(2):135 – 157, 1988. doi: 10.1016/S0022-5193(88)80198-X. URL https://doi.org/10.1016/S0022-5193(88)80198-X.

A. Mader. Aktive Belastungsadaptation und Regulation der Proteinsynthese auf zellulärer Ebene. *Deutsche Zeitschrift für Sportmedizin*, 41(2):40–58, 1990. URL https://www.bisp-surf.de/Record/PU199004042161.

N. A. Maffiuletti. Physiological and methodological considerations for the use of neuromuscular electrical stimulation. *European Journal of Applied Physiology*, 110(2):223–234, Sep 2010. doi: 10.1007/s00421-010-1502-y. URL https://doi.org/10.1007/s00421-010-1502-y.

M. Marina, M. Rios, P. Torrado, A. Busquets, and R. Angulo-Barroso. Force–time course parameters and force fatigue model during an intermittent fatigue protocol in motorcycle race riders. *Scandinavian Journal of Medicine & Science in Sports*, 25(3):406–416, 2014. doi: 10.1111/sms.12220. URL https://doi.org/10.1111/sms.12220.

A. Meyer. Numerical Solution of Optimal Control Problems with Explicit and Implicit Switches. Dissertation, Heidelberg University, 2020. URL https://doi.org/10.11588/heidok.00027701. doi: 10.11588/heidok.00027701.

M. Mitchell, B. Muftakhidinov, T. Winchen, et al. Engauge Digitizer Software. URL https://markummitchell.github.io/engauge-digitizer/. Accessed on 2020-05-06.

K. Mombaur. Stability optimization of open-loop controlled walking robots. Dissertation, Heidelberg University, 2001. URL https://doi.org/10.11588/heidok.00001796. doi: 10.11588/heidok.00002980.

H. Monod and J. Scherrer. Capacité de travail statique d'un groupe musculaire synergique chez l'homme. *Comptes Rendus des Séances de la Société de Biologie et de ses Filiales*, 151(7):1358–1362, 1957.

H. Monod and J. Scherrer. The work capacity of a synergic muscular group. *Ergonomics*, 8(3):329–338, 1965. doi: 10.1080/00140136508930810. URL https://doi.org/10.1080/00140136508930810.

B. Morel, M. Clémençon, S. Rota, G. Y. Millet, D. J. Bishop, O. Brosseau, D. M. Rouffet, and C. A. Hautier. Contraction velocity influence the magnitude and etiology of neuromuscular fatigue during repeated maximal contractions. *Scandinavian Journal of Medicine & Science in Sports*, 25(5):e432–e441, 2015. doi: 10.1111/sms.12358. URL https://doi.org/10.1111/sms.12358.

B. Morel, T. Lapole, C. Liotard, and C. Hautier. Critical Peripheral Fatigue Thresholds Among Different Force-Velocity Conditions: An Individual-Based Model Approach. *Frontiers in Physiology*, 10:875, 2019. doi: 10.3389/fphys.2019.00875. URL https://doi.org/10.3389/fphys.2019.00875.

D. Muniz-Pumares, B. Karsten, C. Triska, and M. Glaister. Methodological Approaches and Related Challenges Associated With the Determination of Critical Power and W'. *The Journal of Strength & Conditioning Research*, December 2018. doi: 10.1519/jsc.0000000000002977. URL https://doi.org/10.1519/jsc.0000000000002977.

D. Neyroud, J. Rüttimann, A. F. Mannion, G. Y. Millet, N. A. Maffiuletti, B. Kayser, and N. Place. Comparison of neuromuscular adjustments associated with sustained isometric contractions of four different muscle groups. *Journal of Applied Physiology*, 114(10):1426–1434, 2013. doi: 10.1152/japplphysiol.01539.2012. URL https://doi.org/10.1152/japplphysiol.01539.2012.

D. Neyroud, B. Kayser, and N. Place. Are There Critical Fatigue Thresholds? Aggregated vs. Individual Data. *Frontiers in Physiology*, 7:376, 2016. doi: 10.3389/fphys.2016.00376. URL https://doi.org/10.3389/fphys.2016.00376.

J. Nocedal and S. J. Wright. *Numerical Optimization*. Springer Series in Operations Research and Financial Enginering. Springer Verlag, New York, 2nd edition, 2006.

J. P. Nunes, A. S. Ribeiro, B. J. Schoenfeld, and E. S. Cyrino. Comment on: "Comparison of Periodized and Non-Periodized Resistance Training on Maximal Strength: A Meta-Analysis". *Sports Medicine*, 48(2):491–494, 2018. doi: 10.1007/s40279-017-0824-x. URL https://doi.org/10.1007/s40279-017-0824-x.

W. L. Oberkampf and C. J. Roy. *Verification and Validation in Scientific Computing*. Cambridge University Press, 2010. doi: 10.1017/cbo9780511760396. URL https://doi.org/10.1017/cbo9780511760396.

D. J. Oranchuk, A. G. Storey, A. R. Nelson, and J. B. Cronin. Isometric training and long-term adaptations: Effects of muscle length, intensity, and intent: A systematic review. *Scandinavian Journal of Medicine & Science in Sports*, 29 (4):484–503, 2019. doi: 10.1111/sms.13375. URL https://doi.org/10.1111/sms.13375.

A. G. Philippe, G. Py, F. B. Favier, A. M. Sanchez, A. Bonnieu, T. Busso, and R. Candau. Modeling the Responses to Resistance Training in an Animal Experiment Study. *BioMed research international*, 2015, 2015. doi: 10.1155/2015/914860. URL https://doi.org/10.1155/2015/914860.

A. G. Philippe, F. Borrani, A. M. Sanchez, G. Py, and R. Candau. Modelling performance and skeletal muscle adaptations with exponential growth functions during resistance training. *Journal of Sports Sciences*, 37(3):254–261, 2019. doi: 10.1080/02640414.2018.1494909. URL https://doi.org/10.1080/02640414.2018.1494909.

N. Place, N. A. Maffiuletti, Y. Ballay, and R. Lepers. Twitch potentiation is greater after a fatiguing submaximal isometric contraction performed at short vs. long quadriceps muscle length. *Journal of Applied Physiology*, 98(2):429–436, 2005. doi: 10.1152/japplphysiol.00664.2004. URL https://doi.org/10.1152/japplphysiol.00664.2004.

J. R. Potvin and A. J. Fuglevand. A motor unit-based model of muscle fatigue. *PLOS Computational Biology*, 13(6):1–30, 06 2017. doi: 10.1371/journal.pcbi.1005581. URL https://doi.org/10.1371/journal.pcbi.1005581.

F. Pukelsheim. *Optimal Design of Experiments*. John Wiley & Sons, 1993. doi: 10.1137/1.9780898719109. URL https://doi.org/10.1137/1.9780898719109.

E. Rashedi and M. A. Nussbaum. Quantifying the history dependency of muscle recovery from a fatiguing intermittent task. *Journal of Biomechanics*, 51:26–31, 2017. doi: 10.1016/j.jbiomech.2016.11.061. URL https://doi.org/10.1016/j.jbiomech.2016.11.061.

G. Q. Rich. Muscular Fatigue Curves of Boys and Girls. *Research Quarterly. American Association for Health, Physical Education and Recreation*, 31(3): 485–498, 1960. doi: 10.1080/10671188.1960.10762056. URL https://doi.org/10.1080/10671188.1960.10762056.

R. Riener, J. Quintern, and G. Schmidt. Biomechanical model of the human knee evaluated by neuromuscular stimulation. *Journal of Biomechanics*, 29(9):1157–1167, 1996. doi: 10.1016/0021-9290(96)00012-7. URL https://doi.org/10.1016/0021-9290(96)00012-7.

D. Rodríguez-Rosell, F. Pareja-Blanco, P. Aagaard, and J. J. González-Badillo. Physiological and methodological aspects of rate of force development assessment in human skeletal muscle. *Clinical Physiology and Functional Imaging*, 2017. doi: 10.1111/cpf.12495. URL https://doi.org/10.1111/cpf.12495.

W. Rohmert. Ermittlung von Erholungspausen für statische Arbeit des Menschen. *Internationale Zeitschrift für angewandte Physiologie einschließlich Arbeitsphysiologie*, 18(2):123–164, 1960. doi: 10.1007/BF00698869. URL https://doi.org/10.1007/BF00698869.

V. Rozand, T. Cattagni, J. Theurel, A. Martin, and R. Lepers. Neuromuscular Fatigue Following Isometric Contractions with Similar Torque Time Integral. *International Journal of Sports Medicine*, 36(01):35–40, 2015. doi: 10.1055/s-0034-1375614. URL https://doi.org/10.1055/s-0034-1375614.

T. Sadamoto, F. Bonde-Petersen, and Y. Suzuki. Skeletal muscle tension, flow, pressure, and EMG during sustained isometric contractions in humans. *European Journal of Applied Physiology and Occupational Physiology*, 51(3):395–408, Sep 1983. doi: 10.1007/BF00429076. URL https://doi.org/10.1007/BF00429076.

K. Sahlin, M. Tonkonogi, and K. Söderlund. Energy supply and muscle fatigue in humans. *Acta Physiologica Scandinavica*, 162(3):261–266, 1998. doi: 10.1046/j.1365-201x.1998.0298f.x. URL https://doi.org/10.1046/j.1365-201x.1998.0298f.x.

H. Sato, J. Ohashi, K. Iwanaga, R. Yoshitake, and R. Shimada. Endurance time and fatigue in static contractions. *Journal of Human Ergology*, 13(2):147–154, 1984. doi: 10.11183/jhe1972.13.147. URL https://doi.org/10.11183/jhe1972.13.147.

D. Schaefer, A. Asteroth, and M. Ludwig. Training plan evolution based on training models. In *2015 International Symposium on INnovations in Intelligent SysTems and Applications (INISTA)*, pages 1–8. IEEE, 2015. doi: 10.1109/INISTA.2015.7276739. URL https://doi.org/10.1109/INISTA.2015.7276739.

J. P. Schlöder and H. G. Bock. Identification of Rate Constants in Bistable Chemical Reactions. In Deuflhard and Hairer, editors, *Numerical Treatment of Inverse Problems in Differential and Integral Equations, Progress in Scientific Computing*, pages 27–47, Basel Boston Berlin, 1983. Birkhäuser. doi: 10.1007/978-1-4684-7324-7_3. URL https://doi.org/10.1007/978-1-4684-7324-7_3.

J. P. Schlöder. Numerische Methoden zur Behandlung hochdimensionaler Aufgaben der Parameteridentifizierung. Dissertation, Rheinische Friedrich-Wilhelms-Universität Bonn, 1988.

B. J. Schoenfeld. The Mechanisms of Muscle Hypertrophy and Their Application to Resistance Training. *The Journal of Strength & Conditioning Research*, 24 (10):2857–2872, 2010. doi: 10.1519/JSC.0b013e3181e840f3. URL https://doi.org/10.1519/JSC.0b013e3181e840f3.

B. J. Schoenfeld, D. Ogborn, and J. W. Krieger. Effects of Resistance Training Frequency on Measures of Muscle Hypertrophy: A Systematic Review and Meta-Analysis. *Sports Medicine*, pages 1–9, 2016. doi: 10.1007/s40279-016-0543-8. URL https://doi.org/10.1007/s40279-016-0543-8.

B. J. Schoenfeld, J. Grgic, D. Ogborn, and J. W. Krieger. Strength and Hypertrophy Adaptations Between Low- vs. High-Load Resistance Training: A Systematic Review and Meta-analysis. *The Journal of Strength & Conditioning Research*, 31(12):3508–3523, 2017. doi: 10.1519/JSC.0000000000002200. URL https://doi.org/10.1519/JSC.0000000000002200.

J. Schott, K. McCully, and O. M. Rutherford. The role of metabolites in strength training. *European Journal of Applied Physiology and Occupational Physiology*, 71(4):337–341, Sep 1995. doi: 10.1007/BF00240414. URL https://doi.org/10.1007/BF00240414.

A. Shield and S. Zhou. Assessing Voluntary Muscle Activation with the Twitch Interpolation Technique. *Sports Medicine*, 34(4):253–267, 2004. doi: 10.2165/00007256-200434040-00005. URL https://doi.org/10.2165/00007256-200434040-00005.

B. Sih, L. Ng, and J. Stuhmiller. Generalization of a Model Based on Biophysical Concepts of Muscle Activation, Fatigue and Recovery that Explains Exercise Performance. *International Journal of Sports Medicine*, 33(04):258–267, 2012. doi: 10.1055/s-0031-1297958. URL https://doi.org/10.1055/s-0031-1297958.

J. L. Smith, P. G. Martin, S. C. Gandevia, and J. L. Taylor. Sustained contraction at very low forces produces prominent supraspinal fatigue in human elbow flexor muscles. *Journal of Applied Physiology*, 103(2):560–568, 2007. doi: 10.1152/japplphysiol.00220.2007. URL https://doi.org/10.1152/japplphysiol.00220.2007.

K. Søgaard, S. C. Gandevia, G. Todd, N. T. Petersen, and J. L. Taylor. The effect of sustained low-intensity contractions on supraspinal fatigue in human elbow flexor muscles. *The Journal of Physiology*, 573(2):511–523, 2006. doi: 10.1113/jphysiol.2005.103598. URL https://doi.org/10.1113/jphysiol.2005.103598.

M. W. Sonne and J. R. Potvin. A modified version of the three-compartment model to predict fatigue during submaximal tasks with complex force-time histories. *Ergonomics*, 59(1):85–98, 2016. doi: 10.1080/00140139.2015.1051597. URL https://doi.org/10.1080/00140139.2015.1051597.

A.-N. Spiess and N. Neumeyer. An evaluation of R2 as an inadequate measure for nonlinear models in pharmacological and biochemical research: a Monte Carlo approach. *BMC Pharmacology*, 10(1):6, 2010. doi: 10.1186/1471-2210-10-6. URL https://doi.org/10.1186/1471-2210-10-6.

G. A. Stull and J. T. Kearney. Recovery of muscular endurance following submaximal, isometric exercise. *Medicine & Science in Sports*, 10(2):109–112, 1978. URL https://europepmc.org/article/med/692299.

B. Tan. Manipulating Resistance Training Program Variables to Optimize Maximum Strength in Men: A Review. *The Journal of Strength & Conditioning Research*, 13(3):289–304, 1999. URL https://journals.lww.com/nsca-jscr/Abstract/1999/08000/Manipulating_Resistance_Training_Program_Variables.19.aspx.

J. L. Taylor, J. E. Butler, and S. C. Gandevia. Altered responses of human elbow flexors to peripheral-nerve and cortical stimulation during a sustained maximal voluntary contraction. *Experimental Brain Research*, 127(1):108–115, 1999. doi: 10.1007/s002210050779. URL https://doi.org/10.1007/s002210050779.

J. L. Taylor, G. M. Allen, J. E. Butler, and S. C. Gandevia. Supraspinal fatigue during intermittent maximal voluntary contractions of the human elbow flexors. *Journal of Applied Physiology*, 89(1):305–313, 2000. doi: 10.1152/jappl.2000.89.1.305. URL https://doi.org/10.1152/jappl.2000.89.1.305.

J. L. Taylor, M. Amann, J. Duchateau, R. Meeusen, and C. L. Rice. Neural Contributions to Muscle Fatigue: From the Brain to the Muscle and Back Again. *Medicine & Science in Sports & Exercise*, 48(11):2294–306, 2016. doi: 10.1249/mss.0000000000000923. URL https://doi.org/10.1249/mss.0000000000000923.

G. Todd, J. L. Taylor, and S. C. Gandevia. Measurement of voluntary activation of fresh and fatigued human muscles using transcranial magnetic stimulation. *The Journal of Physiology*, 551(2):661–671, 2003. doi: 10.1113/jphysiol.2003.044099. URL https://doi.org/10.1113/jphysiol.2003.044099.

M. Toigo and U. Boutellier. New fundamental resistance exercise determinants of molecular and cellular muscle adaptations. *European Journal of Applied Physiology*, 97(6):643–663, 2006. doi: 10.1007/s00421-006-0238-1. URL https://doi.org/10.1007/s00421-006-0238-1.

M. Torres, E. T. Trexler, A. E. Smith-Ryan, and A. Reynolds. A mathematical model of the effects of resistance exercise-induced muscle hypertrophy on body composition. *European Journal of Applied Physiology*, Dec 2017. doi: 10.1007/s00421-017-3787-6. URL https://doi.org/10.1007/s00421-017-3787-6.

J. J. Tufano, L. E. Brown, and G. G. Haff. Theoretical and Practical Aspects of Different Cluster Set Structures: A Systematic Review. *The Journal of*

Strength & Conditioning Research, 31(3):848–867, 2017. doi: 10.1519/JSC.0000000000001581. URL https://doi.org/10.1519/JSC.0000000000001581.

S. Ullmer and A. Mader. A Mathematical Model of Regulation of Protein Synthesis by Activation Feedback: Some Reflections on Its Possibilities and Limits in Describing Muscle Mass Adaptations with Exercise. In *Integration of Medical and Sports Sciences*, volume 37, pages 288–298. Karger Publishers, 1992. doi: 10.1159/000421575. URL https://doi.org/10.1159/000421575.

A. Vanhatalo and A. M. Jones. Influence of prior sprint exercise on the parameters of the 'all-out critical power test' in men. *Experimental Physiology*, 94(2):255–263, 2009. doi: 10.1113/expphysiol.2008.045229. URL https://doi.org/10.1113/expphysiol.2008.045229.

A. Vanhatalo, J. H. Doust, and M. Burnley. Determination of Critical Power Using a 3-min All-out Cycling Test. *Medicine & Science in Sports & Exercise*, 39(3):548–555, March 2007. doi: 10.1249/mss.0b013e31802dd3e6. URL https://doi.org/10.1249/mss.0b013e31802dd3e6.

G. Vernillo, J. Temesi, M. Martin, and G. Y. Millet. Mechanisms of Fatigue and Recovery in Upper versus Lower Limbs in Men. *Medicine & Science in Sports & Exercise*, 2017. doi: 10.1249/MSS.0000000000001445. URL https://doi.org/10.1249/MSS.0000000000001445.

P. Virtanen, R. Gommers, T. E. Oliphant, M. Haberland, T. Reddy, D. Cournapeau, E. Burovski, P. Peterson, W. Weckesser, J. Bright, et al. SciPy 1.0: fundamental algorithms for scientific computing in Python. *Nature Methods*, pages 1–12, 2020. doi: 10.1038/s41592-019-0686-2. URL https://doi.org/10.1038/s41592-019-0686-2.

N. K. Vøllestad. Measurement of human muscle fatigue. *Journal of Neuroscience Methods*, 74(2):219–227, 1997. doi: 10.1016/S0165-0270(97)02251-6. URL https://doi.org/10.1016/S0165-0270(97)02251-6.

H. Wackerhage, B. J. Schoenfeld, D. L. Hamilton, M. Lehti, and J. J. Hulmi. Stimuli and sensors that initiate skeletal muscle hypertrophy following resistance exercise. *Journal of Applied Physiology*, 126(1):30–43, Jan. 2019. doi: 10.1152/japplphysiol.00685.2018. URL https://doi.org/10.1152/japplphysiol.00685.2018.

S. Walter. Structured higher-order algorithmic differentiation in the forward and reverse mode with application in optimum experimental design. Dissertation, Humboldt University of Berlin, 2012. URL https://doi.org/10.18452/16514. doi: 10.18452/16514.

M. A. Williams, W. L. Haskell, P. A. Ades, E. A. Amsterdam, V. Bittner, B. A. Franklin, M. Gulanick, S. T. Laing, and K. J. Stewart. Resistance Exercise

in Individuals With and Without Cardiovascular Disease: 2007 Update. *Circulation*, 116(5):572–584, 2007. doi: 10.1161/CIRCULATIONAHA.107.185214. URL https://doi.org/10.1161/CIRCULATIONAHA.107.185214.

T. D. Williams, D. V. Tolusso, M. V. Fedewa, and M. R. Esco. Comparison of Periodized and Non-Periodized Resistance Training on Maximal Strength: A Meta-Analysis. *Sports Medicine*, 47(10):2083–2100, 2017. doi: 10.1007/s40279-017-0734-y. URL https://doi.org/10.1007/s40279-017-0734-y.

T. D. Williams, D. V. Tolusso, M. V. Fedewa, and M. R. Esco. Author's Reply to Nunes et al.: Comment on: "Comparison of Periodized and Non-Periodized Resistance Training on Maximal Strength: A Meta-Analysis". *Sports Medicine*, 48(2):495–496, 2018. doi: 10.1007/s40279-017-0822-z. URL https://doi.org/10.1007/s40279-017-0822-z.

G. J. Wilson and A. J. Murphy. The Use of Isometric Tests of Muscular Function in Athletic Assessment. *Sports Medicine*, 22(1):19–37, 1996. doi: 10.2165/00007256-199622010-00003. URL https://doi.org/10.2165/00007256-199622010-00003.

K. M. Wisdom, S. L. Delp, and E. Kuhl. Use it or lose it: multiscale skeletal muscle adaptation to mechanical stimuli. *Biomechanics and modeling in mechanobiology*, 14(2):195–215, 2015. doi: 10.1007/s10237-014-0607-3. URL https://doi.org/10.1007/s10237-014-0607-3.

D. D. Wood, D. L. Fisher, and R. O. Andres. Minimizing Fatigue during Repetitive Jobs: Optimal Work-Rest Schedules. *Human Factors*, 39(1):83–101, 1997. doi: 10.1518/001872097778940678. URL https://doi.org/10.1518/001872097778940678.

R. E. Wood, S. Hayter, D. Rowbottom, and I. Stewart. Applying a mathematical model to training adaptation in a distance runner. *European Journal of Applied Physiology*, 94(3):310–316, 2005. doi: 10.1007/s00421-005-1319-2. URL https://doi.org/10.1007/s00421-005-1319-2.

T. Xia and L. A. F. Law. A theoretical approach for modeling peripheral muscle fatigue and recovery. *Journal of Biomechanics*, 41(14):3046–3052, 2008. doi: 10.1016/j.jbiomech.2008.07.013. URL https://doi.org/10.1016/j.jbiomech.2008.07.013.

T. Yoon, B. Schlinder Delap, E. E. Griffith, and S. K. Hunter. Mechanisms of fatigue differ after low- and high-force fatiguing contractions in men and women. *Muscle & Nerve*, 36(4):515–524, 2007. doi: 10.1002/mus.20844. URL https://doi.org/10.1002/mus.20844.

X. Zhou, P. E. Roos, and X. Chen. *Modeling of Muscle Atrophy and Exercise Induced Hypertrophy*, pages 116–127. Springer International Publishing, Cham, 2018. doi: 10.1007/978-3-319-60591-3. URL https://doi.org/10.1007/978-3-319-60591-3.

A. Zignoli and F. Biral. Prediction of pacing and cornering strategies during cycling individual time trials with optimal control. *Sports Engineering*, 23(1), 2020. doi: 10.1007/s12283-020-00326-x. URL https://doi.org/10.1007/s12283-020-00326-x.

M. C. Zourdos, C. Dolan, J. M. Quiles, A. Klemp, E. Jo, J. P. Loenneke, R. Blanco, and M. Whitehurst. Efficacy of daily one-repetition maximum training in well-trained powerlifters and weightlifters: a case series. *Nutricion Hospitalaria*, 33: 437 – 443, 04 2016. doi: 10.20960/nh.129. URL https://doi.org/10.20960/nh.129.

List of figures

4.1 Different experimental conditions result in different parameter estimates and confidence regions thereof. The measurement data obtained by two different experiments are denoted by η and $\tilde{\eta}$. The corresponding parameter estimates are denoted by p and $\tilde{p}$. Confidence regions are illustrated by ellipses. Smaller confidence regions increase the probability of the estimates being close to the 'true' but unknown value. Redrawn in modified form from Walter [2012]. 41

8.1 Model response obtained by fitting the model of Freund and Takala [2001] simultaneously to the data of E1 (shown here) and E2. The top row shows the mean values of the experiments plotted against the model response for the experimental setting. The error bars represent the standard errors of the means. Additionally, the relative force input is illustrated in the bottom row. 72

8.2 Model response obtained by fitting the model of Freund and Takala [2001] simultaneously to the data of E1 and E2 (shown here). The top row shows the mean values of the experiments plotted against the model response for the experimental setting. The error bars represent the standard errors of the means. Additionally, the absolute force input is illustrated in the middle row and the relative force input is illustrated in the bottom row. Note that these two input functions result from using the multi-stage formulation of the model as described in Section 8.6. 73

8.3 Model response obtained by fitting the model of Fayazi et al. [2013] simultaneously to the data of E1 (shown here) and E2. The top row shows the mean values of the experiments plotted against the model response for the experimental setting. The error bars represent the standard errors of the means. Additionally, the relative force input is illustrated in the bottom row. 74

8.4 Model response obtained by fitting the model of Fayazi et al. [2013] simultaneously to the data of E1 and E2 (shown here). The top row shows the mean values of the experiments plotted against the model response for the experimental setting. The error bars represent the standard errors of the means. Additionally, the absolute force input is illustrated in the middle row and the relative force input is illustrated in the bottom row. Note that these two input functions result from using the multi-stage formulation of the model as described in Section 8.6. 75

8.5 Model response obtained by fitting the proposed model simultaneously to the data of E1 (shown here), E2, E3a, and E3c. The top row shows the mean values of the experiments plotted against the model response for the experimental setting. The error bars represent the standard errors of the means. Additionally, the relative force input is illustrated in the bottom row. 76
8.6 Model response obtained by fitting the proposed model simultaneously to the data of E1, E2 (shown here), E3a, and E3c. The top top row shows the mean values of the experiments plotted against the model response for the experimental setting. The error bars represent the standard errors of the means. Additionally, the absolute force input is illustrated in the middle row and the relative force input is illustrated in the bottom row. Note that these two input functions result from using the multi-stage formulation of the model as described in Section 8.6. 77
8.7 Model response obtained by fitting the proposed model simultaneously to the data of E1, E2, E3a (shown here), and E3c. The top row shows the mean values of the experiments plotted against the model response for the experimental setting. The error bars represent the standard errors of the means. Additionally, the relative force input is illustrated in the bottom row. 78
8.8 Model response obtained by fitting the proposed model simultaneously to the data of E1, E2, E3a, and E3c (shown here). The top row shows the mean values of the experiments plotted against the model response for the experimental setting. The error bars represent the standard errors of the means. Additionally, the relative force input is illustrated in the bottom row. 79
8.9 Model response obtained by simulating the calibrated model for the experimental settings of E3b. The top row shows the mean values of the experiments plotted against the model response for the experimental setting. The error bars represent the standard errors of the means. Additionally, the relative force input is illustrated in the bottom row. 79
8.10 Model response obtained by simulating the calibrated model for the experimental settings of E3d. The top row shows the mean values of the experiments plotted against the model response for the experimental setting. The error bars represent the standard errors of the means. Additionally, the relative force input is illustrated in the bottom row. 80
8.11 Model response obtained by simulating the calibrated model for the experimental settings of E4. The top row shows the mean values of the experiments plotted against the model response for the experimental setting. The error bars represent the standard errors of the means. Additionally, the relative force input is illustrated in the bottom row. 80

8.12 Model response obtained by simulating the calibrated model for the experimental settings of E5. The top row shows the mean values of the experiments plotted against the model response for the experimental setting. The error bars represent the standard errors of the means. Additionally, the absolute force input is illustrated in the middle row and the relative force input is illustrated in the bottom row. Note that these two input functions result from using the multi-stage formulation of the model as described in Section 8.6. 81
8.13 Results of the cross-validation with 30 different combinations of calibration and prediction sets. To visualize the deviations, the parameter estimates p_i and the WRSS are normalized to the values obtained in Section 8.10.2. The whiskers illustrate the minimum and maximum value. The boundaries of the box illustrate the first and the third quartiles. The line inside the box illustrates the median. 83

9.1 Model response obtained by simulating the calibrated model for an MVIC effort (shown here) and for a submaximal contraction with the same force-time integral. The top row shows the model response and the relative force input is illustrated in the bottom row. 90
9.2 Model response obtained by simulating the calibrated model for an MVIC effort and for a submaximal contraction (shown here) with the same force-time integral. The top row shows the model response and the absolute force input is illustrated in the bottom row. . . . 91
9.3 Model response obtained by simulating the calibrated model for an MVIC effort (shown here) and for a submaximal contraction inducing the same level of fatigue followed by 10 min of recovery. The top row shows the model response and the relative force input is illustrated in the bottom row. Recovery from the MVIC effort is almost complete after 10 min. 91
9.4 Model response obtained by simulating the calibrated model for an MVIC effort and for a submaximal contraction (shown here) inducing the same level of fatigue followed by 10 min of recovery. The top row shows the model response and the absolute force input is illustrated in the bottom row. Recovery from the submaximal contraction takes longer than 10 min. 92

10.1 Model response obtained by simulating the calibrated model for Session A. The top row shows the model response and the absolute force input is illustrated in the bottom row. 101
10.2 Model response obtained by simulating the calibrated model for Session $B_{70\%}$. The top row shows the model response and the absolute force input is illustrated in the bottom row. 101
10.3 Model response obtained by simulating the calibrated model for Session $B_{90\%}$. The top row shows the model response and the absolute force input is illustrated in the bottom row. 102

10.4 Model response obtained by simulating the calibrated model for Session C. The top row shows the model response and the absolute force input is illustrated in the bottom row. 102
10.5 Model response obtained by simulating the calibrated model for Session D_5. The top row shows the model response and the absolute force input is illustrated in the bottom row. 103
10.6 Model response obtained by simulating the calibrated model for Session D_{50}. The top row shows the model response and the absolute force input is illustrated in the bottom row. 103
10.7 Dependency of the objective functional value on the number of possible contractions for Sessions D_5 to D_{50}. Increasing the number of possible contractions increases the FTI of the computed solution. . 104
10.8 Dependency of the durations of contractions (a) and rests (b) on the number of possible contractions for Sessions D_5 to D_{50}. The horizontal dashed lines illustrate the 1 s mark. Increasing the number of possible contractions decreases the durations of contractions and rests of the computed solution. 104
10.9 Dependency of the durations of contractions (a) and rests (b) on the number of possible contractions for Sessions D_5 to D_{50}. The horizontal dashed lines illustrate the 1 s mark. Increasing the number of possible contractions decreases the durations of contractions and rests of the computed solution. 105
10.10 Model response obtained by simulating the calibrated model for Session E. The top row shows the model response and the absolute force input is illustrated in the bottom row. 105
10.11 Model response obtained by simulating the calibrated model for Session F. The top row shows the model response and the absolute force input is illustrated in the bottom row. 106
10.12 Model response obtained by simulating the calibrated model for Session G. The top row shows the model response and the absolute force input is illustrated in the bottom row. 107
10.13 Model response obtained by simulating the calibrated model for Session H. The top row shows the model response and the absolute force input is illustrated in the bottom row. 107
10.14 Model response obtained by simulating the calibrated model for Session I. The top row shows the model response and the absolute force input is illustrated in the bottom row. 108
10.15 Model response obtained by simulating the calibrated model for Session J. The top row shows the model response and the absolute force input is illustrated in the bottom row. 109
10.16 Model response obtained by simulating the calibrated model for Session K. The top row shows the model response and the absolute force input is illustrated in the bottom row. 109

11.1 Schematic illustration of the power-endurance relationship of constant power tasks (11.2). The curvature of this relationship is determined by W' and its asymptote by P_c. The power that can be sustained for time T_{lim} can be obtained through $P = W'/T_{\text{lim}} + P_c$. 118
11.2 Model response obtained by simulating Scenario SCmax for 5 min. The bottom row illustrates the relative torque input. The dash-dotted lines represent the steady states obtained by simulating the scenario until a plateau of MVIC torque is reached. 121
11.3 Model response obtained by simulating Scenario ICmax for 5 min. The bottom row illustrates the relative torque input. The dash-dotted lines represent the steady states obtained by simulating the scenario until a plateau of MVIC torque is reached. 121
11.4 Model response obtained by simulating Scenario IC80 for 60 min. The dash-dotted lines represent the target torques of the intermittent contractions. The torque input has been omitted for this plot as due to the high number of intermittent contractions the plot would become illegible. 122
11.5 Model response obtained by simulating Scenario IC120 until MVIC torque drops below target torque. The dash-dotted lines represent the target torques of the intermittent contractions. The torque input has been omitted for this plot as due to the high number of intermittent contractions the plot would become illegible. 122
11.6 Highest sustainable torque output of the elbow flexors for intermittent contractions depending on the duty cycle. The duty cycle denotes the ratio $t_c/(t_c + t_r)$, where t_c denotes the duration of a contraction and t_r denotes the inter-repetition rest. 123

12.1 Model response obtained by simulating the intuitive testing session ITS. The bottom row illustrates the relative torque input. All contractions are maximal. 133
12.2 Model response obtained by simulating the optimized testing session OTS200. The bottom row illustrates the relative torque input. All contractions are maximal. 133
12.3 Model response obtained by simulating the optimized testing session OTS400. The bottom row illustrates the relative torque input. All contractions are maximal. 134
12.4 Estimated standard deviations of the model parameters SD(p) and trace tr(C) of the variance-covariance matrix resulting from the intuitive (Scenario ITS) and the optimized testing sessions (Scenarios OTS200 and OTS400). All parameters were scaled to 1 for the OED computations. Furthermore, SD(ICmax) and SD(RTS) denote the standard deviations of the differences of end-MVIC torque of the 10000 perturbed settings from the nominal setting p using the parameter uncertainties resulting from the intuitive testing session (ITS) and from the optimized testing sessions (OTS200 and OTS400). 135

12.5 Model response obtained by simulating Scenario RTS. The bottom row illustrates the relative torque input. This is one of two scenarios used to examine how the parameter uncertainties propagate through the model. 136
12.6 Kernel density estimates obtained by analyzing the differences of end-MVIC torque of the 10000 perturbed settings from the nominal setting p using the parameter uncertainties resulting from the intuitive testing session (ITS) and from the optimized testing sessions (OTS200 and OTS400). This plot shows the results for Scenario ICmax. The parameter uncertainties of the optimized testing sessions result in sharper peaks around the mean value 0. 136
12.7 Kernel density estimates obtained by analyzing the differences of end-MVIC torque of the 10000 perturbed settings from the nominal setting p using the parameter uncertainties resulting from the intuitive testing session (ITS) and from the optimized testing sessions (OTS200 and OTS400). This plot shows the results for Scenario RTS. The parameter uncertainties of the optimized testing sessions result in sharper peaks around the mean value 0. 137

List of tables

8.1 Overview of the model components. 67
8.2 Parameter estimates and their estimated relative standard deviations obtained by fitting the models of Freund and Takala [2001] and Fayazi et al. [2013] simultaneously to the data of E1 and E2. The common factors of these fits are estimated to be 7.45 and 7.82. 71
8.3 Mean absolute errors and weighted residual sum of squares obtained by fitting the models of Freund and Takala [2001] and Fayazi et al. [2013] simultaneously to the data of E1 and E2. 72
8.4 Parameter estimates and their estimated relative standard deviations obtained by fitting the proposed model simultaneously to the data of E1, E2, E3a, and E3c. The common factor for this fit is estimated to be 1.87. 76
8.5 Mean absolute errors and weighted residual sum of squares obtained by fitting the proposed model simultaneously to the data of E1, E2, E3a, and E3c. 77
8.6 Mean absolute errors and weighted residual sum of squares obtained by using the calibrated model to predict the data of E3b, E3d, E4, and E5. 78
8.7 AIC and AIC_c values for the fits of the three presented models to the data of experiments E1 and E2. The minimum value indicates the model to be preferred. 82
8.8 Results of the cross-validation with 30 different combinations of calibration and prediction sets. The table gives the minimum (min), maximum (max), and median estimate of the parameters p_i and the weighted residual sum of squares (WRSS). The last column additionally gives the standard deviations (SD) normalized to the values obtained in Section 8.10.2. 83

10.1 Overview of symbols used in the multi-stage OC problem (10.1). . 95
10.2 Overview of sessions used in this work. If not mentioned otherwise, all sessions last 20 min and allow 25 possible contractions. 97
10.3 Overview of sessions used in this work. If not mentioned otherwise, all sessions last 20 min and allow 25 possible contractions. 98
10.4 Minimum, maximum, and mean durations of contractions δ_c and rests δ_r for all sessions plotted. To a certain extent, this data allows to examine the real-life feasibility of the computed sessions. 110

11.1 Overview of simulation scenarios used in this chapter. 119

List of tables

12.1 Overview of symbols used in OED problem (12.7). 130
12.2 Overview of simulation scenarios used in this chapter. 132